Study of the Molecular Behaviour of Ionic Liquid Colloidal Suspensions Using Rheometry and NMR

By

Catherine Franklin Smith

A thesis submitted to the

University of Birmingham

for the degree of

DOCTOR OF PHILOSOPHY

School of Chemistry
College of Engineering and Physical Sciences
University of Birmingham
September 2016

Abstract

In this thesis, a systematic investigation has been carried out to study the effect of cations and anions on the interactions and aggregation of silica nanoparticles in ionic liquid colloidal suspensions. Suspensions of hydrophobic and hydrophilic silica nanoparticles in four ionic liquids, 1-ethyl-3-methylimidazolium tetrafluoroborate, $[C_2mim][BF_4]$, 1-butyl-3-methylimidazolium tetrafluoroborate, $[C_4mim][BF_4]$, 1-ethyl-3-methylimidazolium bis(trifluoromethylsufonyl)imide, $[C_2mim][NTf_2]$, and 1-butyl-3-methylimidazolium bis(trifluoromethylsufonyl)imide, $[C_4mim][NTf_2]$, have been studied.

Shear thinning rheology was observed in all systems. Suspensions in $[C_2mim][BF_4]$ and $[C_4mim][BF_4]$ showed shear thickening behaviour at high hydrophilic silica nanoparticle concentrations. Magnetic resonance velocity imaging experiments were performed to study the local rheology of the suspensions, which compared well with the bulk rheology, but indicated shear banding in suspensions of $[C_4mim][NTf_2]$ with hydrophilic nanoparticles. No hydrogen bonding, between either cation or anion and silica nanoparticles, was observed by IR spectroscopy. With increasing silica concentration, a decrease in the NMR T_1 relaxation time of protons on the imidazolium ring, of the cation, was observed for all ionic liquids indicating it is the cation that interacts with the nanoparticles. For all ionic liquid suspensions investigated, clusters of nanoparticles were observed by dynamic light scattering. However, for suspensions of hydrophilic silica in $[C_4mim][NTf_2]$ and hydrophobic silica in $[C_4mim][BF_4]$, high proportions of single nanoparticles were also present. These data have been interpreted in terms of the formation of colloidal gels and glasses.

Acknowledgements

First and foremost, I would like to thank my supervisor Melanie Britton. Without her support, encouragement and patience, the research would not have been completed, this thesis would not have been written and I would not be who I am now. I would also like to thank members of the research group, past and present, for their support: Heather, for showing me the ropes; Antoine, for trying to show me his laid back ways; Sue, for looking out for me; Matt and Sarah, for always finding time to chat; Josh, for being a great buddy; and Emma and Amanda, for the endless cups of tea and the conversations, both about research and anything else.

Endless thanks to my supportive friends, who have been there to celebrate with me on the good days and offer me a drink on the bad ones. Thanks also to my brother, Chris, for his cheerful optimism and faith in my ability to complete this degree.

Finally, a huge thanks goes to my parents and to my boyfriend Matt, for being there through the rollercoaster that has been this PhD.

Table of Contents

List of Figures

List of Abbreviations

AFM – atomic force microscopy

BPP – Bloembergen-Purcell-Pound

BF_4 - tetrafluoroborate

C_2mim - 1-ethyl-3-methylimidazolium

C_4mim - 1-butyl-3-methylimidazolium

[C_2mim][BF_4] - 1-ethyl-3-methylimidazolium tetrafluoroborate

[C_2mim][NTf_2] - 1-ethyl-3-methylimidazolium bis(trifluoromethylsufonyl)imide

[C_4mim][BF_4] - 1-butyl-3-methylimidazolium tetrafluoroborate

[C_4mim][NTf_2] - 1-butyl-3-methylimidazolium bis(trifluoromethylsufonyl)imide

[C_6mim][BF_4] - 1-hexyl-3-methylimidazolium tetrafluoroborate

[C_6mim][NTf_2] - 1-hexyl-3-methyimidazolium bis(trifluoromethylsufonyl)imide

CPMG - Carr-Purcell-Meiboom-Gill

DVLO - Derjaguin-Landau-Verwey-Overbeek

DLCA - diffusion limited cluster aggregation

DLS - dynamic light scattering

FID - free induction decay

FT - Fourier Transform

IR - infrared

NMR - nuclear magnetic resonance

NTf_2 - bis(trifluoromethylsufonyl)imide

PGSE - pulse field gradient spin echo

PGSTE - pulse field gradient stimulated echo

rf - radio frequency

1. Introduction

1.1 Colloidal Suspensions

Colloidal suspensions are of significant interest and are widely investigated systems.[1] They are two-component systems consisting of a dispersed phase of particles suspended in a continuous medium. Particle sizes can range from nanometres to micrometres in size and are several orders of magnitude larger than the molecules that make up the suspending liquid, which allows suspensions to be studied as a continuous medium.[1, 2] A wide variety of particles can be used to form colloidal suspensions, from silica and metal nanoparticles to carbon nanotubes and polymers.[1, 3-5] The continuous phase is often water, organic solvents or viscous liquids, such as glycerol. Colloidal suspensions are commonly found in nature and in many areas of science, including food science, formulation, engineering and material science.[1, 3, 5-7] There is a need to understand their chemistry and stability so as to improve applications.[8]

1.1.1 Interactions in Colloidal Suspensions

The interactions between the continuous phase and the nanoparticles define whether a colloidal suspension is formed and its stability. There are several competing forces which determine these factors.[1] Two particles in a medium will have a mutual, electrostatic repulsion, caused by charges that build up on the surface of the particles (figure 1.1a).[1, 2] This causes an electrical double layer, where the charge on the surface attracts species of the opposite charge from the continuous phase. This is described by the Debye-Huckel theory.[2] There is also a long-range attraction between the particles caused by van der Waals forces (figure 1.1b).[2, 9, 10] The balance between this attraction and repulsion is described by the Derjaguin-Landau-Verwey-Overbeek (DVLO) theory (figure 1.1c). If there is no stabilising

force, over time, the van der Waals forces cause the particles to come closer together. Due to a minimum in the DVLO potential, when the particles get close enough together, they form flocculates.[1, 2] At this point, there is still some repulsion between the particles so the flocculation is reversible.[2] If van der Waals forces completely dominate then the particles irreversibly coagulate.[2]

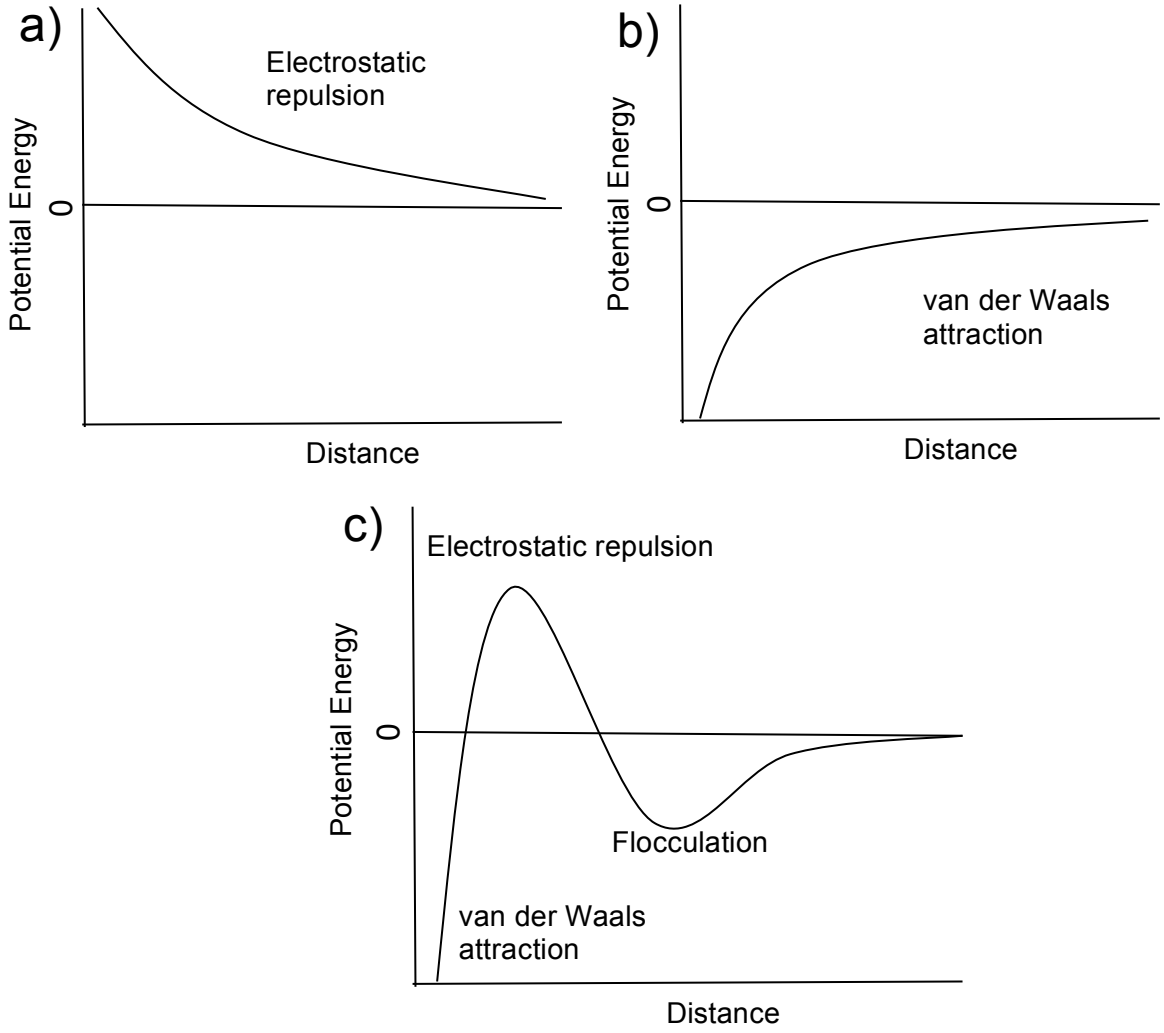

Figure 1.1: Plots of potential energy versus distance showing electrostatic repulsion force (a), van der Waals attraction force (b) and a combination of the two as described by the DVLO theory (c).

If a medium can provide a screening force between the particles, they will be stabilised and thus a stable suspension will be formed. The surface area of the particles, along with their volume fraction, will have a large effect on whether a suspension will be

stable or not; the larger the surface area, or volume fraction, the more area there is for charge to build and hence a larger screening force is required to stabilise the particles.[1] In some systems, aggregation of particles occurs at higher concentrations, as this reduces the surface area and thus enables the system to be stabilised. The properties of the medium, such as its ionic strength and dielectric properties, will also influence this stabilisation. Ultimately, the viscosity of the medium and the volume fraction of the particle are the most significant factors in predicting the stability of a system.[1] However, in different systems, there are different influences on stabilisation, making it very hard to predict how they will behave.[1]

1.1.2 Structure and Rheology of Colloidal Suspensions

The simplest form of a colloidal suspension is a fluid, where hard sphere particles are suspended and able to move freely with Brownian motion (figure 1.2). Hard spheres are model colloidal particles, where the only interaction between the particles is a steric repulsion.[11] In a non-colloidal system, hydrodynamic forces dominate the interactions between particles in solution.[1] In a colloidal suspension, Brownian motion acts to keep particles distributed throughout the suspending medium.[1] When a shear rate is applied to a sample, during rheometry, the equilibrium distribution of the particles is perturbed.[1, 12] At low shear rates, the Brownian motion can then return the particles to equilibrium. The return to a

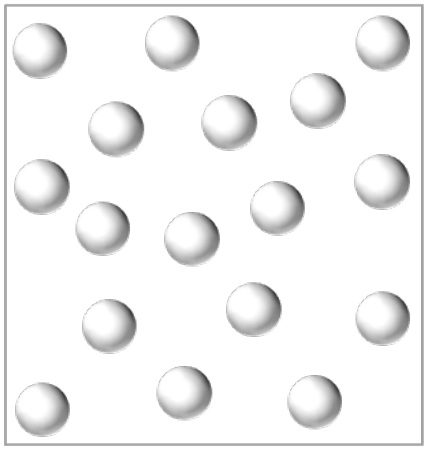

Figure 1.2: Schematic of nanoparticles in a colloidal suspension.

distributed sample means that there will be little change in the suspension viscosity with change in shear rate therefore the suspension will show Newtonian behaviour.[1, 12]

At increased shear rates, the Brownian motion cannot return the system to equilibrium. Small shear stresses can cause a degree of ordering. At these shear rates, instead of returning to their equilibrium structure, the particles form layers, which can then more easily move past each other.[13] Evidence for the layers has been observed using scattering techniques.[14] The layering means there is less of an entropy contribution to the viscosity as well as a decrease in the density of particles, and hence a decrease in the viscosity.[3] A decrease in the viscosity with increasing shear rate is known as shear thinning (figure 1.3).[12] The degree of shear thinning observed depends on the particle concentration; the higher the nanoparticle concentration, the greater the degree of shear thinning observed.[3]

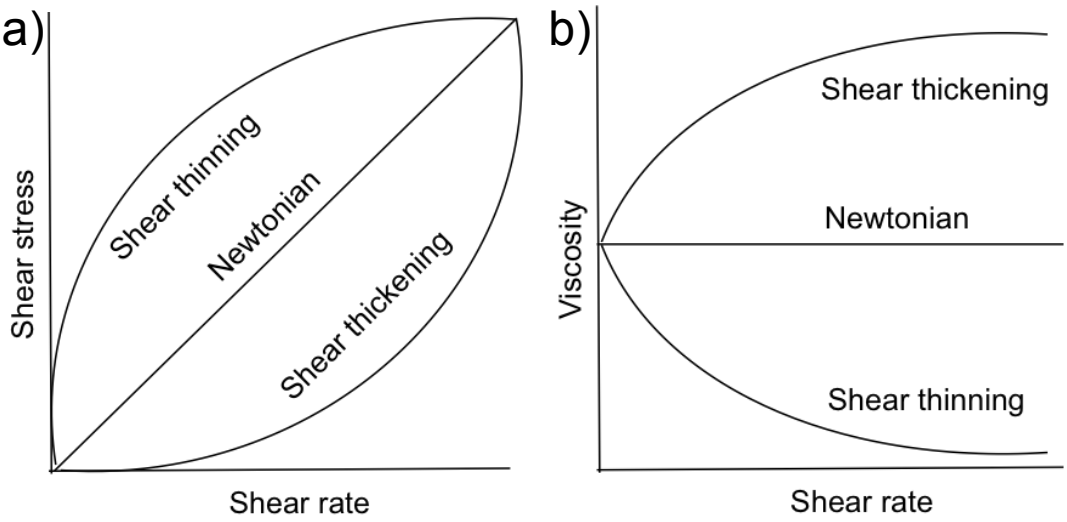

Figure 1.3: Example of rheological responses for a) plot of shear stress versus shear rate and b) plot of viscosity versus shear rate.

After a period of shear thinning in colloidal suspensions, another Newtonian regime is observed (figure 1.4). At this point, the layering that causes the shear thinning has reached a maximum point and therefore the viscosity can decrease no further.[3] However, with a further

increase in the shear rate, the entropic contribution to the viscosity continues to decrease and becomes negligible.[3] Therefore, the only force left is the hydrodynamic contribution to the viscosity.[3] At high shear rates, the decrease in Brownian motion means the particles start to collide. The hydrodynamic forces mean these collisions form temporary clusters. These have been observed as local, transient fluctuations in particle density by rheo-optic experiments and small angle neutron scattering.[1] The presence of the clusters causes an increase in the suspension viscosity. The increase of viscosity with increase in shear rate is known as shear thickening (figure 1.3). Shear thickening occurs at a constant strain, regardless of shear rate - it is the strain that varies between samples of different concentrations.[14-17] As soon as the shear rate drops below the critical strain value required, the cluster formation stops and hence the viscosity drops. Therefore, shear thickening is reversible. At higher concentrations, these clusters will cause the suspension to jam in the rheometer.[13] This is, again, completely reversible.

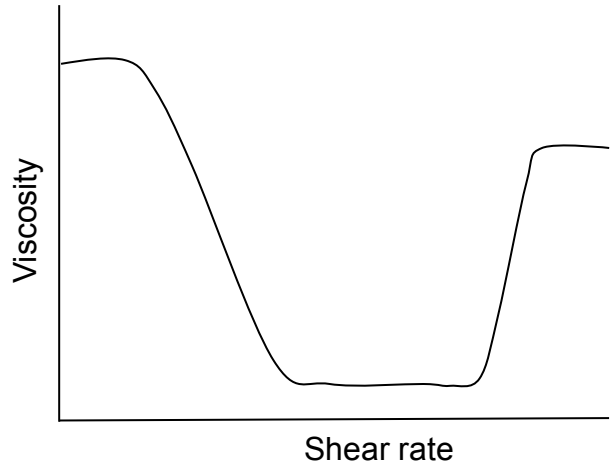

Figure 1.4: Schematic of colloidal suspension rheology on a plot of viscosity against shear rate

At the highest shear rates, lubrication forces between the particles come into play, giving a final shear thinning region as more clusters are destroyed than formed. This general rheology, as shown in figure 1.4, is observed for all colloidal suspensions with particles below

1 μm in diameter, given a large enough range of shear rates.[18] However, all of these phases are not always observed due to limits of instrumentation.[18] Sometimes only the shear thinning regime is observed. The onset of these different regimes is dependent on the size and concentration of the particles.[1] It also depends on the inter-particle interactions, such as the electrostatic repulsion, when suspensions of non-hard spheres are used.[1] Especially for smaller nanoparticles, surface forces have a large role in shear thickening being observed.[1]

1.1.3 Colloidal Gels

Colloidal suspensions of hard spheres are only kinetically stable.[1] Thermodynamically, they are unstable.[1] The most thermodynamically stable form of a suspension is for the material to form at the bottom of the container.[1, 7] Over time or at higher concentrations, colloidal systems will try to move to a thermodynamically stable state.[8] This involves the aggregation of particles. If the particles are not stabilised by the continuous medium, then the particles will aggregate and the system will start to undergo a phase separation.[8] However, at higher particle concentrations, this phase separation becomes interrupted.[8, 19]

At higher concentrations, the instability of the system is greater and therefore aggregation happens faster.[8] As the particles aggregate, particle rich and particle poor regions are formed.[20] These areas of different density mean that the sample starts to undergo phase separation.[20] However, the phase separation is interrupted and the system undergoes spinodal decomposition to a dynamically arrested state of a space spanning gel network (figure 1.5).[21] The particle network is kinetically stable in this arrested state, as no phase separation occurs over time.[19]

The spinodal decomposition is a non-equilibrium process that is triggered by a thermal instability that causes the formation of density fluctuations, which lead to the formation of space spanning clusters and the dynamical arrest of the system, forming a

gel. [11, 19, 22] The diffusion limited cluster aggregation (DLCA) mechanism that is often related to the formation of colloidal gels is an arrested spinodal mechanism – a low density colloid is quenched to a state point where a large attractive interaction dominates and then bonds become effectively irreversible.[19]

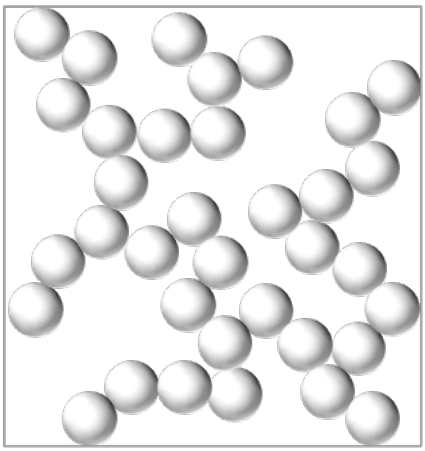

Figure 1.5: Schematic of the network formed by silica nanoparticles in a colloidal gel.

The space spanning network of particles that forms a colloidal gel is the cause of the large increase in viscosity observed in these systems, as when the particles aggregate some of the continuous phase becomes trapped.[23] When these samples are placed under shear, this breaks the gel network, reducing the viscosity and hence leading to the shear thinning that is observed. A colloidal gel can be described as a low density, disordered arrested state which does not flow but possesses solid like properties, such as a yield stress.[19]

Colloidal gels can also show a plateau in a plot of viscosity against shear rate (figure 1.6). This is evidence for the presence of a yield stress, which is the stress that needs to be applied to the sample for it to flow.[24] At very low shear rates, the sample will deform slightly as there is some give in the continuous network of particles that make up the system, leading to a small decrease in viscosity. However, until the shear stress exceeds yield stress, the sample will not flow, causing the viscosity to be constant.[24] Once the yield stress is reached, the sample then begins to flow and the viscosity decreases. This yield stress point

corresponds to the breaking of the network of particles that make up the gel. This network, especially because it can trap continuous phase, is what causes the larger viscosity observed and therefore once it is broken, shear thinning is observed. The observation of a yield stress in the rheology is an indication that a colloidal gel has been formed.[12, 24]

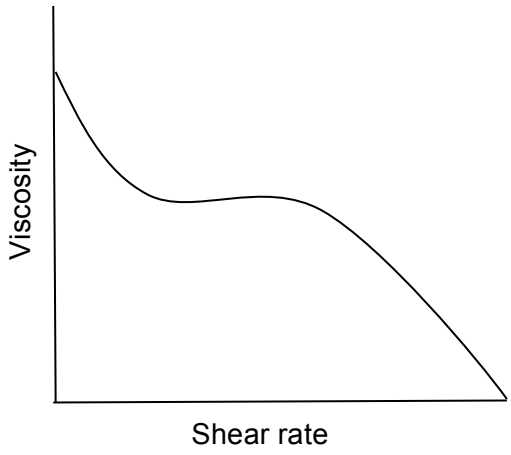

Figure 1.6: Schematic of a plot of viscosity against shear rate showing a yield stress.

1.1.4 Colloidal Glasses

Another arrested state that can form at high particle concentrations is a colloidal glass. A colloidal glass is a disordered and dynamically arrested state in which the particles are trapped in cages by repulsion.[25] In a stable glass, neighbouring particles trap each other into cages that are a regular meso-stable structure (figure 1.7).[25] This means that particle movements are restricted as the motion can only take place with a collective rearrangement of all the particles surrounding it.[20]

Most colloidal systems undergo a gel or glass transition to form 3D disordered states.[26] Gel and glass transitions are types of jamming transitions.[27] The differences in structures formed are dependent on the energy of the formed state. [28, 29] Nucleation and rearrangement processes play a key role in determining the properties of the suspensions, such as the microphase separation and subsequent gelation.[30]

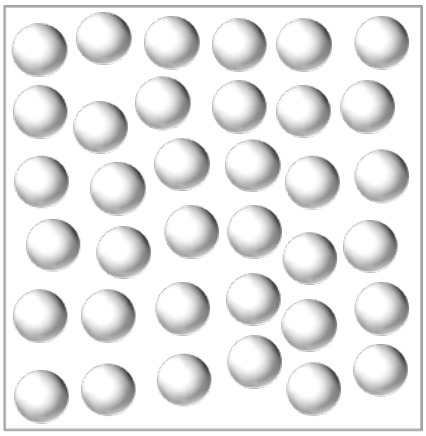

Figure 1.7: Schematic of a nanoparticles in a colloidal glass.

Colloidal glasses and gels are very similar in character and it can be hard to tell them apart. Many systems show characteristics of both a gel and a glass, for example a highly filled system that also contains connected particles.[25] They are both forms of a general jamming transition that occurs within a structure. It has been observed, through using dynamic light scattering (DLS) that there is a slowing down of the dynamics of a system before a jammed state occurs. Before the formation of a gel, the particles have to link together. In some instances, particles have been observed to form clusters before the jamming transition occurs. These clusters are fluid and able to move freely, so the system is not jammed. This is a phase known as a fluid of clusters.

1.1.5 Fluid of Clusters

A fluid of clusters is an intermediate phase between single nanoparticles and a gel; a weakly flocculated structure represents a dynamic equilibrium between clusters and single nanoparticles (figure 1.8).[31, 32] These occur at low nanoparticle concentrations where the particles have not been stabilised and have been observed in a wide range of systems, including silica nanoparticles.[32] These stable fluids are often observed in systems where the nanoparticle concentrations are just below those needed for the systems to form a gel.[22, 33] Clusters are only stable for a short period; over time a gel network will be formed due to the

instability of the nanoparticles.[32, 34] The existence of fluids of clusters have been confirmed using confocal microscopy and they have also been studied using computational methods.[32]

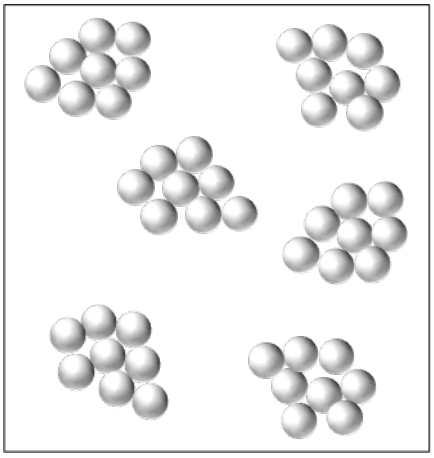

Figure 1.8: Schematic of a fluid of clusters.

Clusters formed in fluids are expected to be transient and are not predicted to exist in a stable state.[33] However, they are found to be thermodynamically stable and form as they represent a minimum in free energy.[32] The clusters represent a balance between competing short range interactions and long range repulsion, or a reversible flocculation.[32] The cluster phase will only appear if the attraction between the particles is strong enough and there must be some repulsion in the system.[32, 33] It has been found experimentally that it is the repulsion between hard spheres that will determine this phase.[33]

What causes the formation of this cluster phase? In colloidal suspensions, the formation of metastable states is often related to a depletion driven collapse, in which the particles quickly flocculate due to the lack of stabilisation [8, 35] One possible cause is that when clusters collide, there is not time for them to reorganise and join before moving apart again.[32, 33] It is also possible that the clusters acquire charge and it is this charge that means that the clusters do not aggregate.[33] It has been proposed that this cluster fluid phase is driven by phase separation, which halts due the higher energy of the bonds that formed during aggregation.[32, 36] In which case, the weak structural forces in the system allow the

clusters to form.[31] The particles are attracted to each other and aggregate but do not form networks due to a competition between the cluster formation and the cluster reorganisation, which causes a variation in the cluster size observed.[11] The morphology of the clusters depends on the inter-particle interaction.[32, 33]

1.1.6 Shear Banding

Colloidal suspensions are complex fluids which can undergo a flow-induced transition to a state where there are co-existing bands of different viscosities and internal structures.[37] This is known as shear banding. It occurs when the flow causes an internal meso-structural reorganisation that feeds back to the flow field, giving non-linear flow properties.[37, 38] Shear banding is a mechanical flow instability which is intrinsic to the material that demonstrates it.[39] Shear banding was first observed in the worm-like micelles and has since been observed in many complex fluids systems, such as surfactants, polymer solutions and soft glasses, as well as colloidal suspensions.[37, 38, 40] It is important to detect and understand shear banding as it may greatly affect the apparent flow properties of the materials.[41] The presence or absence of shear banding will depend on the shear stresses on the sample – there is a variation in the shear rate at the local scale.[41] It can occur at the approach of the interface between a liquid and a solid.[41]

The shear bands are associated with a stress plateau in the flow curve.[38, 42] An apparent discontinuity in the profile of the flowing liquid, when two different shear rates show almost the same shear stress (figure 1.9).[41] Coexisting bands are formed with different shear rates and different microstructures.[42] This allows the system to bypass the unstable part of the constitutive curve.[37] Shear banding can be simply represented by two coexisting phases of high and low viscosity, which represent two different strain rates, $\dot{\gamma}_1$ and $\dot{\gamma}_2$.[38] The bulk strain observed is an average of these local strain rates, as expressed by the level rule (equation 1.1).[38]

$$\dot{\gamma} = (1 - x)\dot{\gamma}_1 + x\dot{\gamma}_2 \quad (1.1)$$

Shear banding can also be detected when a negative slope appears in the flow curve of shear stress against shear rate.[39] If the slope that relates shear stress and shear rate is negative then the homogenous flow is unstable, which leads to bands of different shear rates at a common shear stress (figure 1.9).[37] By knowing the critical shear stress at which shear banding will onset for a particular system, shear banding can be predicted.[39]

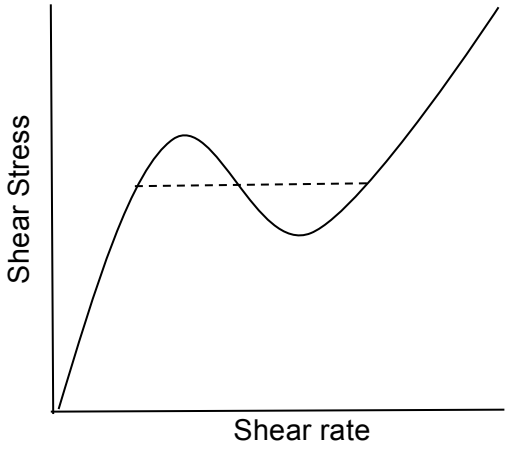

Figure 1.9: Schematic of shear banding on a plot of shear stress against shear rate.

However, bulk rheology provides a spatial average of the sample and is not able to directly relate the complex rheology to the microscopic structure.[43] To observe shear banding locally within a sample ultrasound, heterodyne DLS, as well as other rheo-optic techniques, confocal microscopy, rheology, x-ray scattering and velocity NMR can be used.[37, 41, 42, 44] It can also be detected using small angle neutron scattering measurements.[37] These techniques allow the strain-rate heterogeneities and discontinuities, such as fracture and wall slip to be visualised.[38] These techniques can also provide information about colloidal or molecular aggregation under conditions of flow and with spatial resolution.[38]

There are a wide variety of jammed systems, which have very different structures at the local level.[45] These materials are unable to flow steadily at a shear rate smaller than a critical value and often show a yield stress as well as being able to develop shear banding.[45]

It has been proposed that this shear banding occurs when the restructuring of the system is faster than the relaxation of the system, which is why shear banding occurs in some systems and not others – it is the timescale of the restructuring versus the relaxation of the structures.[45] However, this is an oversimplification to try and explain jammed soft systems as a whole.[45]

There is a difference between shear banding and a yield stress.[41] If there is a progressive decrease towards a velocity of zero in the sample, and therefore there is the same value for the velocity either side of shear and unsheared regions, then there is a yield stress in the sample and not shear banding.[41, 46] Co-existing static and flowing regions are a consequence of a yield stress.[41] Shear banding can be characterised by an abrupt transition from the flowing region to the stationary region in the velocity slope – a discontinuity of the shear at the interface.[41, 47] The increase in thickness of the sheared part will increase with shear rate.[48] Shear banding must also be distinguished from shear localisation. In shear localisation, the material is simply sheared at higher shear rates and the rest is uniform below the critical stress. The part of the material that is shearing can be characterised by a constitutive model, such as the power law.[49]

In shear banding, there is a significant coupling between shear and structure.[44] Shear banding in colloidal suspensions has been linked to particle aggregation.[50] In colloidal systems, there is a competition between the build-up of colloidal aggregates, which increase the viscosity, and their breakdown, which causes a decrease in viscosity.[39] Colloidal suspensions often show highly sheared bands where the reminder of the fluid is not sheared.[39] It has been observed in both colloidal gels and colloidal glasses.[39, 49] It is predicted that weakly or strongly flocculated systems will exhibit shear banding.[49] Silica nanoparticles can form these strongly flocculated systems in colloidal suspensions and have been observed to undergo shear banding.

1.1.7 Silica Nanoparticles

Silica nanoparticles are often used as model hard spheres in colloidal suspensions as they have no long range interactions and only have short-ranged repulsion, whereas model hard spheres only experience a steric repulsion.[1, 15] Due to this, they have been widely studied in various media, including aqueous and viscous media, such as glycerine mixtures.[15 3] They are available in a wide range of sizes, and they have a well-understood surface chemistry. Silica nanoparticles with hydroxide groups are often known as bare silica nanoparticles. It is possible to functionalise this hydroxide surface to create nanoparticles with different properties. For example, studies have attached polymer chains to the silica surface to study the effects on the colloidal stability.[51, 52] Another surface modification is to make the silica nanoparticles hydrophobic, by attaching methyl groups, which allows the effects of surface chemistry on the suspensions to be studied.[36] By changing the hydrophobicity of nanoparticles or the medium in which they are suspended, it is possible to study the interactions between the two, as well as the effect on the stability of the nanoparticles. A medium that can be used to form colloidal suspensions with silica nanoparticles is ionic liquids.

1.2 Ionic Liquid Colloidal Suspensions

Ionic liquids are salts that are liquids at room temperature.[53] They have a wide range of attractive properties such as negligible vapour pressure and a high thermal stability. They have been gaining popularity as a colloidal medium as they can act as an alternative to aqueous and organic solvents.[53] They are essentially polarized organic molecules, which allows them to solvate compounds that have low solubility in other dispersants.[53] They can stabilise nanoparticles that would otherwise aggregate in aqueous or organic media. This has led to applications in nanoparticle synthesis, as the nanoparticles are suspended and do not aggregate after being formed in a reactor.[52] This stabilisation means that nanoparticles

can form colloidal suspensions in the ionic liquids. It is imperative to fully understand the solvation and the aggregation of nanoparticles, as well as the 3D structures formed by nanoparticles in ionic liquids, so that these systems can be applied more efficiently.[54]

In ionic liquid colloidal suspensions, the electrostatic interaction is negligible and long range van der Waals forces between the nanoparticles are shielded by the ionic liquid.[9, 35] However, ionic liquids can stabilise nanoparticles by a steric or solvation force.[9] These are where layers of the ions of the liquid cover the surface of the nanoparticle, preventing the nanoparticles from aggregating.[9] This solvation force has been used to explain why ionic liquids are able to suspend silica nanoparticles for longer than expected periods of time, without the use of stabilisers [36, 55] Silica nanoparticles have also been observed to form gels when suspended in ionic liquids, without significantly altering the conductivity, which is important for electrochemical applications.[56] The stability of the nanoparticles is dependent on the particle concentration and particle sizes as well as the type of nanoparticles and the ionic liquid used.

There are a large number of different ionic liquids available, which have different cation and anion combinations.[57] Imidazolium cations typically have a methyl group on one nitrogen atom and the other nitrogen has an alkyl chain that can be of any length. The length of this chain can affect the properties and the interactions of an ionic liquid. When using an ionic liquid it is possible to change the properties by changing to an ionic liquid with a similar anion or cation. The small differences between ionic liquids can have a large effect on their properties. For example, by changing from an ionic liquid with tetrafluoroborate anion, BF_4, to an ionic liquid with the same cation but a bis(trifluoromethylsufonyl)imide anion, NTf_2, there is a decrease in the viscosity of the ionic liquid and change from hydrophilic to hydrophobic behaviour, due the nature of the anion.[58] These different properties, especially hydrophobicity, have a large effect on the interaction of the ionic liquids with hydrophilic and hydrophobic nanoparticles. These systems have applications in solid-state electrolytes, but the interactions between the silica nanoparticles themselves and with the ionic liquid are not

fully understood. By developing this understanding of the stabilising forces involved, it can help the design of future systems. Changes in the stability of the nanoparticles in ionic liquids have been observed to result in changes in their rheological behaviour.[36]

1.2.1 Macroscopic Structure

The stability of ionic liquid colloidal suspensions has been studied using rheology. When suspensions show Newtonian behaviour it suggests that the nanoparticles have been stabilised.[52, 54, 59] This is due to the suspended particles being able to easily move around in the suspensions when they are fully stabilised, so that Brownian motion can easily restore the equilibrium and hence Newtonian behaviour observed. There have been very few studies of hydrophobic silica nanoparticles in hydrophilic and hydrophobic ionic liquids. Suspensions of hydrophobic nanoparticles in 1-hexyl-3-methylimidazolium tetrafluoroborate, $[C_6mim][BF_4]$, showed a shear thinning interaction, indicating that the hydrophobic nanoparticles are unstable in the hydrophilic ionic liquid.[52] At low concentrations, suspensions of hydrophobic silica nanoparticles in hydrophobic ionic liquids show Newtonian behaviour.[52] However, these suspensions also show shear thinning at high nanoparticle concentrations.[52] The cause of this shear thinning needs to be investigated further. However, these suspensions have only been studied at one or two concentrations in ionic liquids that make it hard to compare the systems. A more systematic study is required to understand the rheology of hydrophobic nanoparticles in hydrophilic and hydrophobic ionic liquids.

At low concentrations, < 1 wt. %, bare silica nanoparticles in a hydrophilic ionic liquid, $[C_6mim][BF_4]$ show Newtonian behaviour, indicating that a stable suspension is formed.[52] This has also been observed for suspensions of bare silica nanoparticles in hydrophilic 1-butyl-3-methylimidazolium tetrafluoroborate, $[C_4mim][BF_4]$.[36] However, suspensions of bare silica nanoparticles in the hydrophobic ionic liquids, 1-ethyl-3-methylimidazolium bis(trifluoromethylsufonyl)imide, $[C_2mim][NTf_2]$ or 1-hexyl-imidazolium

bis(trifluoromethylsufonyl)imide, $[C_6mim][NTf_2]$, show shear thinning behaviour, indicating that the nanoparticles have not been stabilised.[52, 56] It is suggested that this shear thinning is due to the formation of a colloidal gel. There is a moderate repulsion between silica nanoparticles but the steric hindrance or solvation force from the ionic liquid was not strong enough to stabilise the nanoparticles so they aggregate.[56] The applied shear breaks the networks of silica that have formed due to the instability in the hydrophobic ionic liquids and therefore providing the shear thinning response.

Most ionic liquid colloidal suspensions show shear thinning behaviour.[36] However, shear thickening behaviour has been observed for some suspensions of ionic liquids; those with a BF_4 anion and 1-(2-hydroxylethyl)-3-imdazolium bis(trifluoromethylsufonyl)imide. The cause of shear thickening in some hydrophilic ionic liquid suspensions and not others is unknown. Suspensions of $[C_4mim][BF_4]$ and bare silica nanoparticles have been explored in-depth and have been found to show the full range of rheological behaviour that is expected for colloidal suspensions.[13] At low shear rates, they show shear thinning behaviour, which was proposed to be due to the forming of the nanoparticles into layers although no evidence was presented to show this. These suspensions of silica nanoparticles in $[C_4mim][BF_4]$ also showed Newtonian behaviour at moderate shear rates and demonstrated shear thickening at the highest shear rates. It has been proposed that the shear thickening observed is due to the formation of clusters, as it is assumed for bare silica nanoparticles in other solvents.[13] At low concentrations, an increase in viscosity is observed, due to the formation of clusters, but there is not a large increase as there are not enough clusters to jam the rheometer. At high silica nanoparticle concentrations, the clusters are formed before aggregating and jam the rheometer. These structures are transient and the shear thickening is reversible.[13] However, the structures formed and the interactions that cause them are not obvious.[13] The shear thickening response indicates that a stabilised, non-flocculated dispersion has been formed, which implied that a steric hindrance or solvation force was preventing aggregation of the silica nanoparticles.[36] It is possible that the suspension was forming a colloidal glass, where

the nanoparticles are stabilised by a steric or solvation force in the ionic liquids, without any additional stabilisers.[9, 43]

The shear thickening observed in suspensions of $[C_4mim][BF_4]$ and bare silica nanoparticles has also been study using magnetic resonance velocity imaging.[43] This allows the rheological behaviour of a system to be probed at the local level, to observe if there are any inconsistencies in the shear rates that are applied. In the range of shear rates accessed during the velocity imaging of these $[C_4mim][BF_4]$ suspensions, shear thickening behaviour was always observed, which matches the theory that the formation of these clusters is continuous.[13, 43] Hydrophilic bare silica nanoparticles in a hydrophobic ionic liquid with an NTf_2 anion were also studied using velocity imaging. Evidence for shear banding occurring in this system was found, indicating that system demonstrated large shear fluctuations.[43] However, studies of rheology, either in the bulk or at the localised level, only allow predictions to be made about the structure of nanoparticles with the ionic liquids.

1.2.2 Microscopic Structure

Transmission electron microscopy images have been recorded for hydrophilic silica nanoparticles suspended in a hydrophobic ionic liquid, $[C_2mim][NTf_2]$.[56] These show that the nanoparticles are aggregated, indicating that the silica nanoparticles are unstable in the ionic liquid. Scanning electron microscopy has also been used to study the silica before it is suspended in these samples.[52] However, the sample preparation disturbs the structures formed in the suspensions and the presence of the ionic liquids can make the images hard to focus.[6, 54, 59] Optical microscopy has been used to study the stability of silica particles in an ionic liquid.[55] However this technique requires the particles to be large enough to be visible on the optical microscope and therefore cannot be used for smaller nanoparticles, which will have different stabilities.[18] Microscopy techniques have been used in combination with DLS to study the structures formed by particles in ionic liquids.[55]

DLS measurements allow the distribution of nanoparticles in a suspension to be studied.[59, 60] DLS has been used to demonstrate the stability of silica nanoparticles in an ionic liquid.[31] A single distribution was observed for the nanoparticles in protic ionic liquids, indicating that the nanoparticles had been stabilised.[55] The presence of two peaks, one corresponding to single nanoparticles and the other corresponding to clusters of nanoparticles indicated the formation of a weakly flocculated suspension.[31] The clusters of nanoparticles represented a fluid of cluster phase.[31]

Bare silica nanoparticles suspended in the ionic liquid $[C_6mim][BF_4]$ show a narrow distribution that correspond to the size of the single nanoparticles, indicating that they are fully distributed in the ionic liquid and a stable suspension has been formed. These suspensions also showed Newtonian rheology. Rheology and DLS measurements are often used together to characterise systems. For example, both DLS and rheology measurements were used to show that hydrophobic nanoparticles were unstable in hydrophilic ionic liquids but they form stable suspensions in hydrophobic ionic liquids.[54, 59] The structure of silica nanoparticles in imidazolium ionic liquids needs to be studied so that it can be related to their rheology.[60] However, these techniques do not provide any information on the molecular interactions that underpin the stability of a colloidal suspension.

1.2.2 Microscopic Interactions

Atomic force microscopy (AFM) is able to detect solvation layers of ionic liquids next to different surfaces. AFM has been used to study suspensions of ionic liquids with silica, mica and graphite surfaces.[61] The results indicated the formation of solvation shells of the ionic liquids at the surfaces, though the orientations and the part of the ionic liquid interacting with the surfaces depended on the ionic liquid and the nature of the surface.[61] For example, the C_2mim cation, orientates itself so that the alkyl chain is aligned with the graphite

surface.[61] On the mica and silica, the interaction is suggested to be an electrostatic interaction between the cation and the surface, with the ring oriented parallel to the surface.[61]

It has been proposed, using evidence from infrared (IR) spectroscopy that there is a hydrogen bonding interaction between the anion of $[C_4mim][BF_4]$ and hydroxide groups on the surface of silica nanoparticles.[62] In the study by Yang et al., the peak at 3500 cm^{-1} corresponding to the O-H bond, was not observed to alter when the nanoparticles were suspended in $[C_4mim]I$. However, new peaks were observed at ca. 3650 cm^{-1} when silica nanoparticles were suspended in $[C_4mim][BF_4]$. These peaks were attributed to the formation of hydrogen bonds between the BF_4 anion and the silica nanoparticles. This has also been observed in similar studies.[51, 63] However, other studies of the same system, with silica nanoparticles from the same supplier, were unable to repeat these measurements.[36, 64] No evidence was observed of a hydrogen bonding interaction using IR spectroscopy or nuclear magnetic resonance (NMR) spectroscopy. IR and NMR have been used to study ionic liquids as complementary techniques, which allow an insight in the molecular interactions of a system.[65]

Hydrogen bonding in ionic liquids is a debated topic and IR spectroscopy is often used to try and investigate evidence of such an interaction. NMR and IR were used to study a series of ionic liquids, which had the same cation, C_4mim, and different anions.[66] The anions were Cl, Br, I and BF_4. Increasing amounts of water were added to the systems to see the effect on the NMR and IR spectra. In the ionic liquids with Cl, I and Br anions, a change was observed in the chemical shift of the peak in the NMR spectrum and extra peaks appearing in the IR spectrum, which indicated hydrogen bonds being formed in these systems. However, for $[C_4mim][BF_4]$, only very slight changes were observed in the NMR and IR spectra and hence this system did not demonstrate any evidence of hydrogen bonding. This was attributed to a difference in the interaction between the anion and the cation. The halide ions are expected to be located around the most acidic proton of the cation, located between the nitrogens on the imidazolium ring. In the case of BF_4, molecular dynamics

implied that the anion is located above the imidazolium ring, and so further away from the acidic proton, hence [C_4mim][BF_4] demonstrates very weak hydrogen bonding or weak interaction between the cation and anion.[66]

Multinuclear NMR diffusion experiments have been used to study the relative mobilities of cations and anions of ionic liquids in the presence of hydrophilic and hydrophobic surfaces. In several ionic liquids, it has been observed that the cation diffusion coefficient is reduced more than the anion diffusion coefficient in the presence of silica.[56, 67, 68] This indicates that it is the cation preferentially interacting with the hydrophilic silica.

Diffusion NMR measurements, and molecular dynamics simulations have been used to compare the interactions of an ionic liquid, [C_4mim][NTf_2], within silica and carbon pores. These indicated that the ionic liquid preferentially interacted with the surface over itself, though there was exchange between the ionic liquid at the surface and that in the bulk of the pore.[67, 68] This was most evident when the pore was full, as increasing the amount of the ionic liquid increased the thickness of the associated layer at the silica surface.[67] Both ions were found closer to the silica wall than the carbon wall. [68] It was found that electrostatic potential dominates the interaction between the ions and the silica surface.[67, 68] The imidazolium ring of the cation was found to be closer to the wall than the alkyl chain, due to this electrostatic interaction.[67] However, in the carbon nanopore, only weak van der Waals forces were found between the ions and the carbon.[68]

The structure and mobility of the ionic liquid [C_6mim][NTf_2] confined in silica pores was studied using ^{1}H and ^{19}F NMR spectroscopy and diffusion measurements, as well as Raman spectroscopy.[69] A decrease in the diffusion coefficients with an increase in the silica concentration was observed. This decrease was greater in the cation diffusion coefficient. Solid-state heteronuclear ^{29}Si-^{1}H and ^{29}Si-^{19}F NMR measurements have been used to look at the interactions between [C_6mim][BF_4] and silica surfaces.[69] There was no correlation between the silica and the fluorine, indicating that there was no interaction. Correlation was observed in the ^{1}H NMR spectra, but only for the imidazolium ring of the cation, and not the

alkyl chain. This indicated that it is specifically the imidazolium ring of the cation that is interacting with the silica. This has also been observed using computer simulations.[70] An imidazolium cation was placed in different orientations next to a silica surface. In all cases, preferred orientation of the imidazolium ring was next to the silica surface.[70] However, measurements have not been performed to show the interaction of a hydrophobic ionic liquid with silica nanoparticles or ionic liquids with hydrophobic nanoparticles. It is possible that it is a change in this interaction that causes a change in the rheological behaviour observed.

Interactions of $[C_4mim][BF_4]$ and 1-butyl-3-methylimidazolium bis(trifluoromethylsufonyl)imide, $[C_4mim][NTf_2]$, with a silica surface have been studied using molecular dynamics simulations.[71, 72] $[C_4mim][BF_4]$ was found to show ordered layers, whereas the bulky NTf_2 anion prevented $[C_4mim][NTf_2]$ from providing such a structured ionic liquid. This was reflected in the rheology of these suspensions. An applied shear made the $[C_4mim][NTf_2]$ unstable as the shear led to ions of the same charge being located next to one another, significantly destabilising the liquid. This demonstrated that the bulk of an ion in an ionic liquid is important in determining its structure. Whereas, the structure formed by $[C_4mim][BF_4]$ meant that it remained stable when shear was applied as only a small movement of the ions was required to minimise repulsion.

1.3 Thesis Outline

In this thesis, ionic liquid colloidal suspensions have been studied to understand the underlying molecular interactions that cause the non-Newtonian rheology observed. Hydrophilic and hydrophobic nanoparticles have been studied in varying concentrations in two hydrophilic ionic liquids, $[C_2mim][BF_4]$ and $[C_4mim][BF_4]$ and two hydrophobic ionic liquids, $[C_2mim][NTf_2]$ and $[C_4mim][NTf_2]$. Chapter 2 outlines a brief theoretical background behind rheology, NMR and DLS, which were primarily used to study these systems.

In chapter 3, the rheology of suspensions of hydrophilic silica nanoparticles in the ionic liquids is described. Using the four ionic liquids, it was possible to systematically compare the effect of the cations and anions on the rheological behaviour. The suspensions were studied over a range of silica concentrations, which allowed the rheology to be studied at the different concentrations for all four ionic liquids.

The molecular interactions of these suspensions were studied using NMR relaxation and diffusion measurements (chapter 4). By varying the concentration of the silica in the suspensions, the change in the rotational and translation motion of the cations and anions, allowing the interaction with the silica to be compared with the rheological behaviour. DLS measurements allowed the distribution of the nanoparticles in $[C_4mim][BF_4]$ and $[C_4mim][NTf_2]$ to be studied, allowing a comparison of the effect of the anion on the structures formed. These measurements allowed the interactions and structures in these suspensions to be related to the rheological behaviour observed. IR measurements were also performed to investigate whether the nature of the interaction was a detectable hydrogen bond, as has been suggested in the literature.

In chapter 5, magnetic resonance velocity imaging measurements performed on the suspensions in $[C_4mim][BF_4]$ and $[C_4mim][NTf_2]$ under shear were presented. Bulk rheology measurements do not allow complex rheological behaviour to be directly related the microscopic structure of a system.[43] They also assume that the rheological behaviour of the sample is uniform.[43] Magnetic resonance velocity measurements allowed the local rheology of the suspensions to be studied and compared with the bulk rheology.

Finally, hydrophobic silica nanoparticles were studied in $[C_4mim][BF_4]$ and $[C_4mim][NTf_2]$, so that comparisons could be drawn with the hydrophilic system. Rheology was performed to allow the bulk structures to be studied. NMR relaxation measurements were used to observe if the interactions were similar to those observed for the hydrophilic nanoparticles. DLS allowed the study of structures formed by these silica nanoparticles to be compared with the hydrophilic particles. Velocity measurements and IR spectroscopy were

also performed. The structures and the interactions that form these suspensions were investigated and compared to those in the suspensions of hydrophilic nanoparticles in the ionic liquids. This allowed a model of how these suspensions behave to be generated to explain how these interactions cause the different rheological behaviours observed in these systems.

1.4 References

1. J. Mewis and N. J. Wagner, *Colloidal Suspension Rheology*, Cambridge University Press, Cambridge, UK, 2012.
2. P. Atkins and J. d. Paulo, *Atkins' Physical Chemistry*, 7th edn., Oxford University Press, New York, USA.
3. X. Cheng, J. H. McCoy, J. N. Israelachvili and I. Cohen, *Science*, 2011, **333**, 1276.
4. M. M. Britton and P. T. Callaghan, *Magn. Reson. Chem.*, 1997, **35**, 37.
5. N. J. Wagner and J. F. Brady, *Phys. Today*, 2009, **62**, 27.
6. Z. Q. He and P. Alexandridis, *Phys. Chem. Chem. Phys.*, 2015, **17**, 18238.
7. T. Cosgrove, *Colloid Science : Principles, Methods and Applications* 2nd edn., Wiley-Blackwell, Chichester, 2010.
8. V. J. Anderson and H. N. W. Lekkerkerker, *Nature*, 2002, **416**, 811.
9. K. Ueno and M. Watanabe, *Langmuir*, 2011, **27**, 9105.
10. J. N. Israelachvili, *Intermolecular and Surface Forces*, 3rd edn., Elsevier, Amsterdam, 2011.
11. P. J. Lu and D. A. Weitz, in *Annu. Rev. Condens. Matter Phys.*, ed. J. S. Langer, 2013, vol. 4, p. 217.
12. H. A. Barnes, J. F. Hutton and K. Walters, *An Introduction to Rheology*, Elsevier, Amsterdam, 1997.
13. J. Qin, G. Zhang, X. Shi and M. Tao, *J Nano. Res.*, 2015, **17**, 333.

14. H. Watanabe, M. L. Yao, K. Osaki, T. Shikata, H. Niwa, Y. Morishima, N. P. Balsara and H. Wang, *Rheo Acta*, 1998, **37**, 1.

15. H. Watanabe, M. L. Yao, A. Yamagishi, K. Osaki, T. Shitata, H. Niwa and Y. Morishima, *Rheo Acta*, 1996, **35**, 433.

16. H. Watanabe, M. L. Yao, K. Osaki, T. Shikata, H. Niwa and Y. Morishima, *Rheo Acta*, 1997, **36**, 524.

17. H. Watanabe, M. L. Yao, K. Osaki, T. Shikata, H. Niwa and Y. Morishima, *Rheo Acta*, 1999, **38**, 2.

18. B. M. Guy, M. Hermes and W. C. K. Poon, *Phys. Rev. Lett.*, 2015, **115**, 088304.

19. E. Zaccarelli, *J. Phys.-Condens. Mat.*, 2007, **19**, 323101.

20. F. Sciortino and P. Tartaglia, *Adv. Phys.*, 2005, **54**, 471.

21. C. J. Dibble, M. Kogan and M. J. Solomon, *Phys. Rev. E*, 2008, **77**, 050401-I.

22. P. J. Lu, E. Zaccarelli, F. Ciulla, A. B. Schofield, F. Sciortino and D. A. Weitz, *Nature*, 2008, **453**, 499.

23. V. Trappe, V. Prasad, L. Cipelletti, P. N. Segre and D. A. Weitz, *Nature*, 2001, **411**, 772.

24. M. Instruments, *Understanding Yield Stress Measurements*, 2012.

25. J. R. Stokes and W. J. Frith, *Soft Matter*, 2008, **4**, 1133.

26. V. N. Manoharan, *Science*, 2015, **349**, 942.

27. P. N. Segre, V. Prasad, A. B. Schofield and D. A. Weitz, *Phys. Rev. Lett.*, 2001, **86**, 6042.

28. D. A. Weitz, J. S. Huang, M. Y. Lin and J. Sung, *Phys. Rev. Lett.*, 1985, **54**, 1416.

29. W. C. K. Poon and M. D. Haw, *Adv. Colloid Interfac.*, 1997, **73**, 71.

30. T. H. Zhang, J. Klok, R. H. Tromp, J. Groenewold and W. K. Kegel, *Soft Matter*, 2012, **8**, 667.

31. J. Smith, G. B. Webber, G. G. Warr and R. Atkin, *Langmuir*, 2014, **30**, 1506.

32. N. Kovalchuk, V. Starov, P. Langston and N. Hilal, *Adv. Colloid Interfac.*, 2009, **147**, 144.

33. P. J. Lu, J. C. Conrad, H. M. Wyss, A. B. Schofield and D. A. Weitz, *Phys. Rev. Lett.*, 2006, **96**, 028306.

34. A. Zaccone, J. J. Crassous and M. Ballauff, *J. Chem. Phys.*, 2013, **138**, 104908-I.

35. E. K. Hobbie, *Phys. Rev. Lett.*, 1998, **81**, 3996.

36. K. Ueno, S. Imaizumi, K. Hata and M. Watanabe, *Langmuir*, 2009, **25**, 825.

37. S. M. Fielding, *Soft Matter*, 2007, **3**, 1262.

38. P. T. Callaghan, *Rheo. Acta*, 2008, **47**, 243.

39. P. C. F. Møller, S. Rodts, M. A. J. Michels and D. Bonn, *Phys. Rev. E*, 2008, **77**, 041507-I.

40. M. M. Britton, R. W. Mair, R. K. Lambert and P. T. Callaghan, *J. Rheol.*, 1999, **43**, 897.

41. G. Ovarlez, S. Rodts, X. Chateau and P. Coussot, *Rheo. Acta*, 2009, **48**, 831.

42. R. Bandyopadhyay, *Pramana-J. Phys.*, 2013, **81**, 3.

43. J. Novak and M. M. Britton, *Soft Matter*, 2013, **9**, 2730.

44. D. Denisov, M. T. Dang, B. Struth, G. Wegdam and P. Schall, *Scientific Reports*, 2013, **3**, 1631.

45. P. Coussot and G. Ovarlez, *Eur. Phys. J E*, 2010, **33**, 183.

46. H. Wassenius and P. T. Callaghan, *Eur. Phys. J. E*, 2005, **18**, 69.

47. S. Jarny, N. Roussel, S. Rodts, F. Bertrand, R. Le Roy and P. Coussot, *Cement Concrete Res.*, 2005, **35**, 1873.

48. P. Coussot, J. Raynaud, F. Bertrand, P. Moucheront, J. Guilbaud, H. Huynh, S. Jarny and D. Lesueur, *Phys. Rev. Lett.*, 2002, **88**, 218301-I.

49. P. Coussot, L. Tocquer, C. Lanos and G. Ovarlez, *J. Non-Newton. Fluid* 2009, **158**, 85.

50. A. Ragouilliaux, G. Ovarlez, N. Shahidzadeh-Bonn, B. Herzhaft, T. Palermo and P. Coussot, *Phys. Rev. E*, 2007, **76**, 051408.

51. J. Y. Kim, T. H. Kim, D. Y. Kim, N.-G. Park and K.-D. Ahn, *J. Power Sources*, 2008, **175**, 692.

52. A. Wittmar, D. Ruiz-Abad and M. Ulbricht, *J. Nano. Res.*, 2012, **14**, 651.

53. M. Freemantle, *An Introduction to ionic liquids*, RSC Pub., Cambridge, UK, 2010.

54. A. Wittmar, D. Gautam, C. Schilling, U. Dorfler, W. Mayer-Zaika, M. Winterer and M. Ulbricht, *J. Nano. Res.*, 2014, **16**, 14.

55. J. A. Smith, O. Werzer, G. B. Webber, G. G. Warr and R. Atkin, *J Phys Chem Lett*, 2010, **1**, 64.

56. K. Ueno, K. Hata, T. Katakabe, M. Kondoh and M. Watanabe, *J. Phys. Chem. B*, 2008, **112**, 9013.

57. V. P. Ananikov, *Chem. Rev.*, 2011, **111**, 418.

58. A. P. Abbott and K. J. McKenzie, *Phys. Chem. Chem. Phys.*, 2006, **8**, 4265.

59. A. Wittmar, M. Gajda, D. Gautam, U. Dorfler, M. Winterer and M. Ulbricht, *J. Nano. Res.*, 2013, **15**, 12.

60. K. Ueno, A. Iaba, M. Kondoh and M. Watanabe, *Langmuir*, 2008, **24**, 5253.

61. R. Atkin and G. G. Warr, *J. Phys. Chem. C*, 2007, **111**, 5162.

62. H. Yang, C. Z. Yu, Q. L. Song, Y. Y. Xia, F. Y. Li, Z. G. Chen, X. G. Li, T. Yi and C. H. Huang, *Chem. Mater.*, 2006, **18**, 5173.

63. J. Nordstrom, L. Aguilera and A. Matic, *Langmuir*, 2012, **28**, 4080.

64. S. Shimano, H. Zhou and I. Honma, *Chem. Mater.*, 2007, **19**, 5216.

65. A. Wulf, K. Fumino, D. Michalik and R. Ludwig, *Chem. Phys. Chem.*, 2007, **8**, 2265.

66. S. Cha, M. Ao, W. Sung, B. Moon, B. Ahlstrom, P. Johansson, Y. Ouchi and D. Kim, *Phys. Chem. Chem. Phys.*, 2014, **16**, 9591.

67. K. S. Han, X. Q. Wang, S. Dai and E. W. Hagaman, *J. Phys. Chem. C*, 2013, **117**, 15754.

68. S. Li, K. S. Han, G. Feng, E. W. Hagaman, L. Vlcek and P. T. Cummings, *Langmuir*, 2013, **29**, 9744.

69. M. Nayeri, M. T. Aronson, D. Bernin, B. F. Chmelka and A. Martinelli, *Soft Matter*, 2014, **10**, 5618.

70. M. P. Singh, R. K. Singh and S. Chandra, *Chem. Phys. Chem.*, 2010, **11**, 2036.

71. F. F. Canova, H. Matsubara, M. Mizukami, K. Kurihara and A. L. Shluger, *Phys. Chem. Chem. Phys.*, 2014, **16**, 8247.

72. F. F. Canova, M. Mizukami, T. Imamura, K. Kurihara and A. L. Shluger, *Phys. Chem. Chem. Phys.*, 2015, **17**, 17661.

2. Experimental Techniques

2.1 Rheometry

Rheology is the study of the deformation and flow of matter.[1] It is studied by applying a force to a sample and measuring its response.[2] The deformation per unit length of the sample is the strain and the rate of this applied strain is the shear rate.[2] The shear stress is the force parallel to the cross-section divided by the area of the cross-section over which the force is applied.[2] It is possible to conduct shear-controlled and stress-controlled rheology measurements but only shear-controlled rheology measurements are performed in this work. The shear stress, σ, and the shear rate, $\dot{\gamma}$, are related by the viscosity of the sample, η (equation 2.1).[1] The viscosity of a sample is its resistance to flow.[1] When the shear stress and the shear rate are directly proportional, the material is behaving like a Newtonian liquid.[1]

$$\sigma = \eta\dot{\gamma} \tag{2.1}$$

If there is a non-linear relationship between the shear rate and the shear stress, then the sample is behaving as a non-Newtonian liquid.[1] If the viscosity decreases with increasing shear rate, then the sample is shear thinning. When a viscosity increase is observed with increase in shear rate, then the sample is shear thickening.[1] Non-Newtonian rheology can be characterised by a power-law relationship, where K is a constant and n is the power law exponent.[1]

$$\sigma = K\dot{\gamma}^n \tag{2.2}$$

If $n > 1$ then the fluid is shear thickening. If $n < 1$ then it is shear thinning. If $n = 1$, then the viscosity is constant and therefore the sample is showing Newtonian behaviour.[1]

There are different geometries that can be used to apply the shear rate.[3] Details of the shear geometries used in this work are given below.

2.1.1 Cone and Plate geometry

The cone and plate consists of a stationary plate and a rotating cone (figure 2.1a).[2] The cone is rotated to produce the shear rate. The shear rate can be calculated using equation 2.3 when the angle, α, between the cone and plate is small and Ω is the angular velocity of the cone.[1, 2]

$$\dot{\gamma} = \frac{\Omega}{\alpha} \tag{2.3}$$

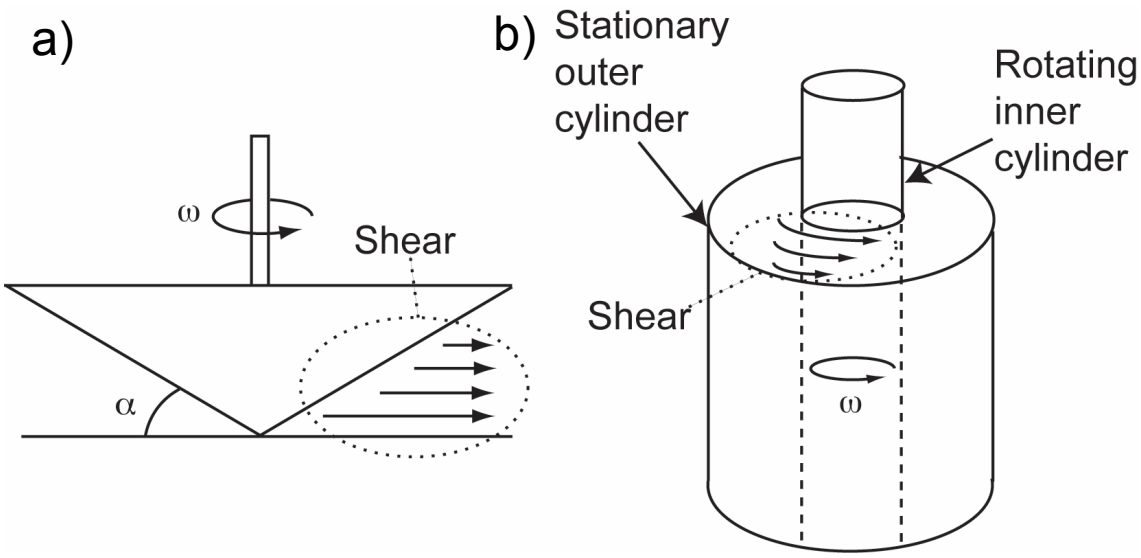

Figure 2.1: Diagram of a) a cone and plate and b) a Couette cell.

2.1.2 Couette cell

A concentric Couette cell consists of a stationary outer cylinder of radius, r_o, and a rotating inner cylinder of radius, r_i.[2] Fluid is placed in the gap between these cylinders. When there is a wide gap between the cylinders there is a heterogeneous shear stress across the gap between the inner and the outer cylinders but it is well controlled.[2, 3] It is assumed that the power law model can describe the shear stress/shear rate relationship over the range of shear rates accessed.[1] The shear rate is given by equation 2.4 where r is the position at any point in the gap.[2]

$$\dot{\gamma} = \frac{2\Omega}{r^2}\left[\frac{1}{r_i^2} - \frac{1}{r_o^2}\right]^{-1} \quad (2.4)$$

Rheology is a bulk technique, which can only study the behaviour of the whole sample. The rheological behaviours observed can be used to infer the structures of a suspension but it does not allow these structures to be directly observed. One such technique that allows microscopic structures to be studied is dynamic light scattering.

2.2 Dynamic Light Scattering

Dynamic light scattering (DLS) is a technique that is able to determine the size and distribution of nanoparticles in suspensions.[4, 5] DLS allows the hydrodynamic radii of moving particles to be determined from the scattering of light.[4, 6] DLS can characterise a wide range of particle sizes, from nm to μm sizes, on a relatively quick timescale.[6, 7] To perform DLS measurements, samples need to be dilute, so that multiple correlations are avoided and it is important that the sample does not absorb the light in any way as this will affect the scattering of the light and hence affect the measurement.[6-8] Due to larger nanoparticles moving slower, they are within the beam path of the light for a longer period of time and hence DLS is weighted towards large nanoparticles.

To obtain a measurement, a monochromatic laser is shone through the sample.[8] The laser then refracts off the particles an angle, θ. This refracted light is then recorded on a screen.[8] As the particles move due to Brownian motion, the scattering of the light and hence the correlation of the light will change.[7] Equation 2.5 is used to convert the fluctuations in light intensity, I_s, over time, τ , (figure 2.2a) into a normalised autocorrelation function $g^2(q,\tau)$ (figure 2.2b).

$$g^2(q,\tau) = \frac{\langle I_s(q,0)\, I_s(q,\tau)\rangle}{\langle I_s(q,0)^2\rangle} \quad (2.5)$$

q is the scattering vector given by equation 2.6, where λ is the wavelength of the incident light and *n* is the refractive index of the solvent.[6, 9]

$$q = \frac{4\pi n}{\lambda \sin\left(\frac{\theta}{2}\right)} \tag{2.6}$$

The normalised autocorrelation function, $g^2(q,\tau)$, is converted to the correlation function of the scattered light, $g^1(q,\tau)$, using the Siegert relationship (equation 2.7).

$$g^2(q,\tau) = |g^1(q,\tau)|^2 + 1 \tag{2.7}$$

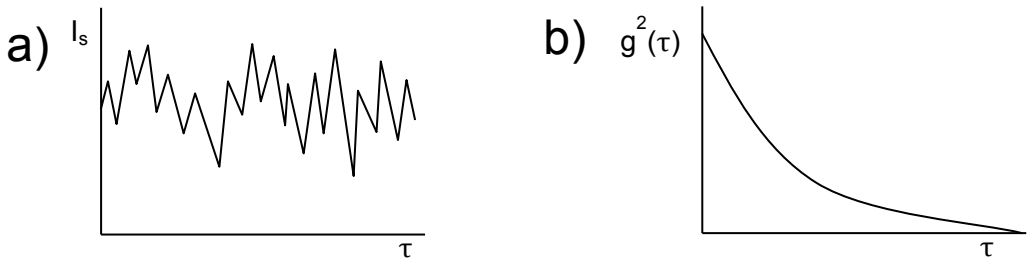

Figure 2.2: (a) Diagram of the intensity change of the light (b) Diagram of the time averaged autocorrelation function.

Small nanoparticles move faster, and therefore the correlation decays faster whereas larger nanoparticles are correlated for much longer.[6, 8] For monodisperse suspensions, there will be a single exponential decay, which can be evaluated using equation 2.8 to give the decay constant, Γ.[9] β is a constant related to the instrument used.

$$g^1(q,\tau) = 1 + \beta \exp(-\Gamma\tau) \tag{2.8}$$

If there is more than one particle size present, there will be a distribution of intensity decay rates, as larger particles diffuse slower and smaller particles move faster.[6, 9] When there are multiple partile sizes present, the autocorrelation function is then written as a sum of the exponentials, equation 2.9, where c is the normalised intensity weight of the particles.[9]

$$g^1(q,\tau) = \sum_{i=1}^{n} c_i \exp(-\Gamma\tau) \tag{2.9}$$

An inverse Laplace transformation is then used to calculate the decay rates of the different size distributions and equation 2.10 is used to produce the size distribution of

diffusion coefficients.[4, 6-8] One of the most commonly used inverse Laplace transformation methods is CONTIN.[10, 11]

$$\Gamma = Dq^2 \tag{2.10}$$

From this distribution of diffusion coefficients it is possible to determine the size of the nanoparticles using the Stokes-Einstein equation (equation 2.11), which relates the diffusion of a nanoparticle, D, and viscosity, η, of the medium to the hydrodynamic radius of the particle, R_h.[6-8]

$$R_h = \frac{k_B T}{6\pi\eta D} \tag{2.11}$$

This produces a distribution of sizes. This distribution of intensities is often converted to a volume or number distribution.[9] The correct distribution is difficult to produce for polydisperse systems, as large particles will scatter the light more than the smaller particles. Hence, the population of larger particles will appear larger than it actually is.[9]

DLS measurements allow the microscopic structure of colloidal suspensions to be observed but does not allow the interactions that cause these structures to be characterised. Nuclear magnetic resonance (NMR) allows systems to be studied at the molecular level.

2.3 Principles of Nuclear Magnetic Resonance

The intrinsic angular momentum of magnetic nuclei is known as spin.[12, 13] The nuclear spin quantum number, I, is used to characterise the nuclei of all atoms.[14] I can take integer and half integer values: 0, $\frac{1}{2}$, 1, $\frac{3}{2}$, 2 etc.[13, 14] For a nuclei to be NMR active, I must not be zero. Nuclei with $I = 0$ are known as 'NMR' silent.[14] The spin quantum number has $2(I + 1)$ states, which are degenerate in the absence of a magnetic field.[13] All nuclei also contain an intrinsic angular momentum, I, with an associated magnetic moment, μ.[12, 13] The magnetic moment and the spin angular momentum are related by equation 2.12 where γ is the gyromagnetic ratio.[12-15]

$$\mu = \gamma I \tag{2.12}$$

The gyromagnetic ratio is different for every spin active nuclei.[13, 15] In the absence of a magnetic field, all orientations of μ are equal in energy and therefore the nuclei are orientated in all directions.[12, 13]

When a magnetic field is applied, the magnetic moments interact with the magnetic field depending on their orientation.[15] Magnetic moments that point in the same direction of the magnetic field are lower in energy than those that in the opposite direction.[15] The interaction with the magnetic field is very weak and can be overcome by thermal motion. However, there is a small net alignment with the magnetic field.[15] The energy of a magnetic moment in the magnetic field is given by equation 2.13 where B_0 is the magnetic field.[13]

$$E = -\mu B_0 \tag{2.13}$$

The application of the magnetic field imposes a torque on the magnetic moment, causing it to precess at a fixed angle to the magnetic field.[12, 14, 15] The angle depends on the initial state of the spin, due to its angular momentum.[12] The frequency of this precession is defined by equation 2.14.[12, 14, 15] This is known as the Larmor frequency of the nucleus.[14]

$$\omega = -\gamma B_0 \ (\text{rad s}^{-1}) \qquad \text{or} \qquad \omega = \frac{-\gamma B_0}{2\pi} \ (\text{Hz}) \tag{2.14}$$

In terms of the spin quantum number, the $2I + 1$ available states are no longer degenerate when the sample is placed in the magnetic field.[13, 14] The states each have different energies (figure 2.3).[13] For a nuclei with I = ½, there are two possible states, $m = +\frac{1}{2}$ or $m = -\frac{1}{2}$. m is the magnetic quantum number.[13] The selection rule for m is $\Delta m = \pm 1$. Equation 2.15 defines the energy required for a spin to move between energy levels.

$$\Delta E = h\nu = \frac{h\gamma B_0}{2\pi} \tag{2.15}$$

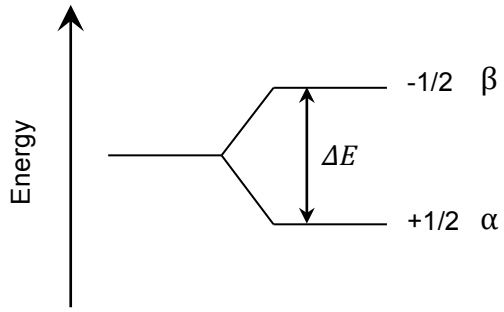

Figure 2.3: Energy level diagram for a nuclei with $I = ½$ in a magnetic field.

The populations of these energy levels are defined by the Boltzmann distribution (equation 2.16) where α is the lower energy spin state and β is the higher spin state.[13]

$$\frac{N_\beta}{N_\alpha} = e^{-\Delta E/k_B T} \qquad (2.16)$$

There are more nuclei in the lower energy level at equilibrium.[15] The slight excess of these lower energy spin states gives rise to a bulk magnetisation vector, M_0.[14] The manipulation of this bulk magnetisation vector is central to NMR.[14]

To change the populations of available spin states, a pulse of electromagnetic radiation is used.[13, 14] This radio frequency (rf) pulse must be equal to the Larmor frequency (equation 2.14).[14] This is known as the applied magnetic field, B_1, which causes the magnetic moments to precess at the Larmor frequency in the transverse plane.[13, 14] The rf pulse is generated by switching on radiofrequency radiation for a given time period, t_p.[13, 14] The duration of this time period defines angle, θ, of this pulse (equation 2.17).

$$\theta = 360 \left(\frac{-\gamma}{2\pi}\right) B_1 t_p \text{ degrees} \qquad (2.17)$$

A 90° pulse equalises the populations of the α and β energy levels.[14, 15] This moves the net magnetisation from the z axis, to the transverse plane.[14] After a 90° pulse, the spins are said to possess phase coherence.[14] A 180° pulse inverts the spin populations, leading to more β than α magnetisation. This means the net magnetisation is pointing in the –z direction.[14]

After a 90° pulse, precession of M_0 in the transverse plane induces a weak oscillating current in the receiver coil, which is the NMR signal.[14, 15] It is only magnetisation in the transverse plane which produces signal.[14] After the pulse, the net magnetisation will move from the x – y axis back to the z axis over a period of time to return to equilibrium. This is known as relaxation.[14, 15] This relaxation causes the signal to decay over time – the free induction decay (FID).[15] A Fourier Transform (FT) is applied to the FID, which translates the data from the time domain to the frequency domain, to produce a NMR spectrum.[14, 15]

In NMR theory, it is common to use a rotating frame to show the movement of the bulk magnetisation vector as a function of the applied rf pulse. This allows the rf field to be viewed as stationary and the time dependence of the rf pulse is removed. It also eliminates B_0, as this is what induces the precession.[14, 15]

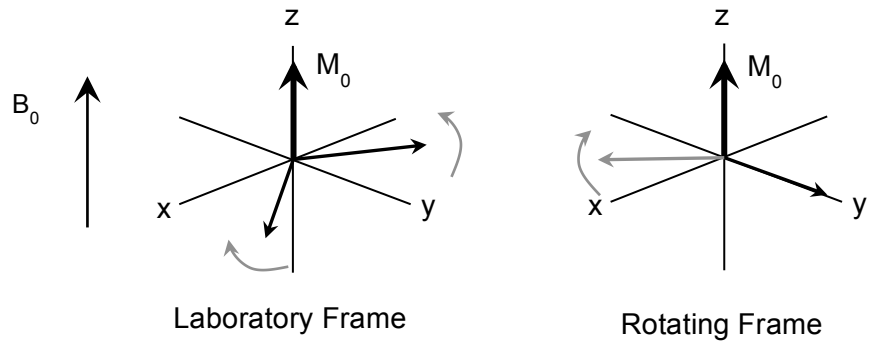

Figure 2.4: Representation of the laboratory frame, where the net magnetisation appears to be moving and the rotating frame, where it appears stationary.

2.3.1 Chemical Shift

The magnetic field experienced by a nucleus depends on its local magnetic field and hence the Larmor frequency of the nucleus is also dependent on its envrionment.[12, 13] The electrons surrounding an atom either enhance or decrease the local magnetic field, and hence change the Larmor frequency of the nucleus.[12] Different nuclei in the molecule will experience slightly different magnetic fields due to the surrounding electronic structure and

therefore will have slightly different Larmor frequencies.[12, 13] This causes them to shift relative to each other and hence produces chemical shift.[12] The more electrons there are to shield the nuclei from the external magnetic field, the greater the chemical shift observed.[13, 14] The chemical shift is field dependent and so is normalised to a ppm scale. It is usually defined in terms of differences in ppm, by δ (equation 2.18), where ν is the chemical shift in Hz and ν_{ref} is the chemical shift of a known compound. [12-14]

$$\delta = 10^6 \left(\frac{\nu - \nu_{ref}}{\nu_{ref}}\right) \quad (2.18)$$

2.4 Nuclear Magnetic Resonance Relaxation

2.4.1 Longitudinal Relaxation

After a radiofrequency pulse, the system is no longer at equilibrium.[15] Over time, the bulk magnetisation vector will return to equilibrium.[15] The return of the bulk magnetisation vector from the x-y plane to the z axis is known as longitudinal relaxation or spin-lattice relaxation.[13-15] The time constant for this process is the T_1 relaxation time which can be measured using an inversion recovery sequence (figure 2.5).[14, 16]

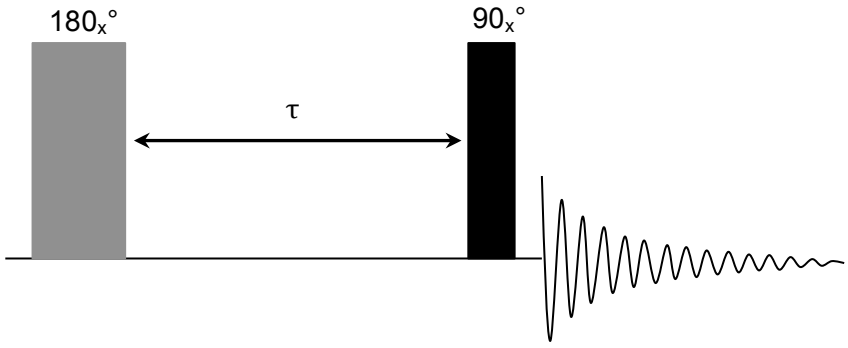

Figure 2.5: Schematic representation of the inversion recovery pulse sequence.

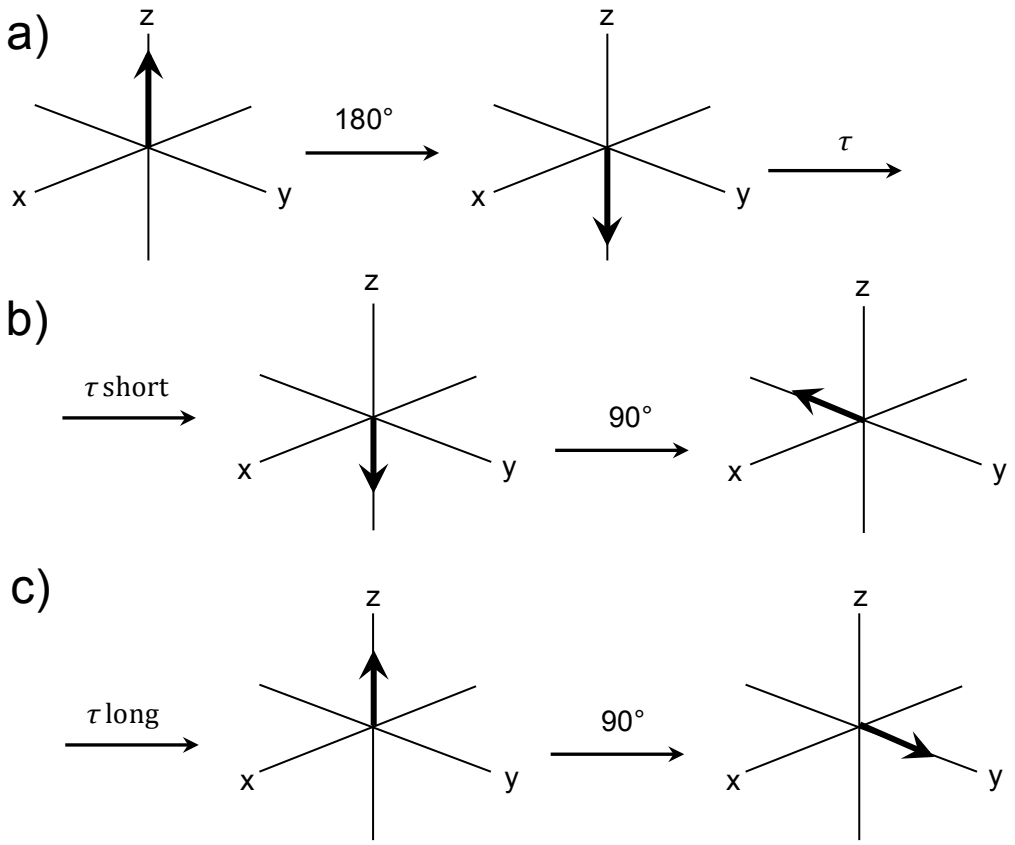

Figure 2.6: A schematic representation showing how the bulk magnetization, M_0, is affected during the inversion recovery pulse sequence.

First, a 180° pulse is used to invert the bulk magnetisation vector onto the –z axis (figure 2.6a).[14] The magnetisation vector immediately starts to return back to the z axis.[14] The progress of this relaxation is monitored by applying a 90_x^o pulse after a time, τ, which places the vector onto the transverse axis so that a signal can be recorded.[14] If τ is 0, then the full intensity is flipped on to the –y axis after a 90_x^o pulse (2.6b). If τ, if 5 * T_1 then the fully magnetisation is placed on the +y axis (2.6c).

By varying τ, a plot of signal intensity against time is produced (figure 2.8). Equation 2.19, where M_t is the net magnetization at time τ, can then be used to obtain a value of the T_1 relaxation time.[13, 14]

$$M_t = M_0\left(1\text{-}2e^{-\tau/T_1}\right) \qquad (2.19)$$

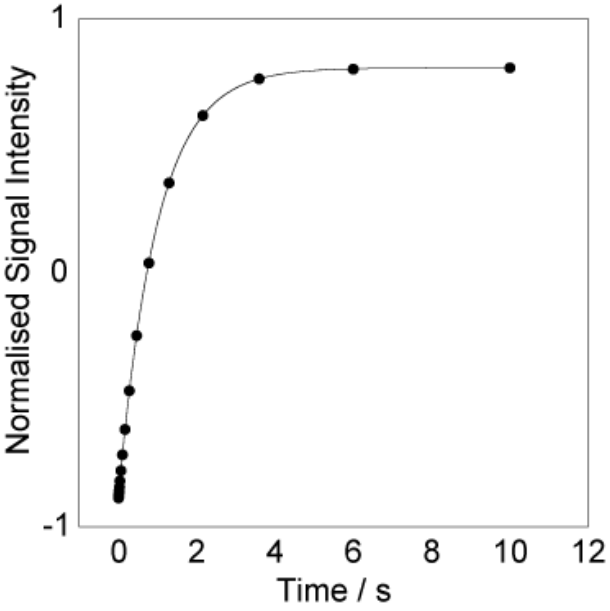

Figure 2.7: An example plot of the signal intensity change over time during a T_1 inversion recovery experiment.

2.4.3 Transverse relaxation

After a 90° pulse, the bulk magnetisation vector is pointed along the transverse plane.[14, 15] The spins are said to possess phase coherence.[14] However, the local fields experienced by the spins that contribute to the bulk magnetisation vector are all slightly different, and hence the spins precess at slightly different frequencies.[14, 15] Over time, the spins will get out of phase and hence the bulk magnetisation vector will decrease to zero.[14, 15] This is called transverse relaxation or spin-spin relaxation.[15]

There are two main sources of transverse relaxation – inhomogeneity in the static magnetic field, $T_{2(\Delta B_0)}$, and local magnetic fields from interaction between and within molecules, T_2.[14] The sum of these effects is expressed by the time constant, T_2^* (equation 2.20).[14]

$$\frac{1}{T_2^*} = \frac{1}{T_2} + \frac{1}{T_{2(\Delta B_0)}} \qquad (2.20)$$

T_2^* corresponds to the full width half maximum of the resonances in the NMR spectrum. When measuring transverse relaxation, a CPMG (Carr-Purcell-Meiboom-Gill) sequence is used to minimise the effects of the inhomogeneous magnetic field and minimise the errors in the 180° pulse angle (figure 2.8).

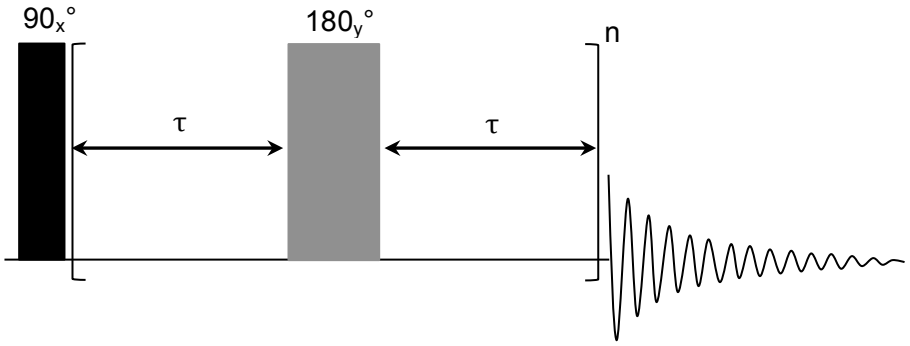

Figure 2.8: A schematic representation of the CPMG pulse sequence.

In a CPMG experiment, a 90_x° pulse puts the bulk magnetisation vector on the transverse plane, where the spins start to lose phase coherence as they precess at slightly different rates, dependent on their local magnetic field (figure 2.9). A 180_y° pulse is then applied, which flips the magnetisation. The spins then continue to precess and eventually refocus. By performing multiple 180_y° pulses, any differences in the precession caused by inhomogeneity in the magnetic field are removed, as these are not refocused.[17] However, some phase is lost due to spin-spin relaxation, T_2, resulting in signal attenuation.[17] Using a short τ value and varying the number of times the echo is refocused allows different time points to be recorded.[14] At longer time points, there is more lost phase due to T_2 relaxation and hence more signal attenuation is observed. This results in an exponential decay curve (figure 2.10). Equation 2.21 then allows the T_2 relaxation time to be obtained.[14]

$$M_t = M_0 e^{-2\tau/T_2} \qquad (2.21)$$

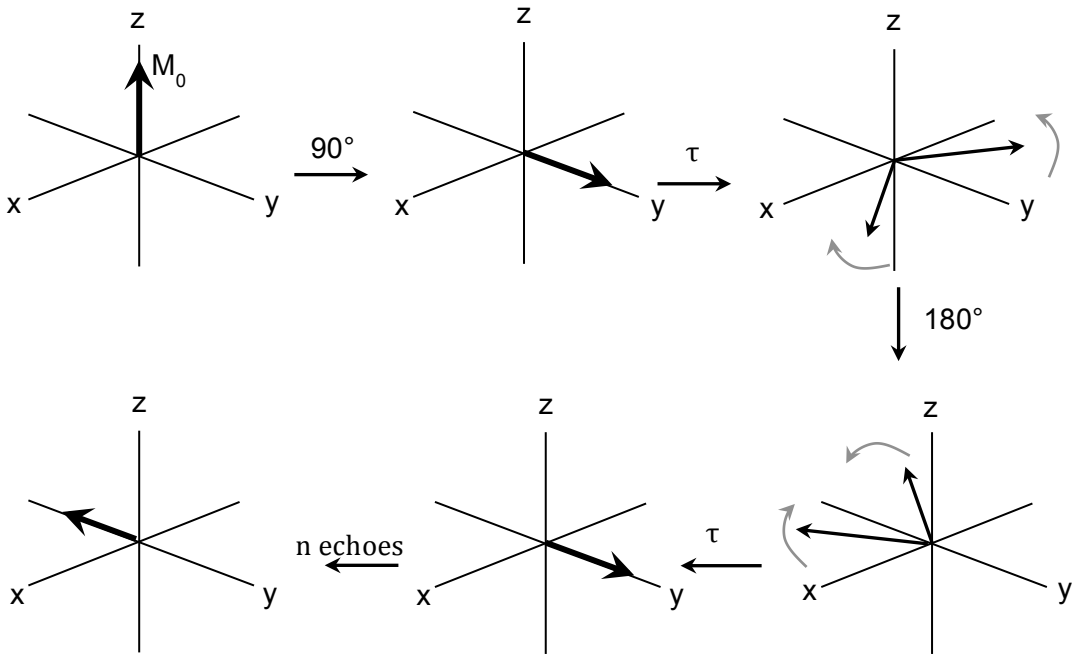

Figure 2.9: A schematic representation of how the bulk magnetization, M_0, is affected during the inversion recovery pulse sequence.

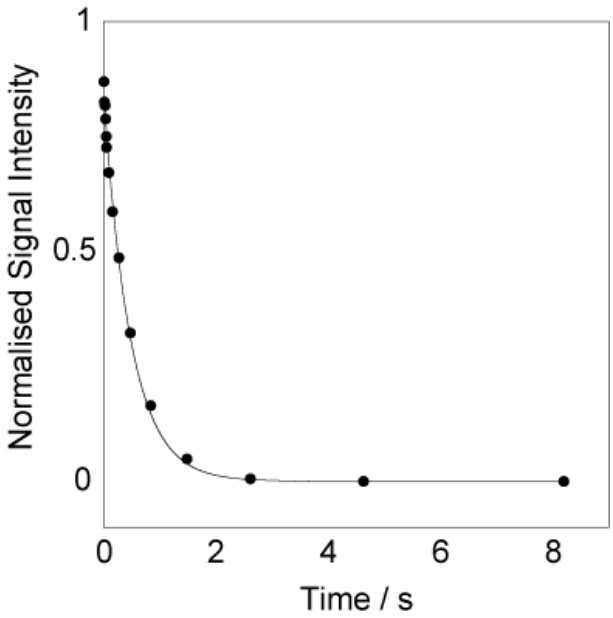

Figure 2.10: An example plot of the signal intensity decay during a CPMG experiment.

2.4.2 Mechanisms for relaxation

Relaxation can be caused by tumbling of the molecules.[14, 15] As the molecules tumble, the local magnetic fields of the nuclei are varying in magnitude and orientation and eventually these lead to the bulk magnetisation returning to equilibrium.[15] Only when a suitable component exists at the Larmor frequency can relaxation then be observed.[14] The rotational motion is characterised by the rotational correlation time, τ_c, which is the average time taken for a molecule to rotate by 1 radian.[13, 14] The frequency distribution of the magnetic fields that are associated with τ_c are known as the spectral density, $J(\omega)$.[13, 14] The spectral density is proportional to the probability of finding a component at a specific frequency, ω.[13, 14] The spectral density is related to the rotational correlation time by equation 2.22.

$$J(\omega) = \frac{2\tau_c}{1 + \omega^2\tau_c^2} \qquad (2.22)$$

For small molecules, there is a larger correlation time which means the spectral densities will be at higher frequencies. This means only a small fraction will be at the Larmor frequency, leading to long T_1 relaxation times.[13, 14] The extreme narrowing limit is where small molecules are in low viscosity solvents, where $\omega_0\tau_c << 1$. This leads to equation 2.19 being reduced to equation 2.23.

$$J(\omega_0) = 2\tau_c \qquad (2.23)$$

Hence, the spectral density is independent of the lower frequency and so the relaxation is now observed.[14, 15] On the other hand, the spectral density is most sensitive to tumbling when $\tau_c = 1/\omega_0$.[15] This is represented in figure 2.11.

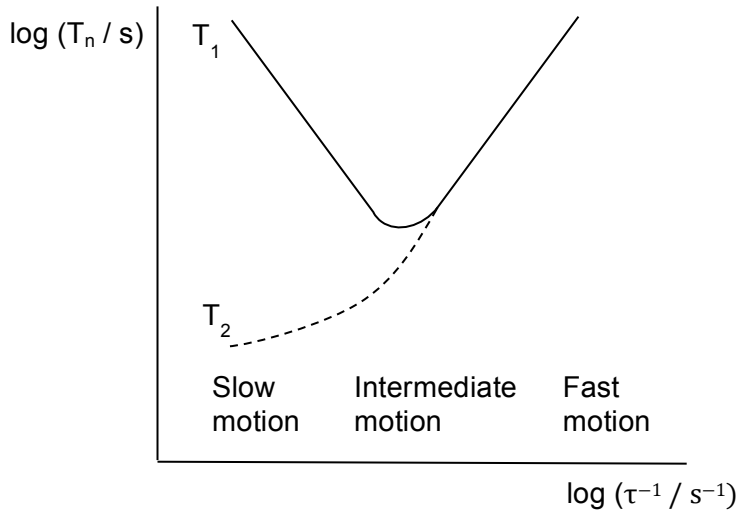

Figure 2.11: Diagram of the dependence of T_1 and T_2 relaxation on the rotational correlation time.

T_1 and T_2 relaxation times are related to the rotational correlation time by BPP (Bloembergen-Purcell-Pound) theory, equation 2.24,

$$R_1^j = \omega_d \left[\frac{16}{15}\frac{x_j}{\left(1+4x_j^2\right)} + \frac{4}{15}\frac{x_j}{\left(1+x_j^2\right)}\right]$$
$$R_2^j = \omega_d \left[\frac{4}{15}\frac{x_j}{\left(1+4x_j^2\right)} + \frac{2}{3}\frac{x_j}{\left(1+x_j^2\right)} + \frac{6}{15}x_j\right] \qquad (2.24)$$

where $R_1^j = 1/T_1$, $R_2^j = 1/T_2$, $x_j = \omega_0\tau_c$, ω_0 is the Larmor frequency and

$$\omega_d = \frac{\gamma^4 h^2}{\omega_0 r_{ij}} I(I+1)$$

is the interaction coefficient. $I = ½$ is assumed and r_{ij} is the mean distance between protons in the molecule.[18]

The relaxation mechanisms that causes T_1 relaxation also affect T_2 relaxation and hence T_2 relaxation cannot be greater that T_1.[14] However, when the motion of the molecules is slow, for example in highly viscous systems, T_2 is less than T_1 as the processes that lead to T_2 relaxation are still active at lower frequencies.[14, 19] Therefore, T_2 is more sensitive to changes in temperature, viscosity and magnetic susceptibility.[14, 19]

2.4.2.1 Dipolar relaxation

The most important relaxation mechanism that occurs in spin-½ nuclei, such as ^{1}H and ^{19}F, is dipolar coupling.[13] This coupling depends on the separation of the nuclei and the angle between their internuclear vector and the static field.[13] When spin-½ nuclei approach, there is an instantaneous interaction between their magnetic fields; there is either an attraction or repulsion.[13, 14] As the molecules tumble in solution, the angle and distance between these nuclei will vary and thus the local field of the nucleus will also vary.[13, 14] If any of these time-dependent local magnetic fields occur at the NMR frequency (equation 2.14) then this radiation will cause the spin of the nuclei to return to equilibrium.[13, 14] Since T_1 relaxation is sensitive to intermolecular separation, this means that it is sensitive to molecular structure.[13] Protons that do not have nearer neighbours will therefore relax more slowly. Those that are nearer other nuclei or near sources of unpaired electrons will relax faster.[14]

2.4.2.2 Chemical Shift Anisotropy

Another source of relaxation is chemical shift anisotropy. The local field of a nucleus is dependent on the interaction with nearby electrons and the applied magnetic field.[13] However, electrons are distributed unsymmetrically in chemical bonds which means the local magnetic field experienced by the nucleus and hence its chemical shift will be dependent on the chemical bond and its orientation.[15] In a solution the rapid tumbling of molecules averages the chemical shift anisotropy, but this fluctuation field can stimulate relaxation if it is sufficiently strong.[15] This is the case for nuclei, such as ^{19}F, that have a larger chemical shift range, as they have a greater chemical shift anisotropy.[14]

2.5 Nuclear Magnetic Resonance Diffusion

The random translational motion of molecules in a liquid can be described by its self-diffusion coefficient, *D*.[14, 20] This self-diffusion coefficient is a measure of the molecular mean square displacement and has units of $m^2\,s^{-1}$.[14] The self-diffusion coefficient of a molecule can give information about the size and shape of the molecule, as well as its mobility and can be measured using a pulse field gradient spin echo (PGSE) NMR sequence (figure 2.12).[14, 21] The application of a magnetic gradient allows the spins to be spatially located.[17] The static magnetic field will vary linearly in the direction of the applied gradient.[22] This means that the spins will experience a different magnetic field gradient, G, depending on their location within the sample, r, and hence will have different precessional frequencies, $\omega(\mathrm{r})$ (equation 2.25).[21]

$$\omega(\mathrm{r}) = \gamma \mathrm{B}_0 + \gamma \mathrm{G}(\mathrm{r}) \tag{2.25}$$

The gradient creates a helix of phase as shown in figure 2.13, where the direction of the spins depends on their local magnetic field as defined by the gradient. Helix has a wavelength, λ, defined by equation 2.26.

$$\lambda = \frac{2\pi}{\gamma \mathrm{G}(\mathrm{t})} \tag{2.26}$$

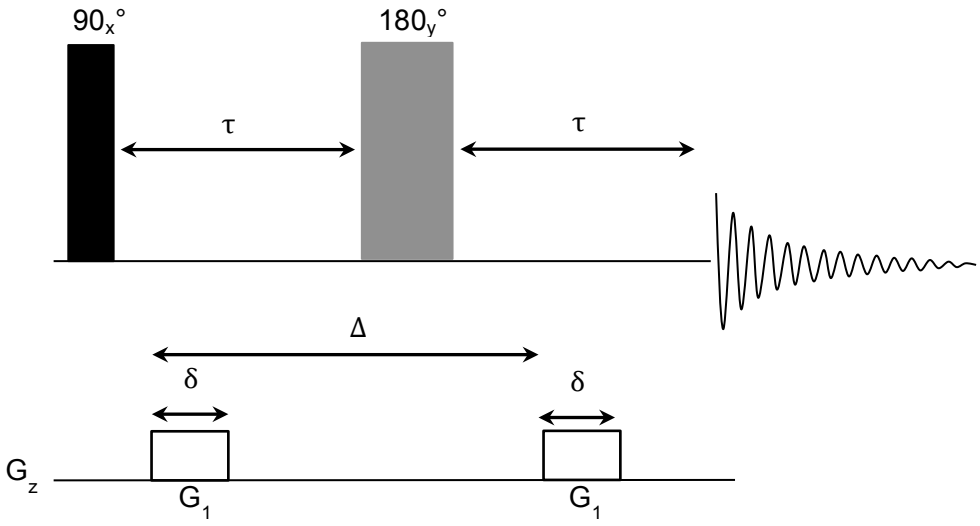

Figure 2.12: Schematic representation of the PGSE pulse sequence.

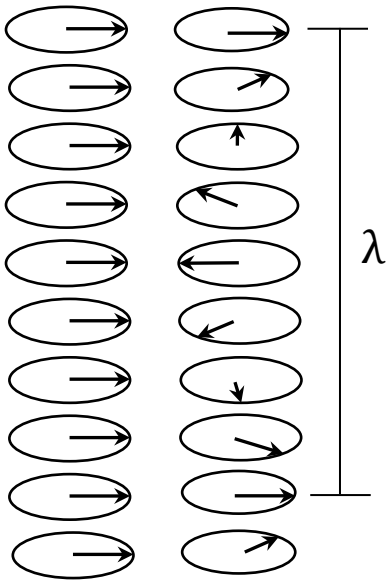

Figure 2.13: Diagram of the positions of spins before and after the application of a magnetic gradient. The wavelength can be calculated using equation 2.26.

After the 90_x^o pulse, the spins are placed on the transverse plane. The applied gradient pulse spatially locates the spins, by giving them a phase shift that depends on their location with respect to the gradient. This winds the spins into a helix of phase. The $180_y°$ pulse flips the spins, so that the second applied gradient will refocus the magnetisation. If there is no movement of the spins, then they will be in the same location and experience the magnetic field for both gradient pulses and hence all the magnetisation will be refocused.[3] However, if the spins move during the observation time, Δ, they will experience a different magnetic field during the second gradient pulse, as they are in a different location. This means the bulk magnetisation will not be completely refocused and the signal will be attenuated. The amount of signal attenuation is dependent on how far the molecule has moved and therefore its diffusion coefficient. The amount of signal attenuation is varied by applying different gradient strengths, resulting in a plot of change in signal attenuation against gradient strength (figure 2.14). The Stejskal-Tanner equation (equation 2.26), where G is the gradient strength and δ is the gradient pulse duration, is used to obtain the diffusion coefficieint.[17]

$$\frac{S(G)}{S(0)} = \exp\left[-\gamma^2\delta^2G^2D\left(\Delta - \frac{\delta}{3}\right)\right] \quad (2.26)$$

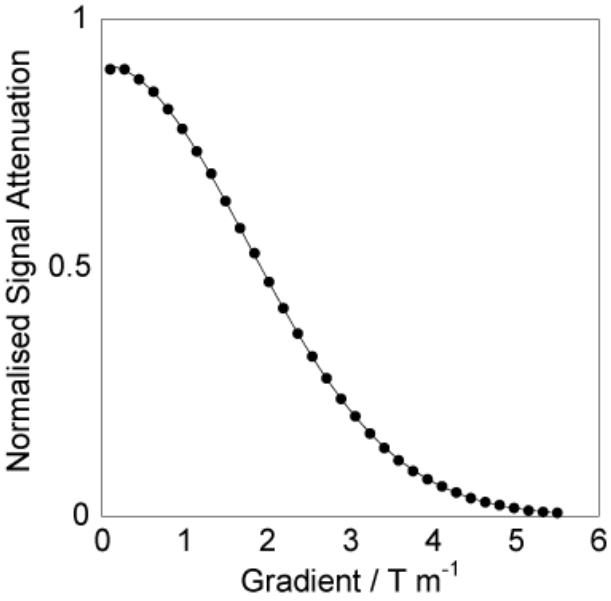

Figure 2.14: An example of the signal attenuation during a PGSE experiment.

The narrow pulse approximation is that $\delta << \Delta$, so that the gradient duration is significantly smaller than the observation time. This means that diffusion whilst the gradient is being applied can be neglected.[22] One issue with the PGSE sequence is that the spins diffuse whilst the magnetisation is on the transverse plane. This means that signal is also lost due to transverse relaxation, T_2, which means the measured diffusion coefficient will be smaller than the actual diffusion coefficient. It leads to errors in the measurement. To avoid this, a pulse field gradient stimulated echo (PGSTE) sequence is used (figure 2.15). In this sequence, a 90_x^o pulse is immediately applied after the first gradient, returning the spins to the longitudinal axis whilst they diffuse. A 90_x^o pulse is then applied before the second gradient, so that the spins are returned to the transverse plane, to be refocused before the signal is acquired. This does mean that the molecules are subjected to longitudinal relaxation during τ_2, but this is often slower than T_2 relaxation, and so affects the signal less. The signal

attenuation is then evaluated using the Stejskal-Tanner equation in the same way as data from the PGSE to produce the diffusion coefficient.

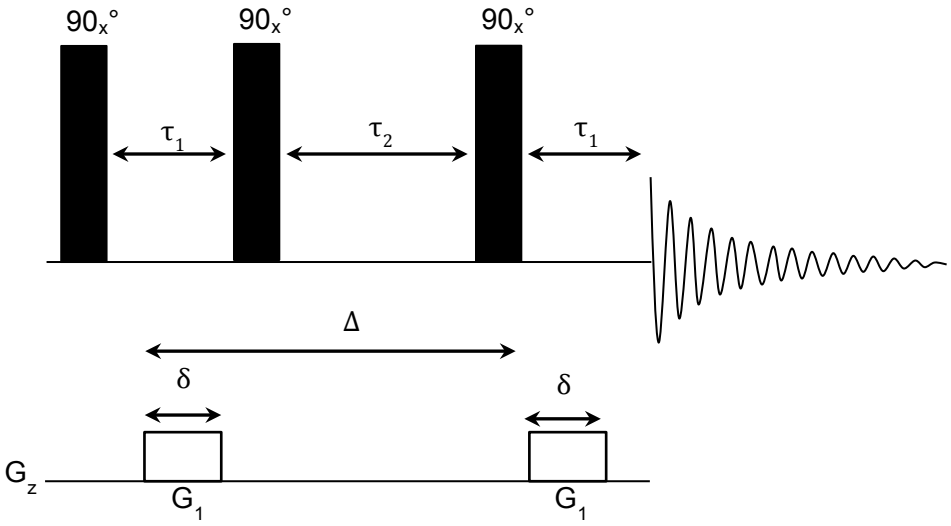

Figure 2.15: Schematic representation of the PGSTE pulse sequence.

2.6 Velocity Imaging

Rheology can be studied using magnetic resonance velocity imaging. This technique allows the local rheology to be studied, and rheological phenomena such as sample fracture and shear banding to be directly observed.[21, 23] The fluid motion involves the bulk movement of the spins within the sample, which can be traced using magnetic resonance imaging.[21]. By applying magnetic gradients, as described in the previous section, in multiple directions, it is possible to produce magnetic resonance images.[24] There are two different methods of applying the gradient that are used in combination to produce images (in 2D or 3D). In phase encoding, the gradient is applied prior to the signal acquisition, meaning that spins will have different phases depending on the frequency applied during the gradient pulse.[24] In frequency encoding, the signal is acquired whilst the gradient is being applied, so the spins will have different frequencies depending on their position.[24] For two-dimensional imaging, a slice selective pulse is required so that only a small region of the third dimension is imaged,

so that the image is not summed along the third dimension.[19, 22, 24] This slice selective, pulse is produced by applying a gradient at the same time as a frequency selective rf pulse or soft pulse.[22] A soft pulse is longer and of lower power than a hard, or broadband, pulse.[19, 24]

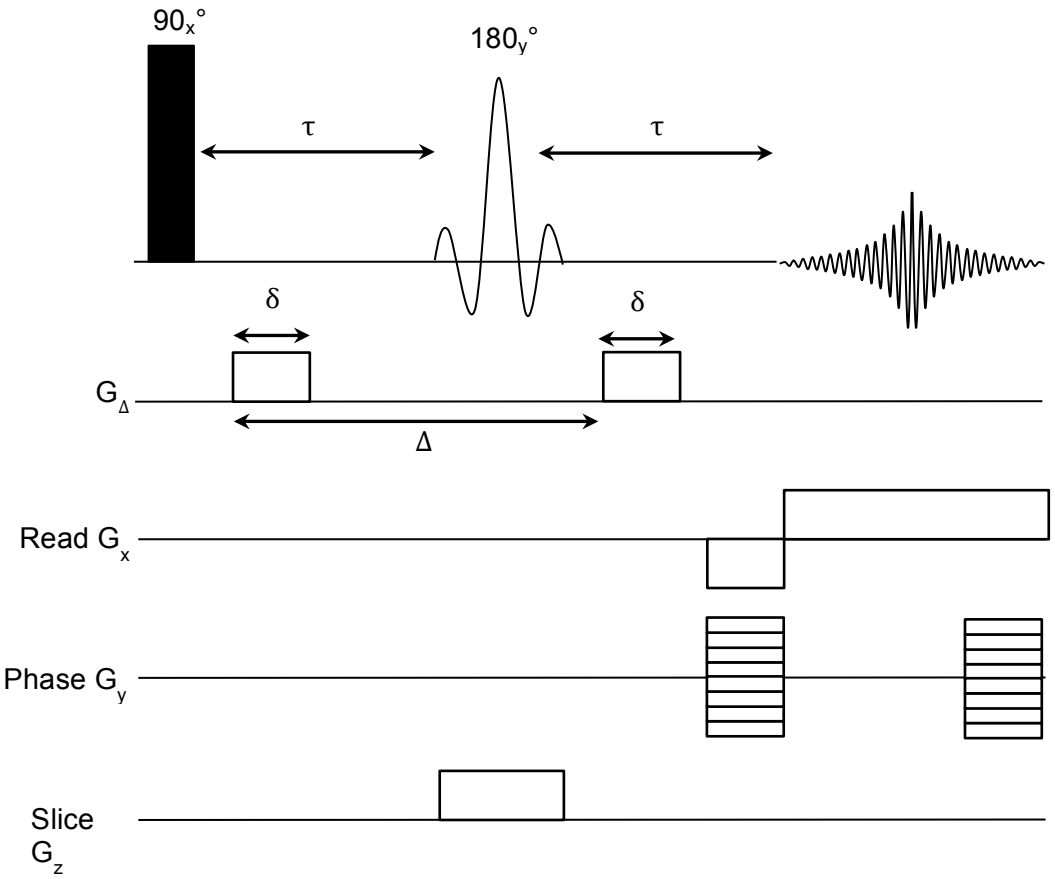

Figure 2.16: Schematic representation of the PGSE pulse sequence used for imaging velocity.

A PGSE imaging sequence (figure 2.16) can be used to study fluids under flow, which produces a map of the local velocity fields in an image (figure 2.17b).[21] It is a 2D imaging sequence combined with a PGSE sequence, so that there are two magnetic field pulses to that spatially encode the spins.[23] The $180_y°$ pulse is a soft pulse. The PGSE sequence gives the spins a phase shift, which arise from molecular displacement over time, Δ.[25] The flow velocity, v, imparts a coherent molecular motion on the samples, resulting in a net phase shift ϕ, (equation 2.27).[22] A series of images are acquired with varying gradient **g,** which allows the velocity of the molecules within each pixel to be extracted.[20, 23, 26] A velocity map

is then produced by measuring the phase shift between the z slices to calculate the velocity of the spins (figure 2.17b).[22] This phase shift is calculated using equation 2.27, where v is the velocity of the sample in that pixel.

$$\phi = \gamma v g \delta \Delta \tag{2.27}$$

The rheological behaviour of the sample can then be characterised by taking a vector across the maximum velocity in the image (figure 2.17 c & d) and fitting this to the power law relationship (equation 2.28) where v_ϕ is the velocity of a power law at radius, r in the Couette cell to give a power law exponent, n.[21, 23] If $n = 1$, then the fluid is Newtonian. If $n > 1$ then the fluid is shear thickening and $n < 1$ is shear thinning.

$$v_\phi = \Omega r_i \frac{R(1- R^{-2/n})}{K(1-K^{-2/n})} \tag{2.28}$$

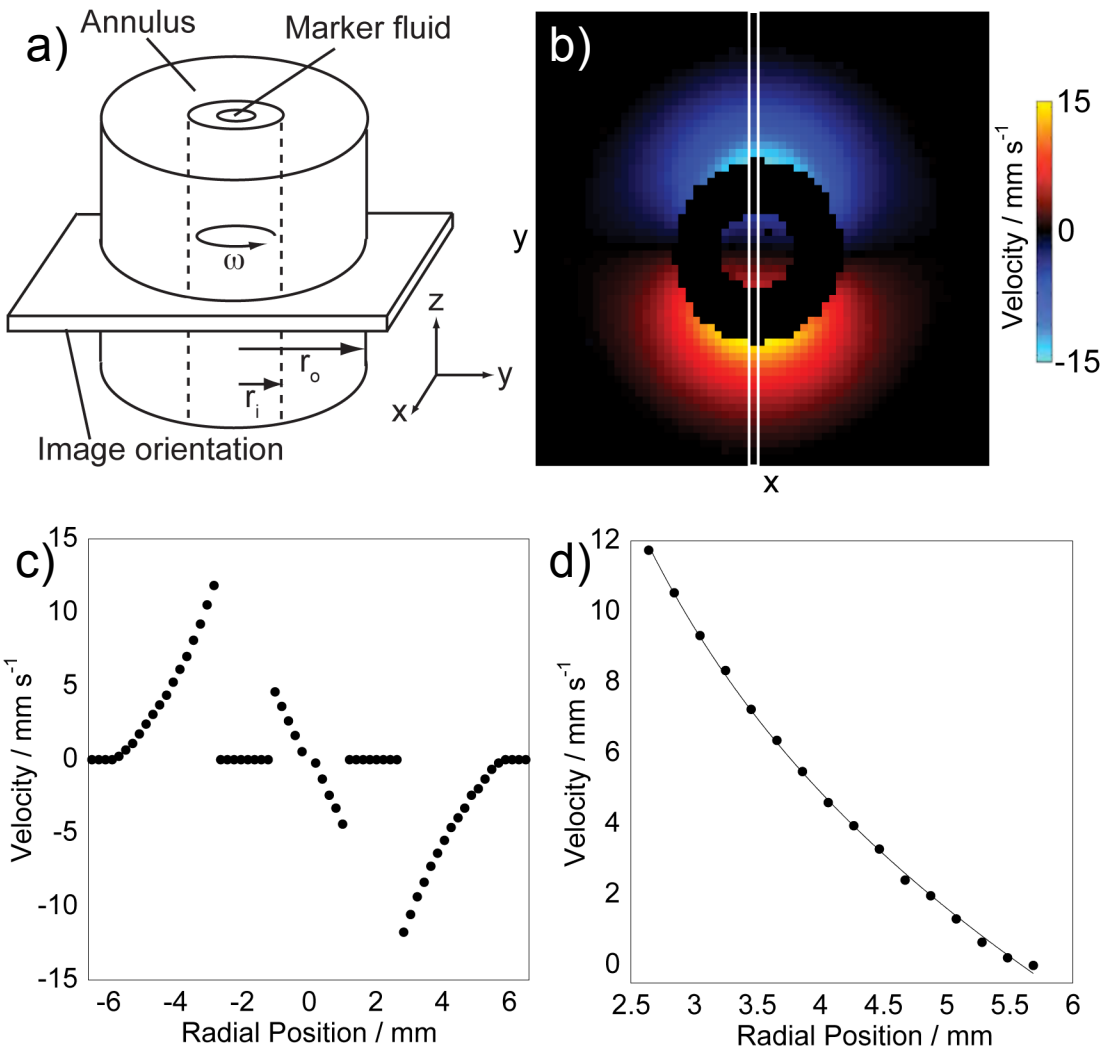

Figure 2.17: a) Diagram of a Couette cell showing image orientation for the horizontal velocity image. b) Velocity image of a Couette cell. c). Profile of the velocities obtained across the image shown obtained from the highlighted region in b). Regions of zero velocity are due to the presence of the Couette cell. d) Region of the velocity profile where fluid between the inner and outer cylinder is under shear. This is fitted to equation 2.28 to produce a value for the power law exponent.

2.4 References

1. H. A. Barnes, J. F. Hutton and K. Walters, *An Introduction to Rheology*, Elsevier, Amsterdam, 1997.
2. J. W. Goodwin and R. W. Hughes, *Rheology for chemists : an introduction*, 2nd edn., RSC Publishing, Cambridge, UK, 2008.
3. M. M. Britton and P. T. Callaghan, *Magn. Reson. Chem.*, 1997, **35**, 37.
4. P. A. Hassan, S. Rana and G. Verma, *Langmuir*, 2015, **31**, 3.
5. K. Ueno, A. Iaba, M. Kondoh and M. Watanabe, *Langmuir*, 2008, **24**, 5253.
6. D. W. Bruce, D. O'Hare and R. I. Walton, *Multi Length-Scale Characterisation*, Wiley, 2013.
7. S. C. Singh, H. B. Zeng and C. Guo, *Nanomaterials : Processing and Characterization with Lasers*, Wiley-VCH, 2012.
8. M. Instruments, *Zetasizer Nano Series User Manual*, 2004.
9. S. J. Law, PhD Thesis, University of Birmingham, 2015.
10. S. W. Provencher, *Comp. Phys. Comm.*, 1982, **27**, 213.
11. S. W. Provencher, *Comp. Phys. Comm.*, 1982, **27**, 229.
12. M. H. Levitt, *Spin Dynamics: Basics of Nuclear Magnetic Resoance*, 2nd edn., John Wiley & Sons, Chichester ; New York, 2002.
13. P. J. Hore, *Nuclear Magnetic Resonance*, Oxford University Press, 1995.
14. T. D. W. Claridge, *High Resolution NMR Techniques in Organic Chemistry*, 2nd edn., Elsevier, Oxford, 2009.
15. J. Keeler, *Understanding NMR Spectroscopy*, 2nd edn., John Wiley & Sons Ltd., Chichister, UK, 2010.
16. R. L. Vold, J. R. Waugh, M. P. Klein and D. E. Phelps, *J. Chem. Phys.*, 1968, **48**, 3831.
17. A. J. Mills, PhD Thesis, Univeristy of Birmingham, 2016.

18. M. Mussel, E. Wilczynski, U. Eliav, J. Gottesman, M. Wilk and U. Nevo, *J. Polym. Sci. Part B*, 2015, **53**, 1620.

19. P. T. Callaghan, *Principles of Nuclear Magnetic Resonance Microscopy*, Oxford University Press, New York, 1991.

20. W. S. Price, *NMR Studies of Translational Motion*, Cambridge University Press, 2009.

21. P. T. Callaghan, *Translational dynamics and magnetic resonance: principles of pulsed gradient spin echo NMR*, Oxford University Press, Oxford, 2011.

22. A. Vallatos, PhD Thesis, University of Birmingham, 2013.

23. J. Novak and M. M. Britton, *Soft Matter*, 2013, **9**, 2730.

24. M. M. Britton, *Chemical Society reviews*, 2010, **39**, 4036.

25. P. T. Callaghan, *Rheo. Acta*, 2008, **47**, 243.

26. P. Callaghan, *Curr. Opin. Colloid In.*, 2006, **11**, 13.

3. Rheometry Studies of Macroscopic Stability and Structure

3.1 Introduction

Silica nanoparticles can be suspended in ionic liquids to form colloidal suspensions.[1] Some ionic liquids are able to stabilise the silica nanoparticles, so that they do not aggregate, without the need for stabilisers, such as surfactants or polymers.[1] These suspensions have applications in electrochemical systems and nanoparticle synthesis.[1] Suspensions of hydrophilic and hydrophobic ionic liquids with hydrophilic silica nanoparticles have been studied using rheology.[1-5] Rheology can be used to study the bulk behaviour of colloidal suspensions as the rheological behaviour is determined by the structures of the nanoparticles within the suspension.[6] The response of the systems to an applied shear rate can provide a way of predicting the stability and underlying structure of colloidal systems.[3, 7-10]

Shear thinning behaviour was observed for suspensions of hydrophilic silica nanoparticles in hydrophobic ionic liquids, such as $[C_2mim][NTf_2]$ and $[C_6mim][NTf_2]$.[2, 4] The shear thinning behaviour indicates the formation of a colloidal gel, where the nanoparticles have not been stabilised and hence aggregate. These aggregates form a space-spanning gel network.[1, 11] When a shear is applied, this network is broken, and hence a shear thinning response is observed. Colloidal gels also can show a yield stress, where a plateau is observed in the shear thinning, as the structure resists the flow.[12] With increases in silica concentration, large increases in zero shear viscosity are also observed in colloidal gels, as the network traps some of the liquid phase, causing the viscosity to increase.[7]

At low silica concentration, Newtonian behaviour was observed for silica nanoparticles suspended in a hydrophilic ionic liquid with a BF_4 anion.[3, 4, 13, 14] The Newtonian behaviour indicated the silica nanoparticles were being stabilised by the hydrophilic ionic

liquids. At higher silica concentrations, shear thickening behaviour was observed. It was suggested that this shear thickening behaviour demonstrated the possible formation of a colloidal glass, where the silica nanoparticles are trapped in cages formed by neighbouring particles in a dynamically arrested state.[1, 5, 11] This arrested state is overcome at high shear rates, so the nanoparticles collide and form temporary clusters, which increase the viscosity, hence shear thickening.[3, 5, 13]

Recently, suspensions of hydrophilic silica nanoparticles in hydrophilic $[C_4mim][BF_4]$ have been studied at a range of silica concentrations.[5] At low shear rates, shear thinning was observed, before a region of shear thickening at the higher shear rates. This shear thinning, Newtonian and then shear thickening behaviour is characteristic of a colloidal suspension. It was proposed that this shear thinning at low silica concentrations was due to the formation of layers of nanoparticles, which can easily move past each other, hence a decrease in viscosity. At higher shear rates, the nanoparticles collide and form clusters, which cause the viscosity to increase, hence shear thickening.[5]

In previous studies, focus generally has either been on studying a range of silica concentrations in one ionic liquid or one silica concentration in several ionic liquids.[2, 3, 5, 14, 15] This means that trends in the concentration effects of the silica nanoparticles cannot easily been compared. In this chapter, a range of silica concentrations has been studied in $[C_2mim][BF_4]$ and $[C_4mim][NTf_2]$, where previously only one concentration has been reported. A wider range of concentrations was studied in $[C_2mim][NTf_2]$ and $[C_4mim][BF_4]$, allowing changes in the rheological behaviour with changes in silica concentration to be observed. Using these four ionic liquids, with either a C_2mim or a C_4mim cation and a BF_4 or an NTf_2 anion has means a systematic approach has been taken to has allow the rheology of these samples to be related to the components of the ionic liquid that the silica is suspended in. By observing a wide range of comparable silica concentrations, the rheological behaviour could be related to similarities and differences in the underlying structure of the suspensions.

3.2 Experimental

3.2.1 Materials and Sample Preparation

1-ethyl-3-methylimidazolium tetrafluoroborate, [C_2mim][BF_4] (98 %); 1-ethyl-3-methylimidazolium bis(trifluoromethylsulfonyl)imide, [C_2mim][NTf_2] (98 %); 1-butyl-3-methylimidazolium tetrafluoroborate, [C_4mim][BF_4] (98 %) and 1-butyl-3-methylimidazolium bis(trifluoromethylsulfonyl)imide, [C_4mim][NTf_2] (98 %) were obtained from Sigma Aldrich, UK and used without further purification. Aerosil 200 silica nanoparticles (Evonik, Germany) have a diameter of 12 nm, a surface area of 200 ± 25 $m^2 g^{-1}$ and Si-OH surface functionalisation. The density of the silica nanoparticles was 2.2 g cm^{-3}. Aerosil 200 was dried overnight at 70 °C in a vacuum oven before use. Aerosil 200 was dispersed in [C_2mim][BF_4] and [C_4mim][BF_4] at concentrations from 0 to 15% wt. and in [C_2mim][NTf_2] and [C_4mim][NTf_2] from 0 to 8% wt. The suspensions were stirred until they appeared homogeneous and placed in a vacuum oven overnight at a temperature of at least 70 °C to minimise the water content. Water content was monitored by observing the water peak in the ^{1}H NMR spectrum. During the course of these experiments, it was found that the rheological behaviour varied depending on the stirring method used. This is investigated for suspensions of [C_4mim][BF_4] in this chapter.

3.2.2 Rheometry

Rheometry measurements were performed on an AR-G2 rheometer (TA Instruments) with a cone and plate geometry. The measurements were performed at 20 ± 0.1 ^oC, with shear stress recorded logarithmically with 10 points per decade, between shear rates of 0.1 and 1000 s^{-1}. For the neat ionic liquids, a 60 mm diameter cone with a 2^o angle was used. For the ionic liquid suspensions, a cone with a 20 mm diameter and a 2^o angle was used.

3.2.3 Calculating Silica Concentration in Ionic Liquids

In the literature the concentration of silica in ionic liquids suspensions is often referred to in terms of wt. %. This is the most practical way to deal with the systems, however this does not allow a suitable comparison between different ionic liquids. Volume fraction can be calculated but this requires assumptions about the densities of the ionic liquid and the silica, as well as assuming that the hydrodynamic radii do not change. Depending on the method used to calculate the volume fraction, different answers can be obtained.[16] In this work, molar fractions of silica have been calculated for the systems as it allows the relative weights of the cations and the anions to be taken into account (table 3.1). The method used to calculate the mole fractions and volume fractions is shown in appendix 1.

Table 3.1: Table showing calculated values for mole fraction and volume fraction of silica.

$[C_2mim][BF_4]$			$[C_2mim][NTf_2]$		
Weight %	Mole Fraction	Volume Fraction	Weight %	Mole Fraction	Volume Fraction
0	0.00	0.000	0	0.00	0.000
5	0.15	0.029	1	0.06	0.007
8	0.22	0.047	3	0.17	0.020
10	0.27	0.060	5	0.26	0.034
15	0.37	0.092	8	0.37	0.056
$[C_4mim][BF_4]$			$[C_4mim][NTf_2]$		
Weight %	Mole Fraction	Volume Fraction	Weight %	Mole Fraction	Volume Fraction
0	0.00	0.000	0	0.00	0.000
1	0.04	0.005	1	0.07	0.006
3	0.10	0.016	3	0.18	0.019
5	0.16	0.027	5	0.28	0.032
8	0.25	0.044	8	0.39	0.052
10	0.29	0.056			
15	0.40	0.086			

3.3 Results and Discussion

3.3.1 Rheological Behaviour

The rheological behaviour for suspensions of $[C_2mim][NTf_2]$ with silica nanoparticles is shown in figure 3.1. The neat ionic liquid demonstrates a linear change in shear stress with increase in shear rate and is therefore behaving as a Newtonian liquid.[2, 3] When silica nanoparticles were added, a large increase in the zero shear viscosity is observed. In all suspensions of silica and $[C_2mim][NTf_2]$ shear thinning is observed, as there is a decrease in viscosity with an increase in shear rate.

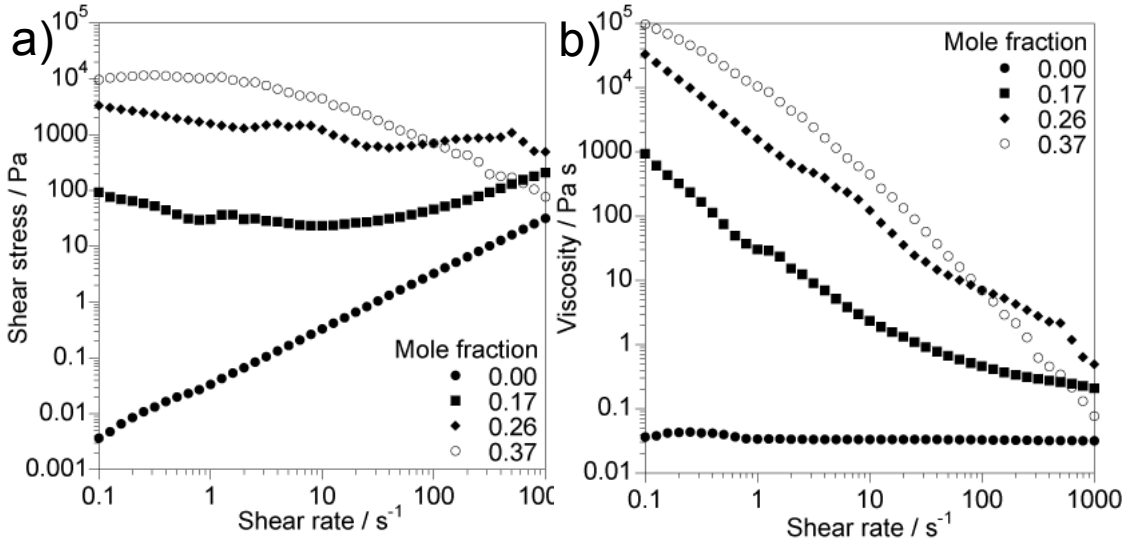

Figure 3.1: Plot of shear stress against shear rate (a) and plot of viscosity against shear rate (b) for $[C_2mim][NTf_2]$ with hydrophilic silica.

The large increases in zero shear viscosity can be linked to the formation of a colloidal gel.[7] If the nanoparticles are not fully stabilised by the liquid phase, then they will aggregate.[17] During this aggregation, some continuous phase becomes trapped in the aggregates of the nanoparticles.[7] Hence, the formation of this network causes a large increase in viscosity. The instability of nanoparticles in the ionic liquid could be linked to a repulsion between the hydrophilic silica and the hydrophobic ionic liquid.[4] It has been calculated, in previous work using DVLO theory, that the silica nanoparticles are attracted to each other, through van der Waals forces, and the electrostatic stabilisation by the ionic

liquid [C_2mim][NTf_2] is not sufficient to prevent the nanoparticle aggregation.[15] This aggregation is formed by weak van der Waals attraction between the particles and therefore can be easily broken. The application of shear in a rheometer is able to break these networks of nanoparticles, causing a decrease in viscosity. This shear thinning is often observed in colloidal gels.[1, 2, 8] The formation of a gel in suspensions in [C_2mim][NTf_2] has been confirmed in previous studies.[2, 3] In figure 3.1a, there appears to be a negative slope in the flow curve of [C_2mim][NTf_2] with 0.17 and 0.26 mole fractions of silica. This could indicate unsteady flow occurring in the sample, due to shear localization or shear banding.

The rheological behaviour of [C_2mim][NTf_2] and silica nanoparticles is very similar to that observed for suspensions of [C_4mim][NTf_2], as shown in figure 3.2. Both neat ionic liquids show Newtonian behaviour. There is a large increase in the zero shear viscosity observed with increase in silica concentration. The increase in viscosity observed is larger in suspensions in [C_2mim][NTf_2] that in [C_4mim][NTf_2] with the same concentration of silica added. This could be a reflection of the silica nanoparticle stability in each of these ionic liquids. It has been calculated, using the DVLO theory, that hydrophilic silica nanoparticles are unstable in both of these ionic liquids.[15] However, the potential curve calculated for

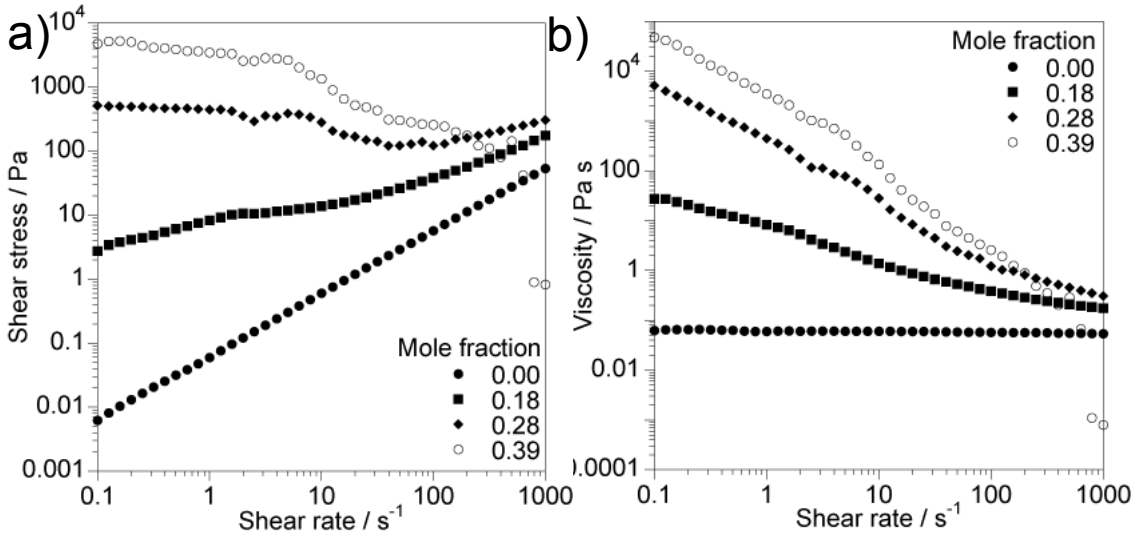

Figure 3.2: Plot of shear stress against shear rate (a) and plot of viscosity against shear rate (b) for [C_4mim][NTf_2] with hydrophilic silica.

$[C_2mim][NTf_2]$ is more negative than that for suspensions of $[C_4mim][NTf_2]$.[15] This is most likely to do the small change in the alkyl chain length affecting the structure of the ionic liquids, i.e. the interactions between the cations and the anions and hence the difference in the rheological behaviours. This indicates that the silica nanoparticles are more unstable in $[C_2mim][NTf_2]$. As they are more unstable, this means that they will aggregate faster and therefore more $[C_2mim][NTf_2]$ will get trapped in the aggregates, leading to a larger increase in the zero shear viscosity.[17]

A decrease in viscosity with increase in shear rate is observed for all suspensions in $[C_4mim][NTf_2]$, indicating that this system is shear thinning, like suspensions in $[C_2mim][NTf_2]$. This indicates that suspensions in $[C_4mim][NTf_2]$ are also forming a colloidal gel. There is a large decrease in viscosity observed for $[C_4mim][NTf_2]$ with 0.39 mole fraction of silica. This is possibly due to a complete collapse of the gel network to single nanoparticles. A negative slope is not observed in the flow curve, figure 3.1a, which is observed for $[C_2mim][NTf_2]$. Shear banding was observed for suspensions of an ionic liquid with an NTf_2 anion and hydrophilic silica nanoparticles.[13] The shear banding was suggested by a plateau in the bulk rheology and observed at a localised level using magnetic resonance velocity imaging.[13] This technique is used to investigate suspensions in $[C_4mim][NTf_2]$ in chapter 5.

The rheological behaviour for suspensions in $[C_2mim][BF_4]$ is shown in figure 3.3. The neat ionic liquid demonstrates Newtonian behaviour.[3] At the lowest silica concentration, 0.15 mole fraction, a large increase in the zero shear viscosity and shear thinning are observed. This behaviour is similar to that shown for suspensions in $[C_2mim][NTf_2]$ and $[C_4mim][NTf_2]$ at this silica concentration and indicates the silica is unstable. However, at higher silica concentrations, a decrease is observed in the zero shear viscosity. At low shear rates, at 0.22 and 0.37 silica mole fractions in $[C_2mim][BF_4]$, there is no change in the viscosity, indicating that these suspensions are showing Newtonian behaviour. This indicates that the silica has been stabilised at these higher concentrations.[4] At higher shear rates, an increase

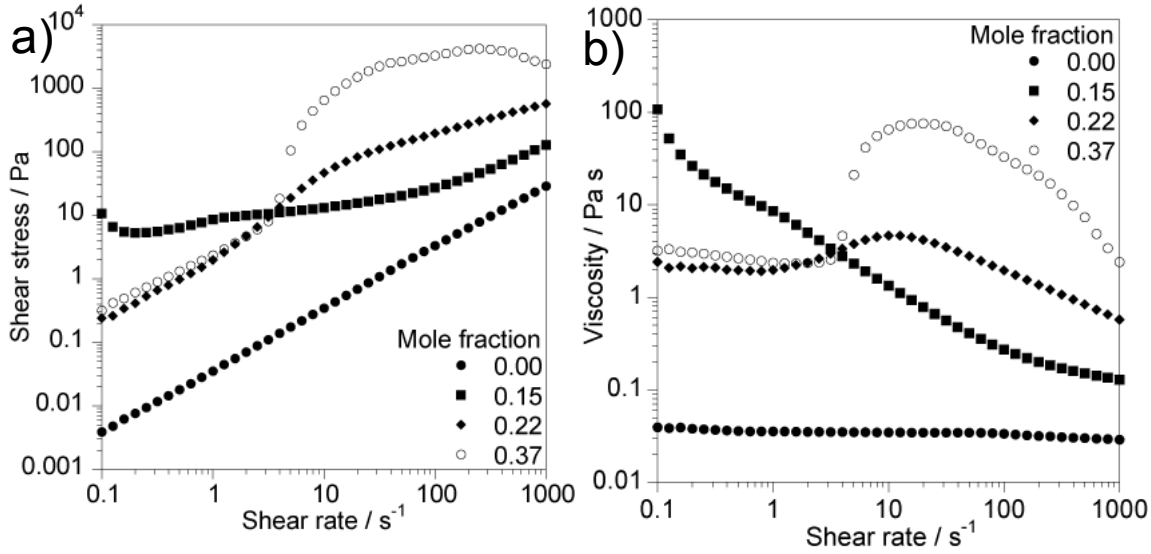

Figure 3.3: Plot of shear stress against shear rate (a) and plot of viscosity against shear rate (b) for $[C_2mim][BF_4]$ with hydrophilic silica.

is observed in the viscosity, indicating that the samples are shear thickening. The degree of shear thickening is higher when there is more silica present in the sample. This shear thinning at low silica concentration and shear thickening at higher concentrations indicate that different structures are forming at these different silica concentrations. It also indicates that the silica is forming different structures in $[C_2mim][BF_4]$ to those formed in $[C_2mim][NTf_2]$ and $[C_4mim][NTf_2]$. Shear thickening has been previously observed in suspensions of $[C_2mim][BF_4]$ and hydrophilic silica nanoparticles, however this is the first time this shear thinning at low silica concentrations has been observed, as other studies have not measured these low silica concentrations.[3, 14]

The rheological behaviour for $[C_4mim][BF_4]$ with silica nanoparticles is shown in figure 3.4. Again, the ionic liquid is observed to show Newtonian behaviour.[3, 13] At low silica nanoparticle concentrations, shear thinning is observed. This is observed at the same silica concentrations as observed in $[C_2mim][BF_4]$. There is the same large increase in zero shear viscosity at these low silica nanoparticle concentrations. The rheology for these low silica nanoparticle concentrations has not previously been reported. It indicates that an unstable suspension has been formed. At silica nanoparticle mole fractions of 0.25 and above, a lower

zero shear viscosity and shear thickening behaviour are observed, indicating the formation of a stable suspension. These are similar to the concentrations at which the shear thickening is observed in $[C_2mim][BF_4]$ suspensions. Suspensions in $[C_4mim][BF_4]$ are also showing different rheological behaviour to that observed in $[C_2mim][NTf_2]$ and $[C_4mim][NTf_2]$ at the highest silica concentrations. These results indicate that the anion, and therefore possibly the hydrophobicity, of the ionic liquids is influencing the rheological behaviour.

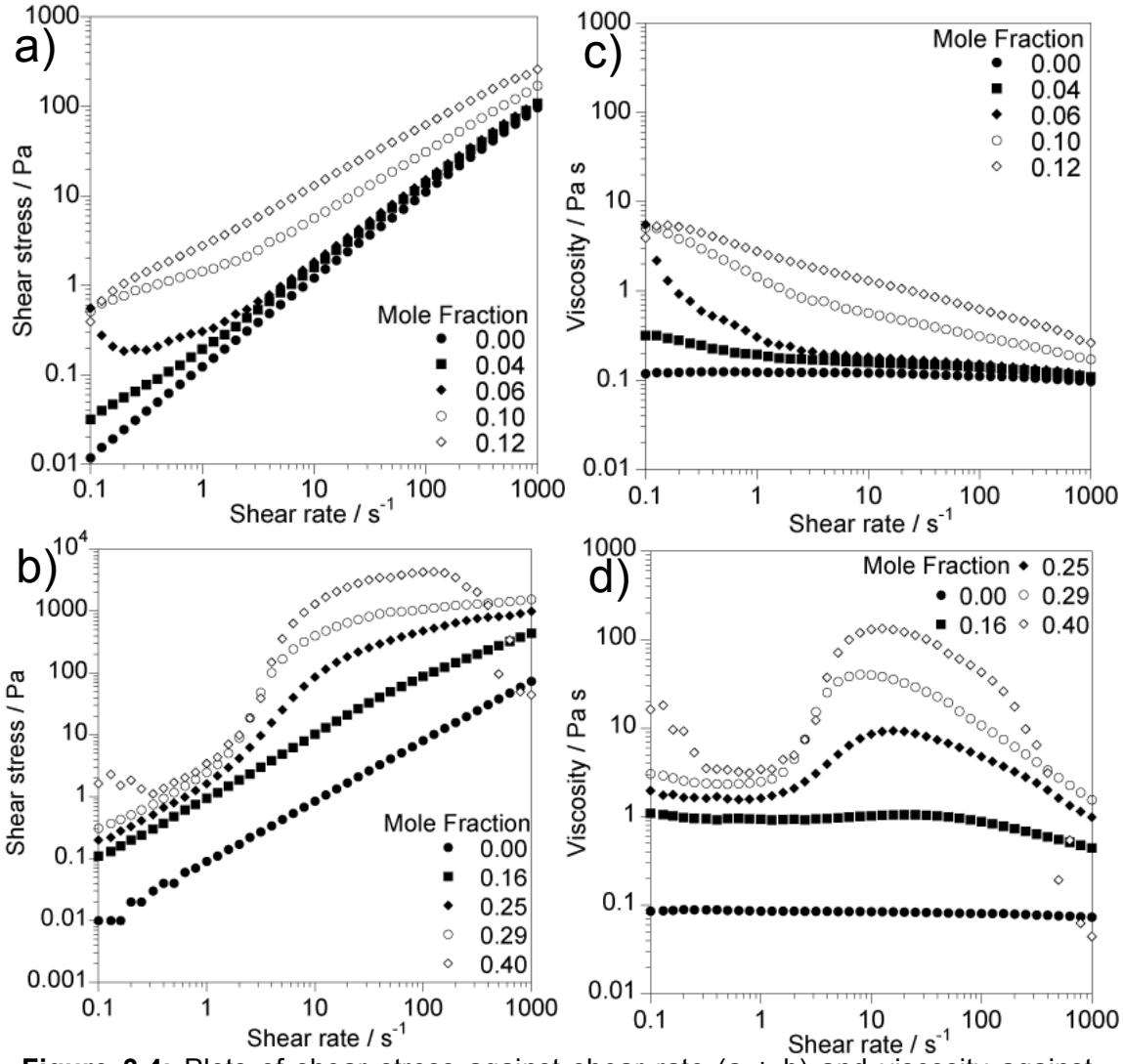

Figure 3.4: Plots of shear stress against shear rate (a + b) and viscosity against shear rate (c + d) for $[C_4mim][BF_4]$ with silica. (a) and c) show rheology at low silica mole fraction. b) and d) show rheology at high silica mole fraction.

At silica mole fraction of 0.16 in $[C_4mim][BF_4]$, Newtonian behaviour is observed. Newtonian behaviour indicates that a stable suspension has been formed. Shear thickening may be observed in this silica concentration at higher shear rates than those recorded in this experiment. This silica concentration represents a balance between the forces that cause shear thinning and shear thickening behaviour.

It is possible that the shear thinning observed in these suspensions in $[C_2mim][BF_4]$ and $[C_4mim][BF_4]$ is due to the breaking up of aggregates of nanoparticles, as has been proposed for the suspensions in $[C_2mim][NTf_2]$ and $[C_4mim][NTf_2]$.[1] The shear thinning could also be due to the layering of the nanoparticles.[5] At low shear rates, nanoparticles sometimes form layers, which means they can more easily move past each other, which causes a decrease in the viscosity. Without knowing the structures of these suspensions, it cannot be determined which mechanism is occurring. In order to investigate whether there is aggregation of silica nanoparticles in $[C_4mim][BF_4]$, dynamic light scattering measurements were performed and are reported in chapter 4.

Colloidal suspensions are known to show shear thickening at higher shear rates.[8, 18] In systems that show shear thickening, Newtonian behaviour is often observed at the lower silica concentrations. The Newtonian behaviour indicates that the nanoparticles are stabilised and able to move freely by Brownian motion.[8] However, at a critical shear rate, the Brownian motion is overwhelmed and the particles start to collide and form transient clusters.[8, 10] It is the formation of these clusters that causes the increase in viscosity. A region of shear thinning is observed after the shear thickening in figure 3.3b. At the highest shear rates, the hydrodynamic forces that contribute to the formation of the clusters are overwhelmed and hence the clusters are broken up, causing the viscosity to decrease.[8, 10]

The general rheology observed for colloidal suspensions is shear thinning at low shear rates, followed by Newtonian behaviour at moderate shear rates before shear thickening at the highest shear rates.[8] All of these stages are not observed in all colloidal suspensions, due to a limit of the range of shear rates that can be accessed in a

rheometer.[6, 9] In suspensions of $[C_2mim][BF_4]$ and $[C_4mim][BF_4]$, the shear thinning is observed at lower silica nanoparticle concentrations and the shear thickening only observed at the highest silica nanoparticle concentrations. Shear thickening is expected to be observed at higher nanoparticles concentrations, as more silica nanoparticles means that are more likely to collide at lower shear rates.[8, 9] However, for the same concentrations of silica in $[C_2mim][NTf_2]$ and $[C_4mim][NTf_2]$, only shear thinning is observed. These indicate that different structures are being formed in these suspensions at higher silica concentrations. They also imply that it is the anion and not the cation influencing the rheological behaviour. However, these structures can only be inferred using the bulk rheology and it is not clear whether different interactions are causing these different structures to form. In order to investigate the structures of nanoparticles within these suspensions and the interactions that form them, NMR and DLS measurements have been performed on these systems and are reported in chapter 4.

3.3.2 Effects of Sample Preparation

The rheological behaviour of these lower mole fraction samples is very sensitive to their preparation. During the course of these experiments, it was found that a difference in the rheological behaviour observed for suspensions in $[C_4mim][BF_4]$ and $[C_2mim][BF_4]$ that is dependent on the stirring method was used. In both cases, the suspension was stirred until a homogenous suspension was observed. A comparison of this behaviour for suspensions in $[C_4mim][BF_4]$ can be found in figure 3.5. When the sample is stirred using a spatula, a higher zero shear viscosity is observed before shear thinning. When a magnetic stirrer bar is used Newtonian behaviour is observed, with a lower initial viscosity. This is possible due to the magnetic stirrer breaking any initially large aggregates formed in the suspension, and therefore giving a more homogenous distribution of aggregates. Spatula stirring allows a more diverse range of particle sizes to be formed, which give the suspension a higher

viscosity. Spatula stirring was used in all further suspensions, as at higher silica concentrations, the use of magnetic stirrer bars was not possible as the suspensions were too viscous. It is important to note that in the cases observed here, shear thinning is observed regardless of the stirring method. It is the initial viscosity and the shear thinning at low shear rates that most affected. Above a shear rate of 10 s^{-1}, the suspensions stirred by the different methods show the same rheological behaviour. It is possible that if spatula stirred samples were run again, the structures, such as aggregations of nanoparticles, causing the higher viscosity would now be broken and a lower zero shear viscosity observed. More measurements are required to determine whether this would be true. If it is true, a pre-shear would allow the effects of different stirring methods to be eliminated. A pre-shear was used during these measurements, but if this is the case, a longer pre-shear would be required to eliminate the effects of the different stirring methods.

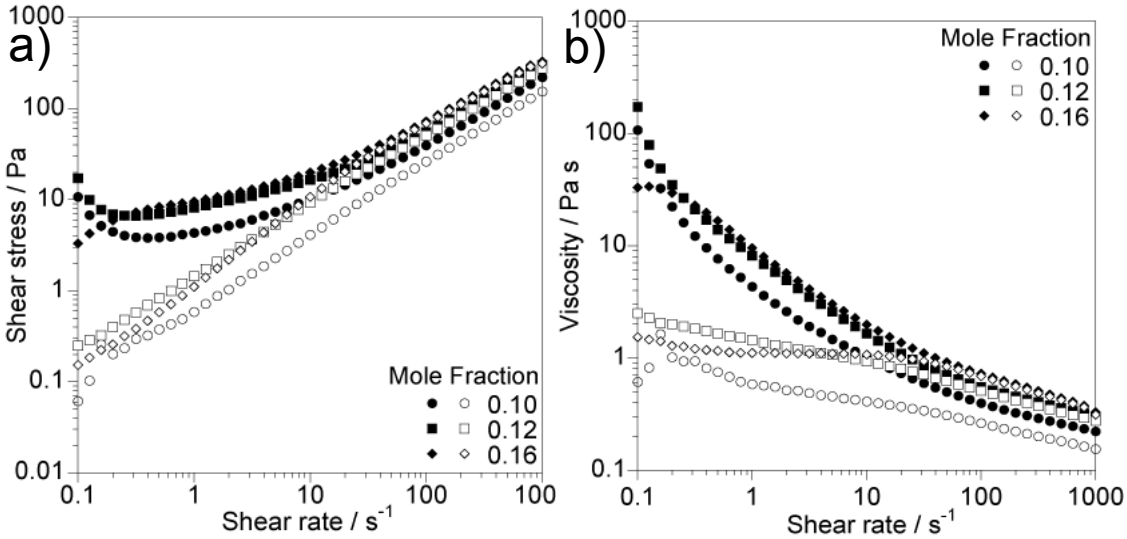

Figure 3.5: Plots of shear stress against shear rate (a) and viscosity against shear rate (b) for [C_4mim][BF_4] with 0.10 – 0.16 mole fractions of silica. Open markers were stirred using a magnetic stirrer bar and filled markers were stirred using a spatula.

3.4 Conclusion

Four different ionic liquids were studied with a wide range of hydrophilic silica nanoparticle concentrations for the first time. All the neat ionic liquids showed Newtonian behaviour. Suspensions in $[C_2mim][NTf_2]$ and $[C_4mim][NTf_2]$ showed large increase in the zero shear viscosity with increase in silica concentrations. All silica concentrations in these ionic liquids showed shear thinning behaviour. These indicated the formation of a colloidal gel in these systems. Suspensions in $[C_2mim][BF_4]$ and $[C_4mim][BF_4]$ also showed shear thinning behaviour at low silica concentrations. However, at higher silica concentrations, shear thickening was observed in these ionic liquids, indicating a change in the structure of these suspensions. The differences indicate that it is the anion, and not the cation, that is influencing the rheology.

These results indicate that there are significant differences in the way the silica nanoparticles interact with the hydrophobic and hydrophilic ionic liquids at higher silica nanoparticle concentrations. However, rheology is not able to probe the interactions that cause these changes nor can the structures formed be observed. In the next chapter, NMR relaxation and diffusion measurements, along with dynamic light scattering are used to probe the interactions and structures within these suspensions. Also, in chapter 5, magnetic resonance velocity imaging is used study the rheological behaviour of these systems at a local level.

3.5 References

1. K. Ueno and M. Watanabe, *Langmuir*, 2011, **27**, 9105.
2. K. Ueno, K. Hata, T. Katakabe, M. Kondoh and M. Watanabe, *J. Phys. Chem. B*, 2008, **112**, 9013.
3. K. Ueno, S. Imaizumi, K. Hata and M. Watanabe, *Langmuir*, 2009, **25**, 825.
4. A. Wittmar, D. Ruiz-Abad and M. Ulbricht, *J. Nano. Res.*, 2012, **14**, 651.

5. J. Qin, G. Zhang, X. Shi and M. Tao, *J Nano. Res.*, 2015, **17**, 333.

6. B. M. Guy, M. Hermes and W. C. K. Poon, *Phys. Rev. Lett.*, 2015, **115**, 088304.

7. H. A. Barnes, J. F. Hutton and K. Walters, *An Introduction to Rheology*, Elsevier, Amsterdam, 1997.

8. J. Mewis and N. J. Wagner, *Colloidal Suspension Rheology*, Cambridge University Press, Cambridge, UK, 2012.

9. N. J. Wagner and J. F. Brady, *Phys. Today*, 2009, **62**, 27.

10. X. Cheng, J. H. McCoy, J. N. Israelachvili and I. Cohen, *Science*, 2011, **333**, 1276.

11. J. R. Stokes and W. J. Frith, *Soft Matter*, 2008, **4**, 1133.

12. M. Instruments, *Understanding Yield Stress Measurements*, 2012.

13. J. Novak and M. M. Britton, *Soft Matter*, 2013, **9**, 2730.

14. J. Qin, G. Zhang, Z. Ma, J. Li, L. Zhou and X. Shi, *RSC Adv.*, 2016, **6**, 81913.

15. K. Ueno, A. Iaba, M. Kondoh and M. Watanabe, *Langmuir*, 2008, **24**, 5253.

16. T. Cosgrove, *Colloid Science : Principles, Methods and Applications* 2nd edn., Wiley-Blackwell, Chichester, 2010.

17. V. J. Anderson and H. N. W. Lekkerkerker, *Nature*, 2002, **416**, 811.

18. W. C. K. Poon and M. D. Haw, *Adv. Colloid Interfac.*, 1997, **73**, 71.

4. Studying Microscopic Structure Using NMR and DLS measurements

4.1 Introduction

In chapter 3, the rheological behaviour of hydrophobic and hydrophilic ionic liquids with hydrophilic silica nanoparticles was studied. Suspensions in $[C_2mim][BF_4]$ and $[C_4mim][BF_4]$ showed shear thinning behaviour at low silica concentrations and shear thickening at higher silica concentrations. This observation agrees with the theory that clusters form with increasing shear rate and that the formation of these clusters is reversible.[1] Suspensions in $[C_2mim][NTf_2]$ and $[C_4mim][NTf_2]$ exhibited shear thinning behaviour. These results suggest that the interactions between the ionic liquids and the silica are very different and depend on the anion of the ionic liquid.[2, 3] However, rheology does not allow the structures that make up these systems to be observed.

Dynamic light scattering (DLS) gives the size distribution of nanoparticles within a suspension.[4] This distribution allows the stability of the nanoparticles to be studied. If a single distribution is observed, then the nanoparticles have been stabilised.[5, 6] If the nanoparticles have not been stabilised then they aggregate, producing multiple peaks that correspond to aggregates of different sizes.[5, 7] The stability determined by DLS measurements are comparable with observations from rheology.[7, 8] For example, if a suspension demonstrates Newtonian behaviour, then it indicates that the nanoparticles have been stabilised and therefore will show a single size distribution in the DLS measurements. Whereas, unstable suspensions of nanoparticles that give multiple peaks in the DLS measurements tend to show shear thinning behaviour, as the structures are broken on the application of shear, hence there is a reduction in the viscosity.[6, 9]

Previously, rheometry and DLS have been used to study nanoparticles in hydrophilic and hydrophobic ionic liquids.[2, 6, 8-10] ZnO and TiO_2 nanoparticles are stable in hydrophilic

ionic liquids as single, narrow size distributions and Newtonian behaviour were observed. However, they were unstable in hydrophobic ionic liquids.[6, 9] Bare silica nanoparticles were observed to show narrow size distributions and Newtonian rheology in hydrophilic ionic liquids, and broader distributions as well as shear thinning behaviour in hydrophobic distributions, indicating that the silica was more stable in the hydrophilic ionic liquids.[8] However, DLS measurements have been used to show that silica nanoparticles are not fully stabilised in hydrophilic ionic liquids, as broad distributions which corresponded to aggregated nanoparticles were observed.[10] Also, the suspensions of ionic liquids with silica nanoparticles are not stable for long periods of time as silica nanoparticles have been observed to settle over 24 hours.[10]

The stability of silica nanoparticles in ionic liquids has been investigated by calculating the Derjaguin-Landau-Verwey-Overbeek (DVLO) interparticle interaction profiles.[10] It was shown that smaller silica nanoparticles (diameter < 100 nm) would always be unstable and aggregate in hydrophobic or hydrophilic ionic liquids.[10] This does not match with the rheology that is observed for hydrophilic ionic liquids with silica nanoparticles. The Newtonian behaviour at low shear rates and shear thickening behaviour that is observed at higher shear rates for the hydrophilic ionic liquids, $[C_2mim][BF_4]$ and $[C_4mim][BF_4]$, imply that stable suspensions have been formed with the silica nanoparticles.[2, 11] This is investigated further in this chapter. DLS measurements are used to investigate the distributions of the silica in the ionic liquids but cannot provide information on the molecular interactions between the silica and the ionic liquids.

Infrared (IR) spectroscopy can identify which bonds are present in a system by studying changes in the spectra on the addition of silica to the ionic liquid.[12, 13] It has been proposed that the ionic liquid and silica nanoparticles interact through hydrogen bonds between the silica and the anion.[14, 15] The evidence for the hydrogen bonds was suggested to be the presence of resonances at ca. 3000 cm^{-1} in the IR spectrum of $[C_4mim][BF_4]$ with silica nanoparticles. These peaks were not present in the neat ionic liquid IR spectrum, or for

suspensions of [C_4mim]I, which indicated that these resonances were due to hydrogen bonding between the fluorine, located on the BF_4 anion, with the silica nanoparticles.[14] However, other studies of [C_4mim][BF_4] with silica nanoparticles using nuclear magnetic resonance (NMR) and IR spectroscopy have found no evidence for hydrogen bonding in the ionic liquid [C_4mim][BF_4].[2, 13, 16] IR measurements for [C_4mim][BF_4] and [C_4mim][NTf_2] with and without silica have been reported in this chapter.

To observe the effect of adding silica on the translational motion of the ions, NMR diffusion measurements have been used.[17, 18] The cations and anions can be studied separately using ^{1}H and ^{19}F NMR measurements, respectively. Diffusion NMR measurements of imidazolium ionic liquids have previously shown that although both the cation and the anion diffusion coefficients decrease with the addition of silica, there is a greater decrease in the cation diffusion coefficient.[10, 17-21] This implies that it is the cation of the ionic liquids that interacts with the silica. Solid-state 2D ^{1}H-^{29}Si NMR experiments demonstrated peaks that show strong correlations between silica and the imidazolium ring of the cation in [C_6mim][NTf_2].[18] This interaction was not observed for 2D ^{19}F-^{29}Si NMR experiments, indicating that it is the imidazolium ring of the cations that is interacting with the silica.

In this chapter, four ionic liquids with hydrophilic silica nanoparticles have been studied using ^{1}H and ^{19}F NMR measurements of T_1 and T_2 relaxation, and diffusion. This has enabled the changes of the cation and anion motion, in the presence of the silica, to be studied. The ionic liquids, [C_4mim][BF_4] and [C_4mim][NTf_2], have also been studied with and without silica using IR spectroscopy, to see if there are any changes to suggest hydrogen bonding within these systems. Lastly, DLS measurements were performed to observe the structure formed by the silica at different concentrations and in the presence of different anions.

4.2 Experimental

4.2.1 Materials and Sample Preparation

1-ethyl-3-methylimidazolium tetrafluoroborate, [C_2mim][BF_4]; 1-ethyl-3-methylimidazolium bis(trifluoromethylsulfonyl)imide, [C_2mim][NTf_2]; 1-butyl-3-methylimidazolium tetrafluoroborate, [C_4mim][BF_4] and 1-butyl-3-methylimidazolium bis(trifluoromethylsulfonyl)imide, [C_4mim][NTf_2] were obtained from Sigma Aldrich, UK and used without further purification. Aerosil 200 silica nanoparticles (Evonik, Germany) had a diameter of 12 nm, a surface area of 200 ± 25 $m^2\,g^{-1}$ and Si-OH surface functionalisation. Aerosil 200 was dried overnight at 70 °C in a vacuum oven prior to use. Aerosil 200 was dispersed in [C_2mim][BF_4] and [C_4mim][BF_4] at concentrations from 0 to 15% wt. (0.40 silica mole fraction) and in [C_2mim][NTf_2] and [C_4mim][NTf_2] from 0 to 8% wt. (0.39 silica mole fraction). The suspensions were stirred until they appeared homogeneous and placed in a vacuum oven overnight at least 70 °C to minimise the water content. These were then transferred into screw cap NMR tubes (Wilmad, UK), which were used to reduce the contact with moisture in the air during the NMR measurements. Water content was monitored by observed the water peak in the ^{1}H NMR spectrum.

4.2.2 Magnetic Resonance

All NMR measurements were performed on a Bruker DMX 300 spectrometer, which has a ^{1}H NMR resonance frequency of 300.13 MHz and a ^{19}F NMR resonance frequency of 282.37 MHz. All measurements were performed at 20 ± 0.3 °C. Data was acquired using 10 mm ^{1}H resonator or 10 mm ^{19}F resonator in a Bruker Diff30 probe, which has a maximum field gradient value of 12 Tm^{-1}. A 90° pulse duration of ca. 45 μs was used during the ^{1}H NMR experiments. For the ^{19}F NMR experiments using the Bruker Diff30 probe, a 90° pulse duration of ca. 30 μs was used. For ^{19}F NMR relaxation measurements, a 30 mm ^{19}F

birdcage radio-frequency resonator with a maximum gradient strength of 96 G cm^{-1} was use with a 90° pulse duration of ca. 20 μs. All data was analysed using Prospa (Magritek, New Zealand). Each measurement was repeated at least three times and the error determined from an analysis of the variation in the value obtained for a given system.

4.2.2.1 ^{1}H NMR T_1 Relaxation Measurements

An inversion recovery sequence was used to measure T_1 relaxation times.[22] 16k points were collected across 8 signal averages with a spectral width of 10 kHz. A variable delay list with 20 points logarithmically spaced between 5 ms and $5 \times T_1$ was used. T_1 values were obtained from curve fitting (equation 2.19) in Kaleidagraph (Synergy, USA).

4.2.2.2 ^{1}H NMR T_2 Relaxation Measurements

T_2 relaxation times were measured using a Carr-Purcell-Meiboom-Gill (CPMG) experiment.[23, 24] 8 signal averages were used across 16k data points, with a spectral width of 10 kHz. A repetition time of at least $5 \times T_1$ was used. The variable counter lists for the CPMG experiments were spaced with values from 0 to 512 and a τ value of 2 ms. T_2 values were obtained from curve fitting (equation 2.21) in Kaleidagraph.

4.2.2.3 ^{19}F NMR Relaxation Measurements

T_1 and T_2 relaxation maps were collected of 5 mm NMR tubes in a phantom. Images were acquired using a RARE (Rapid Acquisition with Relaxation Enhancement)[25] spin-echo imaging sequence with Paravision 3.0. Horizontal images were acquired with a 25 × 25 mm field of view with 64 × 64 pixels and a slice thickness of 4 mm. A repetition time of $T_R > 5 \times T_1$ was used. T_1 relaxation maps were produced from 12 images with inversion delays spaced logarithmically between 5 mm and T_R and a RARE factor of 8. T_2 relaxation maps

were produced from 100 echo images with echo times from 2 – 200 ms and a RARE factor of 1. The T_1 and T_2 relaxation times for each sample were obtained by taking an average of the pixels for each sample using Prospa.

4.2.2.4 Diffusion Measurements

^{1}H and ^{19}F NMR diffusion measurements were performed using a pulsed gradient stimulated echo (PGSTE) sequence.[25] An observation time, Δ, of 100 ms was used, with 32 gradient steps and 16 signal averages. Two dummy scans were used and a repetition time of 2 s was used. A gradient duration, δ, of 2 ms was used and the maximum gradient value, $\boldsymbol{G}_{max}$, was varied between 0.2 and 0.4 T m^{-1} to achieve maximum signal attenuation. The diffusion coefficients were determined by fitting the data to the Stejskal-Tanner equation (equation 2.26) using Kaleidagraph.

4.2.3 IR Measurements

A Perkin-Elmer Spectrum 100 FT-IR spectrometer was used to record the IR spectra between 4000 cm^{-1} and 650 cm^{-1}, with 4 signal averages. IR spectra were recorded for $[C_4mim][BF_4]$ with 0 and 5 % wt. silica (0.16 silica mole fraction) and $[C_4mim][NTf_2]$ with 5% wt. silica (0.26 silica mole fraction). Water was added drop wise to these systems, with each drop of water equivalent to ca. 2 % volume. An IR spectrum was recorded for each additional drop of water.

4.2.4 DLS Measurements

DLS measurements were performed on a Zetasizer Nano ZS (Malvern Instruments, UK). The samples were allowed to equilibrate at 20.0 °C for 60 seconds and the data was accumulated for 120 seconds with 6 repetitions. A refractive index of 1.42, viscosity of 99.6

mPa s and a dielectric constant of 11.7 were used for measurements of $[C_4mim][BF_4]$ suspensions.[10] A refractive index of 1.43, viscosity of 49.9 mPa s and a dielectric constant of 11.5 were used for measurements of $[C_4mim][NTf_2]$ suspensions.[10] The time domain correlation method was used with CONTIN analysis, which applies a constrained form of the inverse Laplace transformation to generate the particle sizes.[26-28] The intensity distribution is reported.[29] The volume distributions for polydisperse plots are shown in appendix 5. The experiments were repeated three times for each silica mole fraction recorded. The error was determined by calculating the standard deviation of the values obtained.

4.3 Results

4.3.1 Spectra

Molecular structures for the ionic liquids are shown in figure 4.1. The ^1H NMR spectra for the C_2mim and C_4mim cations are shown in figure 4.2 and the assignments for these spectra are given in table 4.1. The ^{19}F NMR spectrum for $[NTf_2]$ has a single resonance. The ^{19}F NMR spectrum for BF_4 shows two overlapping resonances due to the two spin active isotopes of boron – ^{10}B and ^{11}B.

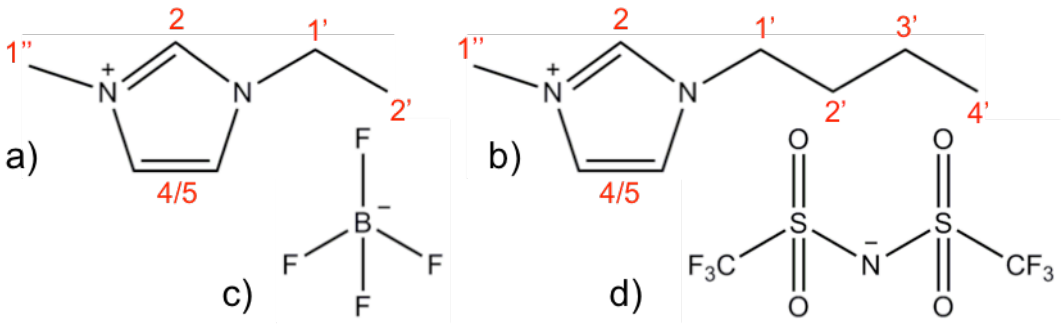

Figure 4.1: Structures of 1-ethyl-3-methylimidazolium, C_2mim (a); 1-butyl-3-methylimidazolium, C_4mim (b); tetrafluoroborate, BF_4 (c) and bis(trifluoromethylsufonyl)imide, NTf_2 (d). Proton labels are shown on the cations.

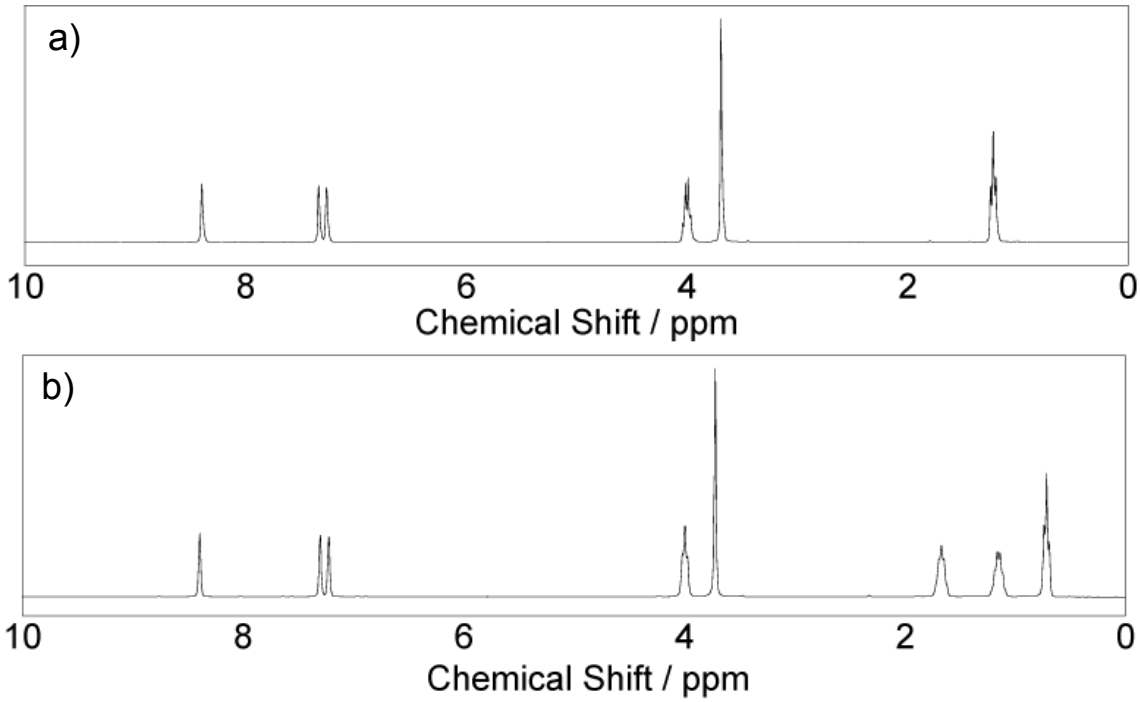

Figure 4.2: ^{1}H NMR spectrum for C_2mim (a) and C_4mim (b) cations. Spectral assignments are shown in table 4.1.

Table 4.1: ^{1}H NMR peak assignments for [C_2mim] and [C_4mim] cations.

Cation	δ / ppm						
	H2	H4/5	H1'	H2'	H3'	H4'	H1"
C_2mim	8.40	7.34,7.27	4.00	1.23	-	-	3.69
C_4mim	8.39	7.30,7.22	4.00	1.68	1.17	0.72	3.72

4.3.2 NMR Relaxation Measurements

The ^{19}F and ^{1}H T_2 relaxation times for the ionic liquids with varying silica concentration are shown in figure 4.3. There is a decrease in the ^{1}H and ^{19}F T_2 relaxation time with increasing silica concentration for the cation and anion respectively. This decrease in T_2 relaxation time is possibly due to the presence of the solid silica nanoparticles, which decrease the magnetic susceptibility of the suspension. Solid materials have a lower magnetic susceptibility than liquids and T_2 relaxation is sensitive to the magnetic susceptibility of the sample.[30] T_2 relaxation is also sensitive to changes in viscosity; an increase in the viscosity is reflected by a decrease in the T_2 relaxation time as the molecules are less mobile.[30] With an increase in silica concentration, there is a decrease in the magnetic susceptibility and an increase in the viscosity in the sample and this is reflected in the decrease of the T_2 relaxation time. It is likely to be a combination of the change in magnetic susceptibility and viscosity having this effect on the T_2 relaxation times.

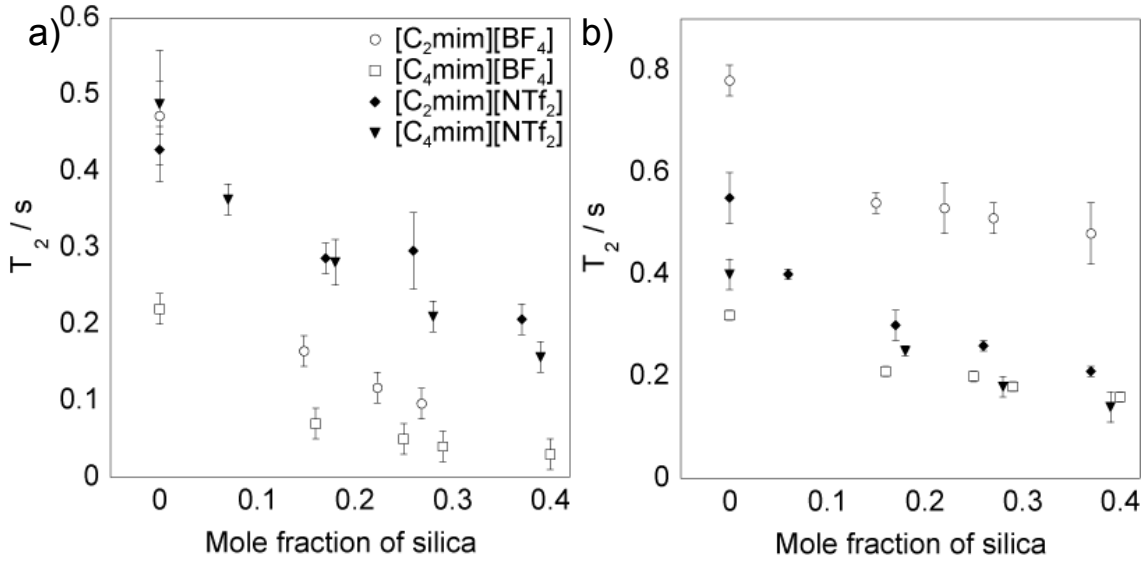

Figure 4.3: Plot of T_2 relaxation times against mole fraction of silica for cations (a) and anions (b). The ^{1}H relaxation data shown is for H(4/5).

A plot showing the ^{19}F NMR T_1 relaxation times for all four ionic liquids is presented in figure 4.4. There is very little change in the ^{19}F T_1 relaxation times with changing silica concentration. The BF_4 anion has a higher T_1 relaxation time than the NTf_2 anion suggesting greater mobility. The BF_4 and NTf_2 anions with the C_2mim have a greater mobility than those with the C_4mim cation. This indicates that these ions are associated in solution, as the larger C_4mim cations will have a lower mobility, which will decrease the mobility of the anions associated with them.

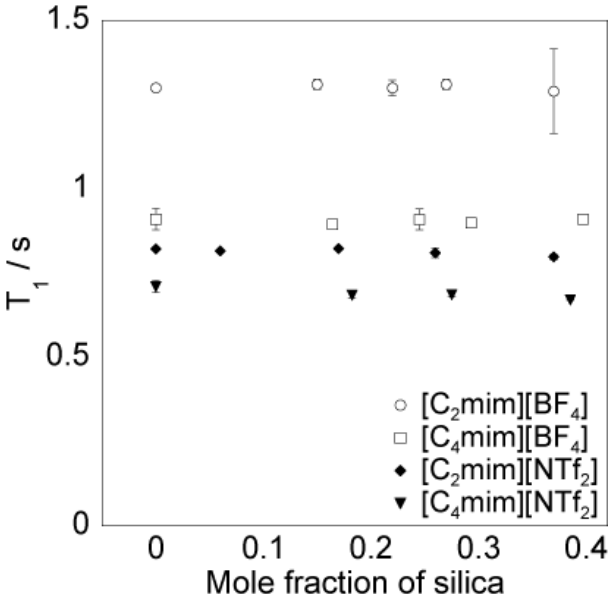

Figure 4.4: Plot of ^{19}F NMR T_1 relaxation time against mole fraction of silica.

Figure 4.5 shows the ^{1}H NMR T_1 relaxation times for the H(4/5) protons that are located on the imidazolium ring of the cation. Across all ionic liquids, there is a decrease in these T_1 relaxation times with increase in silica concentration. This indicates that there is a reduction in the mobility of the protons located on the imidazolium ring of the cation. This suggests the imidazolium protons on the cation could be interacting with the silica as the reduction in the T_1 indicates that their tumbling is slowed. The silica nanoparticles are larger and will be tumbling slower, and therefore if the imidazolium ring protons interact with the

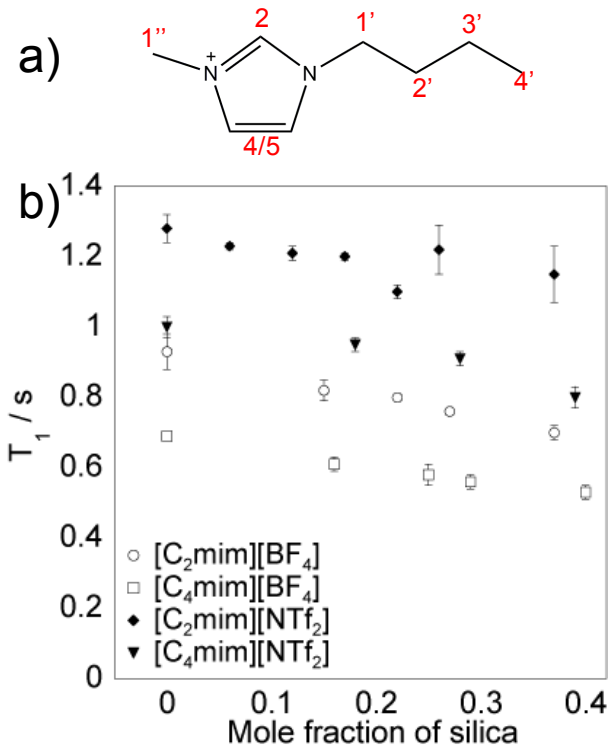

Figure 4.5: a) Structure of the C_4mim cation. b) Plot of H(4/5) T_1 relaxation times against mole fraction of silica.

silica nanoparticles, then their tumbling will be reduced and hence there will be a decrease in the T_1 relaxation time.

The imidazolium ring protons in [C_2mim][NTf_2] show a decrease in their T_1 relaxation time with decrease in silica concentration, but the decrease is not as linear as observed in the other ionic liquids. The ^{1}H T_1 relaxation times of the [C_2mim][NTf_2] suspensions have a higher error than is found for the ^{19}F T_1 relaxation times, especially at higher silica concentrations. This large error in the ^{1}H T_1 values is potentially due to a large variation in the distribution of the silica nanoparticles. [C_2mim][NTf_2] is known to form gels above 0.15 mole fraction of silica.[17] When the samples form a gel, it makes them harder to mix and obtain a homogenous suspension, especially at the higher mole fractions of silica, hence the variation in composition. This demonstrates that the imidazolium ^{1}H T_1 relaxation time in [C_2mim][NTf_2] is affected by variations in composition, hence also demonstrating that there is

an interaction between the cation and the silica. A higher error in the T_1 relaxation times is not observed for the anions. Therefore, as each sample is mixed to different extents, there is a large variation in the amount of silica present in a sample extracted for NMR. This variation in the composition of the samples has a greater effect on the cation relaxation time, implying the cation is interacting with the silica.

Figure 4.6 shows the T_1 relaxation times for the methyl group located at the end of the alkyl chains on the cations: H(2') for the C_2mim cations and H(4') for the C_4mim cations. There is little change in these T_1 relaxation times with variation in silica concentration. For suspensions of [C_2mim][BF_4] and [C_2mim][NTf_2], there is very little change in the T_1 relaxation time of the H(2') as a function of silica concentrations. The H(4') protons in [C_4mim][BF_4] and [C_4mim][NTf_2] show a small decrease in relaxation time with increasing silica concentration. The methyl group is known to rotate rapidly, and so it is unlikely to be affected by an interaction with the silica surface.

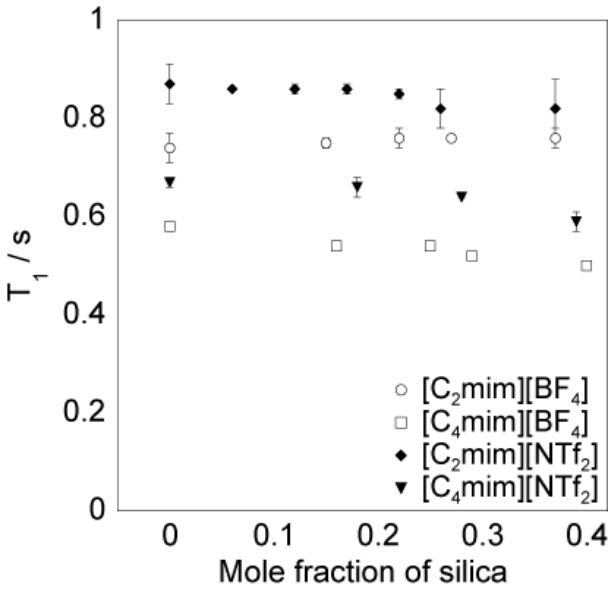

Figure 4.6: Plot of T_1 relaxation time against mole fraction of silica for the H(2') and H(4') protons.

4.3.3 NMR Diffusion measurements

The diffusion coefficients for the cations and the anions of the different ionic liquids with varying silica concentrations are shown in figure 4.7. There is a decrease in the diffusion coefficient of the cations and the anions in all ionic liquids with increase in silica concentration. To allow this decrease to be compared between the ionic liquids, the diffusion coefficients for suspensions in $[C_4mim][BF_4]$ and $[C_4mim][NTf_2]$ have been normalised and are shown in figure 4.8. The normalised diffusion coefficients for suspensions in $[C_2mim][BF_4]$ and $[C_2mim][NTf_2]$ are shown in appendix 2.

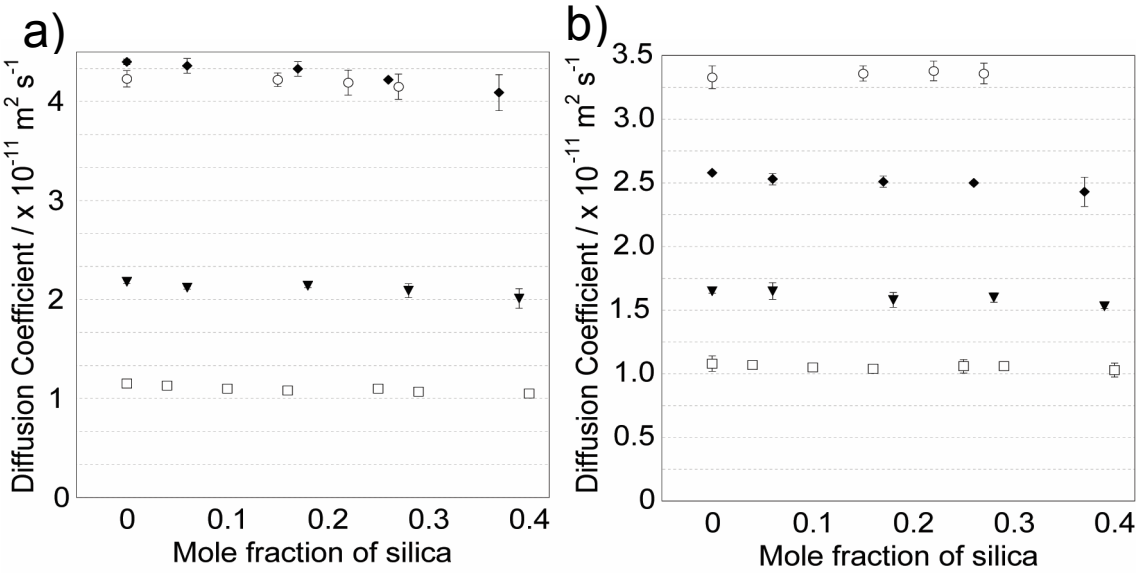

Figure 4.7: Plots of diffusion coefficient against mole fraction of silica for a) cations and b) anions. $[C_2mim][BF_4]$ – empty circles. $[C_4mim][BF_4]$ – empty squares. $[C_2mim][NTf_2]$ – filled diamonds. $[C_4mim][NTf_2]$ – filled triangles.

In suspensions containing both ionic liquids, there is a similar decrease of the cation and anion diffusion coefficients. Above a silica mole fraction of 0.20, an increase is observed in the diffusion coefficients before a further decrease at higher silica concentrations. This change is observed at similar mole fractions in $[C_4mim][BF_4]$ but different mole fractions in $[C_4mim][NTf_2]$: the anion diffusion coefficient also shows an increase above 0.25 mole fraction of silica whereas this increase is observed at 0.20 mole fraction in the cation. Again,

this indicates a change in the structure of the suspension. Diffusion coefficient and viscosity are inversely linked by the Stokes-Einstein relationship, shown in equation 4.1 where k_B is the Boltzman constant, T is the temperature and R_h is the hydrodynamic radius of the diffusion object.[28] An analysis was considered where diffusion coefficient and the reciprocal viscosity were plotted to investigate the relationship between these parameters with varying silica concentration. However, for this analysis, more accurate values of the zero shear viscosity would need to be obtained by performing more repeats of the rheology measurements over a wider range of shear rates.

$$D = \frac{k_B T}{6\pi\eta R_h} \tag{4.1}$$

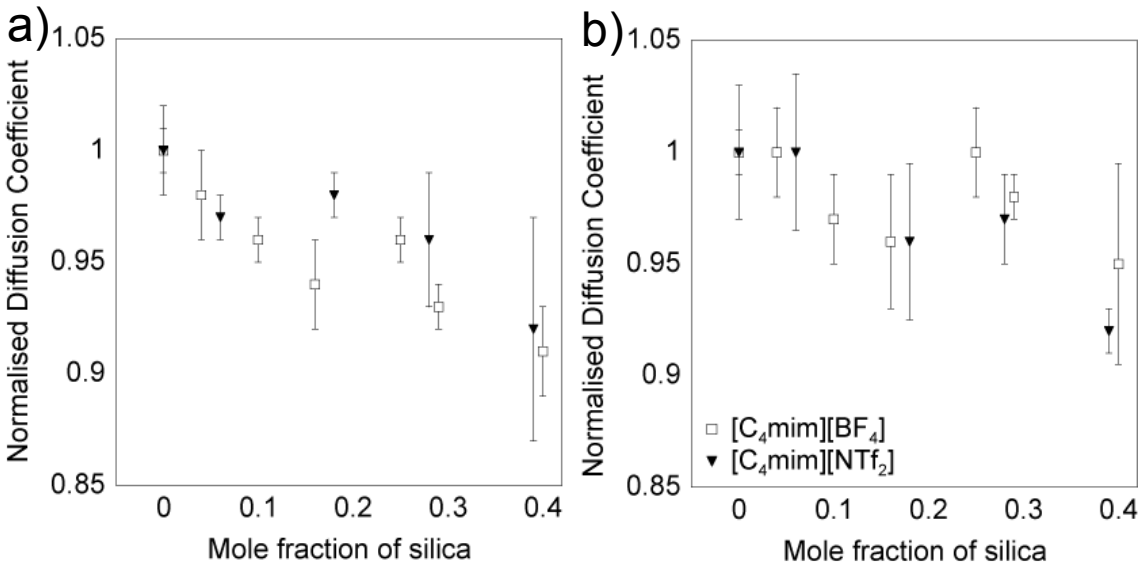

Figure 4.8: Plots of normalised diffusion coefficient against mole fraction of silica for a) cations and b) anions.

4.3.4 Infrared Spectroscopy

The IR spectrum for the hydrophilic silica nanoparticles is shown in figure 4.9. In figure 4.10, the IR spectra for $[C_4mim][BF_4]$ with and without hydrophilic nanoparticles are shown. The insets show the O-H stretching region of the IR spectrum. Little change in observed in the IR spectra of $[C_4mim][BF_4]$ on the addition of hydrophilic silica nanoparticles.

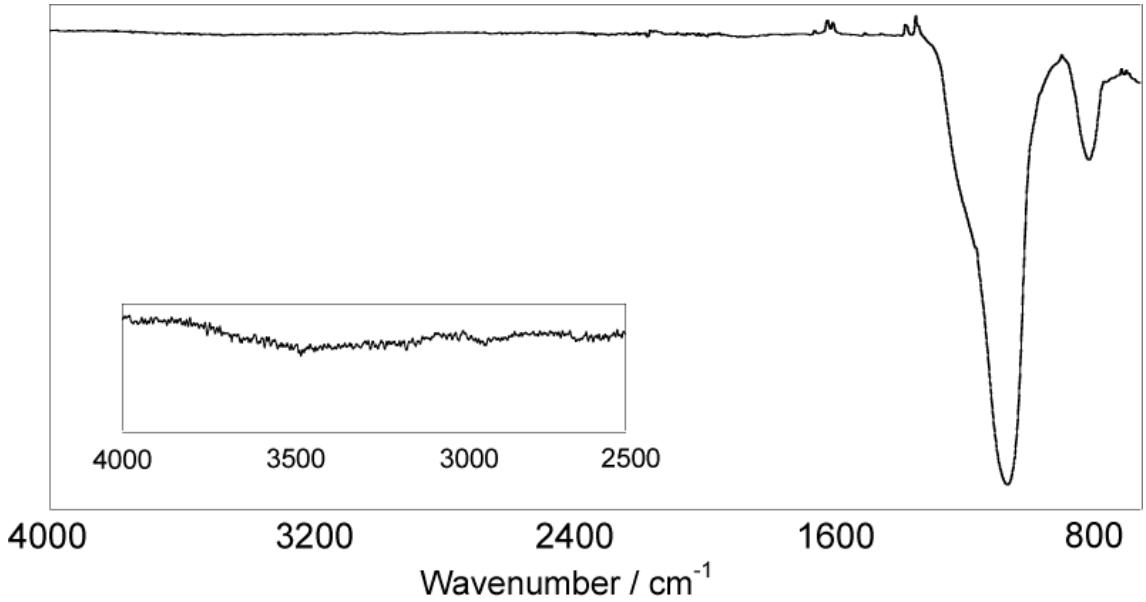

Figure 4.9: IR spectrum of hydrophilic silica nanoparticles. Inset shows the O−H stretching region.

The inset showing the O-H stretching region of the IR spectrum for $[C_4mim][BF_4]$ has two peaks at ca. 3650 cm^{-1} and 3550 cm^{-1} (figure 4.10a). These peaks are due to the presence of water in the ionic liquid. It is very difficult to remove this last trace of water from ionic liquids. These peaks are also present in the O-H stretching region for $[C_4mim][BF_4]$ with 0.16 mole fraction of silica (figure 4.10b). The peaks are at the same wavenumber and at a similar intensity. If the peaks were due to an interaction between the ionic liquid and the silica, they would appear at a different wavenumber. This indicates that these peaks are most likely also due to the presence of water in the suspension.

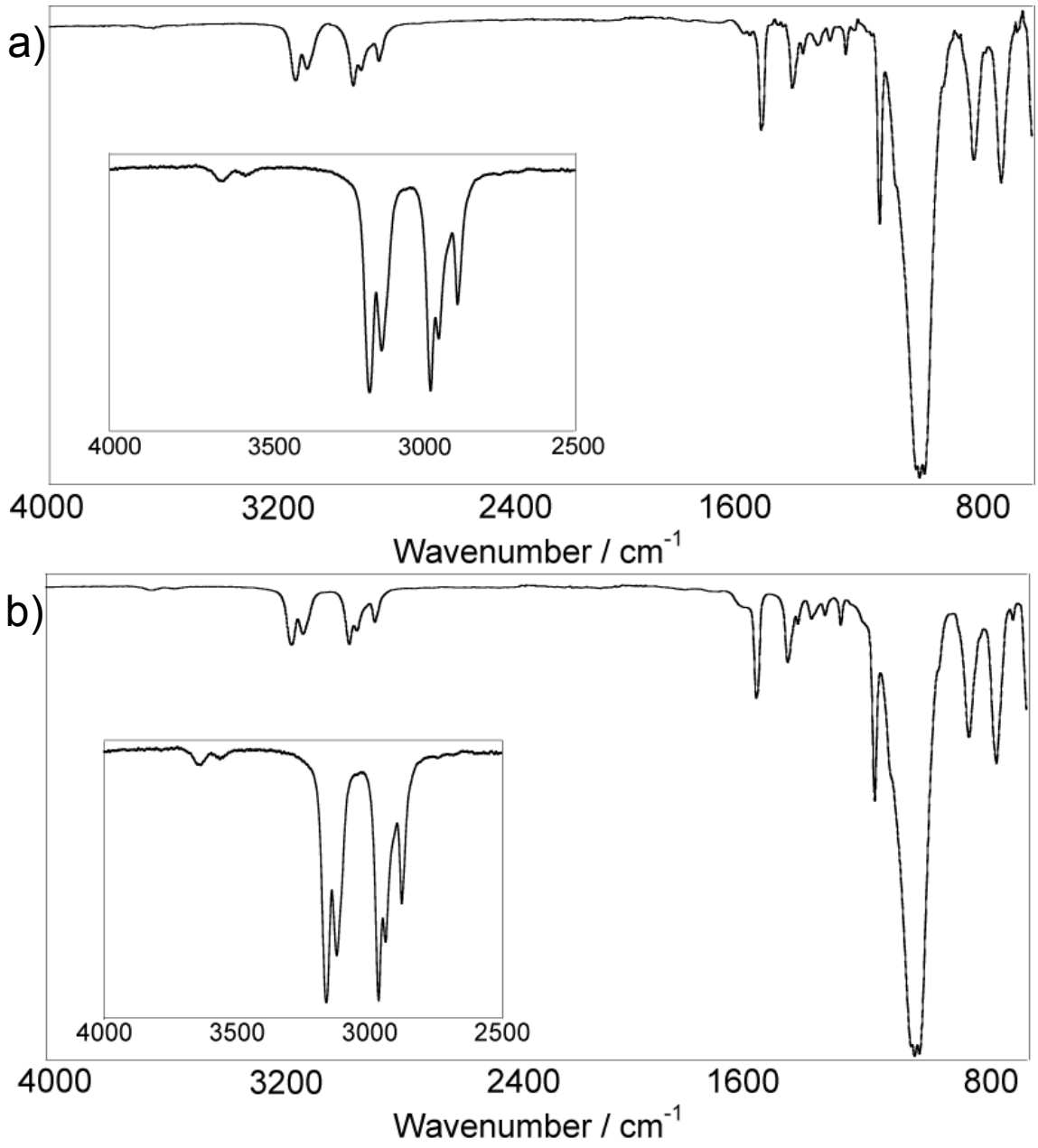

Figure 4.10: IR spectrum for neat [C_4mim][BF_4] (a) and with 0.16 mole fraction of silica (b). Inset shows the O−H stretching of the IR spectrum.

Figure 4.11 shows the 4000 – 2500 cm^{-1} region of the IR spectrum for [C_4mim][BF_4] with and without hydrophilic silica, on the addition of water. The peaks at ca. 3650 cm^{-1} and 3550 cm^{-1} increase in intensity and slightly shift to lower wavenumbers on the addition of water to the neat ionic liquid and the suspension. This increase in intensity and shift of the peaks is due to the addition of water to the systems. This indicates that the peaks at ca. 3650

cm^{-1} and 3550 cm^{-1} are due to water and not due to an interaction between the ionic liquid and the silica nanoparticles.

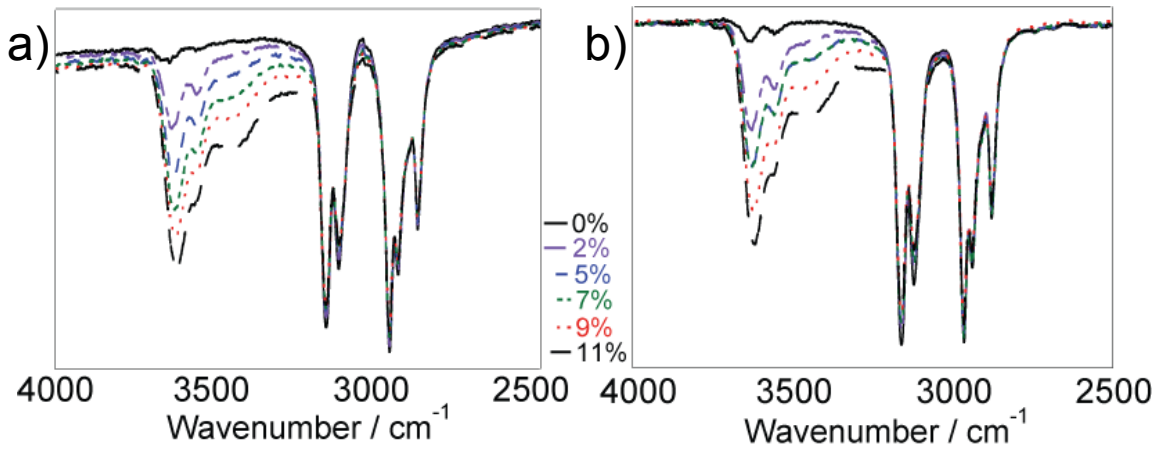

Figure 4.11: O−H stretching of the IR spectrum for neat [C_4mim][BF_4] (a) and with 0.16 mole fraction of silica (b) with additions of water. Legend refers to the volume % of water added.

The IR spectra for [C_4mim][NTf_2] with and without hydrophilic silica nanoparticles can be found in figure 4.12. There is little change in the IR spectrum of [C_4mim][NTf_2] on the addition of the hydrophilic nanoparticles. The inset shows the O-H stretching region of the ionic liquid. There are no peaks around 3650cm^{-1} and 3550cm^{-1}, which is where peaks attributed to water appeared in the IR spectra of [C_4mim][BF_4] with and without silica nanoparticles. [C_4mim][NTf_2] does not contain residual water as it is a hydrophobic ionic liquid.

As [C_4mim][NTf_2] is a hydrophobic ionic liquid, it is not miscible with water. When water was added to the neat [C_4mim][NTf_2] and [C_4mim][NTf_2] with 0.27 mole fraction of

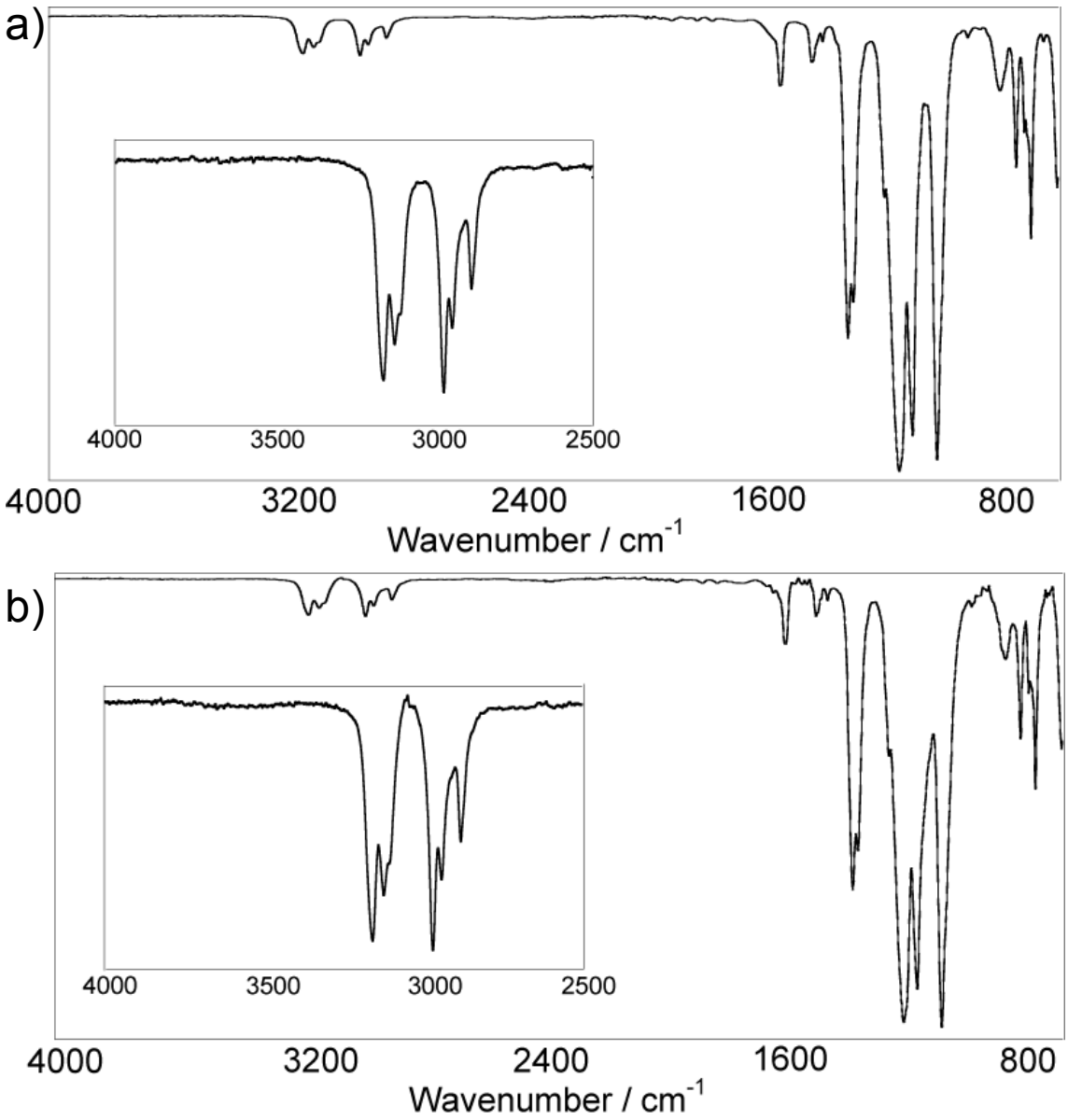

Figure 4.12: IR spectrum for neat [C_4mim][NTf_2] (a) and with 0.27 mole fraction of silica. Inset shows the O−H stretching of the IR spectrum.

silica, an emulsion was formed. Figure 4.13 shows the 4000 – 2500 cm^{-1} region of the IR spectrum for [C_4mim][NTf_2], with and without silica, on the addition of water. Peaks at ca. 3650cm^{-1} and 3550 cm^{-1} are observed in both the ionic liquid and its suspension with water. These peaks are due to the water in the emulsion, and not present in [C_4mim][NTf_2].

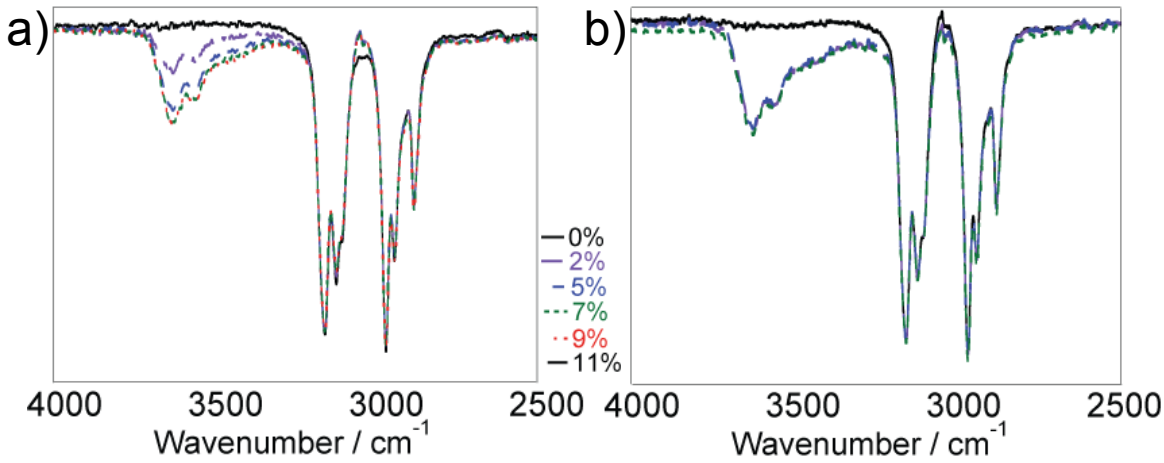

Figure 4.13: O−H stretching of the IR spectrum for neat [C_4mim][NTf_2] (a) and with 0.27 mole fraction of silica (b) with additions of water. Legend refers to the volume % of water added.

Previously, peaks have been observed at 3648 and 3572 cm^{-1} in the IR spectrum for [C_4mim][BF_4] with hydrophilic silica nanoparticles.[14] These peaks were not observed when the neat ionic liquid was present. There was a broad peak at 3500 cm^{-1} in the spectrum of the bare silica nanoparticles. The presence of the peaks at 3648 and 3572 cm^{-1} were attributed to a hydrogen bonding interaction between [C_4mim][BF_4] and the silica nanoparticles. As there peaks were not present in a suspensions of [C_4mim]I with silica nanoparticles, it was proposed that a hydrogen bond between the BF_4 anion and hydroxide on the silica nanoparticles was allowing the ionic liquid to stabilise the silica nanoparticles.[14] This has been reported for ionic liquid and silica suspensions.[15, 31] However, other studies have not been able to repeat these measurements.[2, 16] Here, it has been shown that these peaks at around 3500 cm^{-1} are not present in suspensions of the hydrophobic [C_4mim][NTf_2]. However, peaks appear in the region at the same wavenumbers on the addition of water in the both [C_4mim][BF_4] and [C_4mim][NTf_2], regardless of whether silica is present. Therefore these peaks are due to the presence of water with the systems, and not due to a hydrogen bonding interaction between the ionic liquid and the silica nanoparticles

4.3.5 DLS Measurements

DLS measurements allowed size distribution of the nanoparticles in the ionic liquids to be measured. The intensity distributions of the sizes from the DLS measurements for all concentrations of silica in $[C_4mim][BF_4]$ showed one peak, indicating a uniform size distribution (figure 4.14). The nanoparticles cluster sizes determined by DLS measurements for $[C_4mim][BF_4]$ can be found in figure 4.15. A plot showing the scatter of this data can be found in appendix 3. The sizes observed in the DLS demonstrate that the silica nanoparticles have formed clusters. There is an overall decrease in the cluster size with increase in silica concentration. There is also a decrease in the distribution of the sizes of the clusters. At low silica concentrations, there is a wide variation in the cluster size, indicating that the clusters formed are not very uniform. At high silica concentrations, the clusters formed are smaller and more uniform. At 0.25 mole fraction of silica, there appears

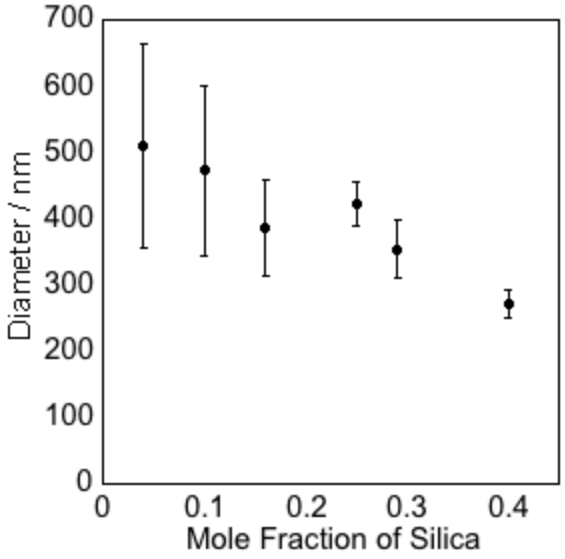

Figure 4.15: Plot of diameter against mole fraction of silica for $[C_4mim][BF_4]$.

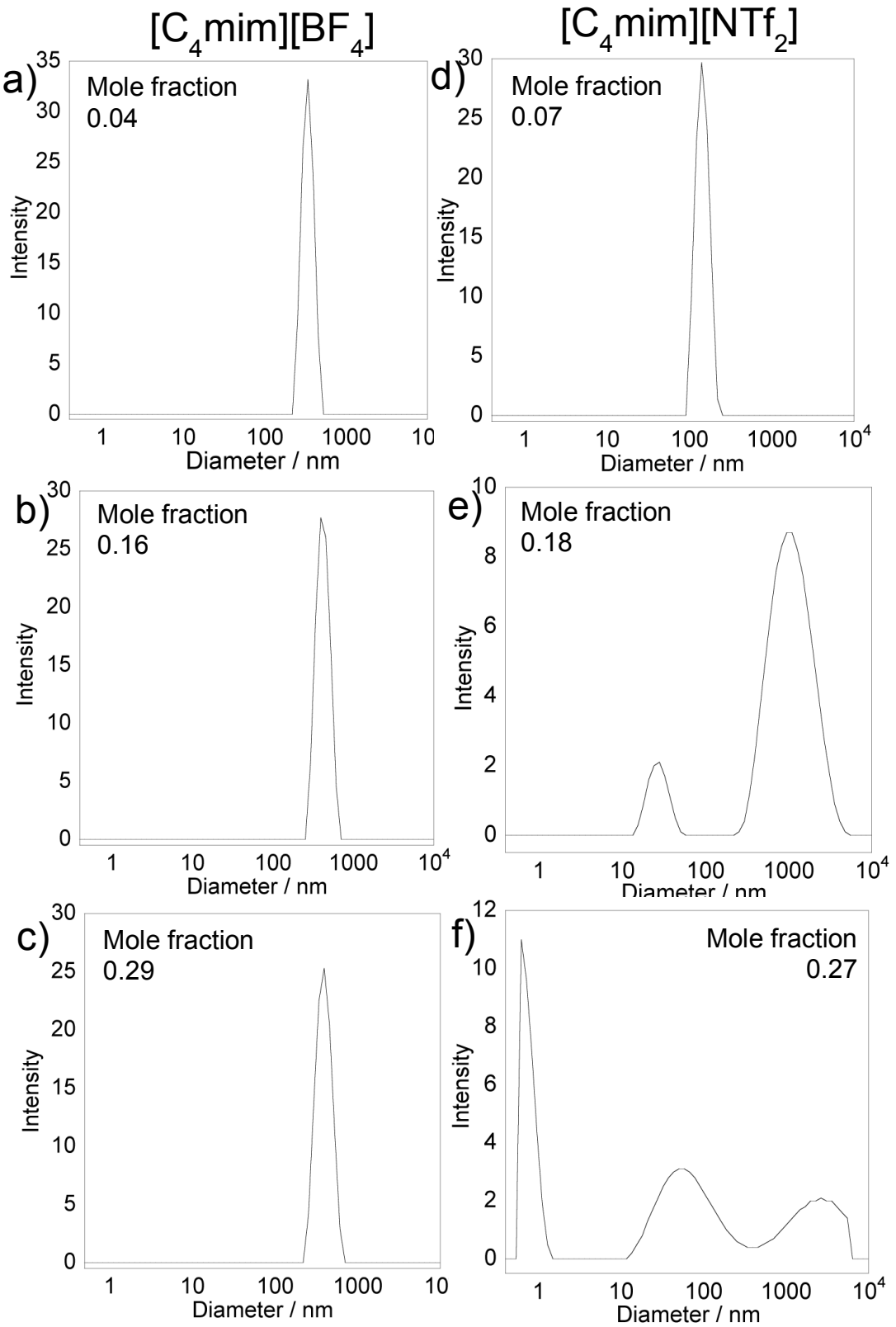

Figure 4.14: Plots of intensity against diameter for $[C_4mim][BF_4]$ with 0.04 (a), 0.16 (b) and 0.29 (c) mole fractions of silica and $[C_4mim][NTf_2]$ with 0.07 (d), 0.18 (e) and 0.27 (f) mole fractions of silica. The variation in these plots is shown in appendix 4.

to be an increase in the diameter size at the same time a reduction in the scatter. This is discussed below.

For suspensions of $[C_4mim][NTf_2]$ with more than 0.07 mole fraction of silica, multiple peaks were observed in the size distribution plots. Representative distributions at different concentrations are shown in figure 4.14. The distributions at similar mole fractions of silica are show for $[C_4mim][BF_4]$ to provide a comparison. The distribution for $[C_4mim][BF_4]$ shows a narrow distribution and one peak at all silica concentrations. The lowest concentration of silica in $[C_4mim][NTf_2]$ also shows a single, narrow distribution of particle sizes. However, at a mole fraction of 0.18, two broad size distributions are observed, indicating a wide range in the size of the clusters and the formation of larger structures. At the highest concentration of silica that was able to measured using DLS, large size distributions are observed. This suggests that the silica is completely interlinked as a 3D network, as has previously been observed using scanning electron microscopy.[17] This variation in the DLS data indicates that there is a fundamental difference in the structure of these systems formed by the different ionic liquids at the mesoscopic level that is also indicated in the very different rheological responses.

4.3.5.1 Effects of Sample Preparation

Figure 4.16 shows the DLS data for two samples of $[C_4mim][BF_4]$ with 0.10 mole fraction of silica, which were prepared by two different stirring methods. In previous chapters, the sample stirred with the magnetic stirrer bar showed Newtonian behaviour, whereas the sample stirred using a spatula showed shear thinning behaviour. When a spatula was used, smaller clusters of nanoparticles are observed in the DLS size distribution data, whereas the larger clusters of nanoparticles were formed when a magnetic stirrer bar was used. The formation of larger nanoparticle clusters could be due to the longer period of stirring giving the nanoparticles more time and more opportunities to aggregate and therefore the larger

clusters are formed. The Newtonian behaviour of this system implies that these larger clusters are a stable phase. Whereas, the smaller clusters formed when a spatula is used show a shear thinning response, which either indicates that these smaller clusters are less stable and are being broken up on the application of shear or that they are able to form layers that more easily move past each other, which also gives a shear thinning response. This requires further investigation.

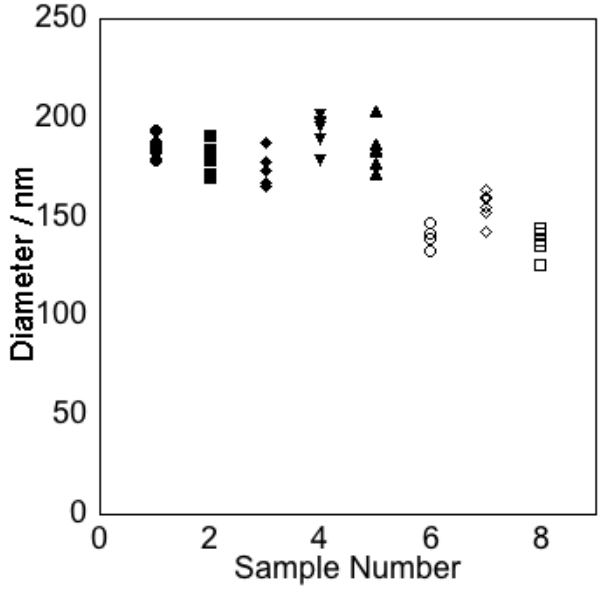

Figure 4.16: Plot of diameter against sample number for $[C_4mim][BF_4]$ with 0.10 mole fraction of silica. Filled markers – stirred with a magnetic stirrer. Empty markers – stirred using a spatula.

4.4 Discussion

4.4.1 $[C_4mim][BF_4]$ with hydrophilic silica nanoparticles

NMR relaxation measurements have been used to study the interaction between the ionic liquids and the silica nanoparticles. There was little change in the ^{19}F NMR T_1 relaxation times with increase in silica concentration in all of the ionic liquids, suggesting that there was little change in the tumbling of the anions and hence there is no detectable interaction between the anion and the silica. The protons on alkyl chain attached to the imidazolium ring

showed the same trend. However, T_1 relaxation times for the protons located on the imidazolium ring, H(4/5), decreased with increasing silica concentration. This likely to be real as the cations are small molecules and therefore will have a fast correlation time, so a slowing of the correlation time would lead to a decrease in T_1 (see figure 2.11). This shows that the tumbling of these protons is slowing in the presence of silica, indicating that they are interacting with the silica nanoparticles. This is observed for all four ionic liquids over the same increase in silica concentration, which implies that there is the same association between the cations and the silica, regardless of which anion is present. This is consistent with other findings.[18] This contrasts with the rheology of these systems, where suspensions of ionic liquids with different anions show different rheological behaviour. This shows that the behaviours of these systems is more complex than just the anion interaction with the silica nanoparticles.

At low silica concentrations, below 0.16 mole fraction of silica, suspensions of both $[C_4mim][BF_4]$ and $[C_4mim][NTf_2]$ show shear thinning behaviour. Below this silica concentration, they also show the same relative decrease in cation and anion diffusion coefficient. In addition, suspensions of both show a single size distribution in the DLS data. This single size distribution corresponds to a diameter of ca. 500 nm in $[C_4mim][BF_4]$ and ca. 400 nm in $[C_4mim][NTf_2]$. The nanoparticles have a diameter of 12 nm so this size distribution shows clusters of nanoparticles having formed in the ionic liquids. The rheology and DLS measurements at these concentrations imply suspensions of silica in both ionic liquids are behaving in the same way by forming a fluid of clusters. The clusters of silica nanoparticles reorganise over time to minimise their free energy and hence after a few days these low silica concentration suspensions are observed to phase separate into a clear upper phase and a cloudy lower phase.[32]

Above 0.18 mole fraction of silica in $[C_4mim][NTf_2]$, shear thinning behaviour is still observed in the rheology. However, multiple peaks are observed in the DLS size distribution. There is also an increase in the diffusion coefficient observed for both the cations and the

anions, indicating a change in the underlying structure of the system. At higher silica concentrations, the silica aggregates into networks leading to silica rich and silica poor regions being formed.[33] These areas of different density mean that the sample starts to undergo phase separation.[33] However, the phase separation is interrupted and the system undergoes spinodal decomposition to a dynamically arrested state of a space spanning gel network.[34] The particle network is kinetically stable in this arrested state.[35]

A gel can be described as a low density, disordered arrested state that possesses solid like properties, such as a yield stress.[35] This is observed in the rheology data for $[C_4mim][NTf_2]$ with silica nanoparticles. This space spanning gel network is the cause of the large increase in zero shear viscosity observed in these systems.[36] When these samples are placed under shear, this breaks the gel network, reducing the viscosity and hence leading the shear thinning that is observed. The formation of this 3D network can also be observed in the multiple peaks in the DLS size distributions, as the silica aggregates link with one another. These indicate a space spanning network has been formed which is characteristic of a colloidal gel.[37]

While suspensions of silica and $[C_4mim][NTf_2]$ go through a gel transition, $[C_4mim][BF_4]$ with silica nanoparticles undergoes a glass transition. The main difference is that gel arrest occurs when a space spanning mechanism is formed whereas glasses are local cages of nanoparticles formed through short range bonds and repulsion.[35] These are both forms of jamming transitions, which are where the dynamics of the suspended particle are arrested and are controlled by the volume fraction, the size of the particles and the internal energy of the system.[36, 38, 39] The only difference between these systems is the anion of the ionic liquid – silica nanoparticles have been theoretically calculated to be slightly more stable in $[C_4mim][NTf_2]$ than in $[C_4mim][BF_4]$, leading to the formation of different metastable structures.[10, 39]

At a silica mole fraction of 0.25 in $[C_4mim][BF_4]$, a slight increase in the cluster size is observed in the DLS data, along with a decrease in the distribution of the cluster sizes. This

also corresponds with a similar change in the diffusion coefficients; a slight increase in the cation and anion diffusion coefficient is observed. This increase is due the reduced silica surface when there are larger cluster sizes. Above this silica concentration, the anion diffusion coefficient shows little change, whilst the cation diffusion coefficient keeps on decreasing with further increases in silica concentration. This change observed in the DLS and diffusion data also corresponds to where the rheological behaviour of these suspensions changes from shear thinning or Newtonian to shear thickening, indicating a change in the underlying structure of this system.

At higher silica concentrations in $[C_4mim][BF_4]$, discreet clusters are still observed as evidenced by the single peak in the DLS size distributions. At these silica concentrations, the system undergoes a glass transition, whereby the clusters are trapped in cages, either by repulsion or the overall large solid volume.[37] Glass and liquid phases are structurally similar but dynamically different.[40] In a stable glass structure, neighbouring clusters trap each other into caged structures, forming a regular structure.[37] This means particle movements are restricted as the motion of the particles can only take place with a collective rearrangement of the particles forming the cage to allow a passage for the arrested particles.[33] The formation of a glass occurs before the formation of colloid-rich and colloid-poor regions and therefore the glass transition interrupts the phase separation that occurs in dense regions by the spinodal mechanism.[40]

Suspensions in $[C_4mim][BF_4]$ appear to undergo a glass transition above a silica mole fraction of 0.16.[37] After the glass transition, the cation diffusion coefficient is reduced with increasing silica concentration, as it is interacting with the silica surface. Whereas, the anions are able to freely diffuse in and amongst the clusters after the transition, hence the little change in their diffusion coefficients once this transition has occurred. The clusters of silica nanoparticles are able to move past each other at low shear rates, hence the small increase in viscosity, compared to $[C_4mim][NTf_2]$ suspensions, and the Newtonian behaviour observed. The slight shear thinning that is observed for $[C_4mim][BF_4]$ with 0.40 mole fraction

of silica at low shear rates could be due to the ordering of the clusters in layers which then can more easily move past each other. At a critical shear rate, the clusters to collide, hence the shear thickening effect observed in these systems.

The glass state formed by high silica concentrations in $[C_4mim][BF_4]$ is stable over longer periods of time, as the repulsion between the clusters prevents them from aggregating.[41, 42] Normally, an increase in volume fraction would lead to an increased cluster size, however, this is not observed here.[41, 43] A decrease in cluster size is related to an increase in short range interactions, which again is not observed here.[43] More investigation into these systems is required to determine the cause of this decrease in cluster size with increasing silica concentration.

It has previously been reported that $[C_4mim][NTf_2]$ forms a colloidal gel on the addition of bare silica nanoparticles, where the nanoparticles form a space spanning network.[3] $[C_4mim][BF_4]$ has not previously been reported to form a fluid of clusters, though the rheological behaviour has been previously detailed.[1, 10, 44] Practically there is not a well-defined difference between a gel and glass, as they are both jammed states that have restricted particle movements.[39] These jammed states are formed because colloidal suspensions are not thermodynamically stable as the energy would be lower in a simple solid. However they become trapped in kinetically arrested states.[39, 40] Only the anion is different between the ionic liquids, so it is the difference in the ionic liquid caused by the anion that affects the stability of the silica and hence different structures formed and the rheological behaviours observed. The behaviour at the glass and gel transitions is very similar, shown by the slowing down of the dynamics, observed in the diffusion data before the jamming is observed.[40] After this transition, suspensions of $[C_4mim][NTf_2]$ form a well-documented colloidal gel, with an interconnected network, which is broken to cause the shear thinning behaviour. The suspensions of $[C_4mim][BF_4]$ are more complicated as a colloidal glass-like state, consisting of nanoparticle clusters, is formed.

4.6 Conclusion

In this chapter, it is shown that the interactions between ionic liquids and the silica nanoparticles are not hydrogen bonds as previously reported, but an interaction between the imidazolium ring of the cation and the silica nanoparticles, regardless of the anion. At low silica concentrations, less than 0.10 mole fraction, these systems form metastable fluids of clusters, which can be characterised by the single peak in the DLS, shear thinning rheology and a similar decrease in the cation and anion diffusion coefficient. At higher silica concentrations, the ionic liquid suspensions undergo a jamming transition, determined by the ionic liquid. The ionic liquids with an NTf_2 anion form a colloidal gel, which is reflected in the slowing of the translational motion of the ions, as well as the increasing number of peaks in the DLS and the shear thinning rheology. A transition to a colloidal glass-like state of clusters is observed for the ionic liquids with a BF_4 anion, which allows the anions to move freely, while the cations are slowed by interactions with the silica. The repulsion, which causes the long-lived stability of these glass systems, is overwhelmed on the application of shear, causing the shear thickening rheology observed.

4.7 References

1. J. Qin, G. Zhang, X. Shi and M. Tao, *J Nano. Res.*, 2015, **17**, 333.
2. K. Ueno, S. Imaizumi, K. Hata and M. Watanabe, *Langmuir*, 2009, **25**, 825.
3. K. Ueno and M. Watanabe, *Langmuir*, 2011, **27**, 9105.
4. P. A. Hassan, S. Rana and G. Verma, *Langmuir*, 2015, **31**, 3.
5. J. A. Smith, O. Werzer, G. B. Webber, G. G. Warr and R. Atkin, *J Phys Chem Lett*, 2010, **1**, 64.
6. A. Wittmar, M. Gajda, D. Gautam, U. Dorfler, M. Winterer and M. Ulbricht, *J. Nano. Res.*, 2013, **15**, 12.
7. J. Smith, G. B. Webber, G. G. Warr and R. Atkin, *Langmuir*, 2014, **30**, 1506.

8. A. Wittmar, D. Ruiz-Abad and M. Ulbricht, *J. Nano. Res.*, 2012, **14**, 651.

9. A. Wittmar, D. Gautam, C. Schilling, U. Dorfler, W. Mayer-Zaika, M. Winterer and M. Ulbricht, *J. Nano. Res.*, 2014, **16**, 14.

10. K. Ueno, A. Iaba, M. Kondoh and M. Watanabe, *Langmuir*, 2008, **24**, 5253.

11. J. Qin, G. Zhang, Z. Ma, J. Li, L. Zhou and X. Shi, *RSC Adv.*, 2016, **6**, 81913.

12. P. Atkins and J. d. Paulo, *Atkins' Physical Chemistry*, 7th edn., Oxford University Press, New York, USA.

13. S. Cha, M. Ao, W. Sung, B. Moon, B. Ahlstrom, P. Johansson, Y. Ouchi and D. Kim, *Phys. Chem. Chem. Phys.*, 2014, **16**, 9591.

14. H. Yang, C. Z. Yu, Q. L. Song, Y. Y. Xia, F. Y. Li, Z. G. Chen, X. G. Li, T. Yi and C. H. Huang, *Chem. Mater.*, 2006, **18**, 5173.

15. J. Y. Kim, T. H. Kim, D. Y. Kim, N.-G. Park and K.-D. Ahn, *J. Power Sources*, 2008, **175**, 692.

16. S. Shimano, H. Zhou and I. Honma, *Chem. Mater.*, 2007, **19**, 5216.

17. K. Ueno, K. Hata, T. Katakabe, M. Kondoh and M. Watanabe, *J. Phys. Chem. B*, 2008, **112**, 9013.

18. M. Nayeri, M. T. Aronson, D. Bernin, B. F. Chmelka and A. Martinelli, *Soft Matter*, 2014, **10**, 5618.

19. X. Han and D. W. Armstrong, *Acc. Chem. Res.*, 2007, **40**, 1079.

20. K. S. Han, X. Q. Wang, S. Dai and E. W. Hagaman, *J. Phys. Chem. C*, 2013, **117**, 15754.

21. K. Hayamizu, S. Tsuzuki, S. Seki and Y. Umebayashi, *J. Phys. Chem. B*, 2012, **116**, 11284.

22. R. L. Vold, J. R. Waugh, M. P. Klein and D. E. Phelps, *J. Chem. Phys.*, 1968, **48**, 3831.

23. H. Carr and E. Purcell, *Phys. Rev.*, 1954, **94**, 630.

24. S. Meiboom and D. Gill, *Rev. Sci. Inst.*, 1958, **29**, 688.

25. P. T. Callaghan, *Translational dynamics and magnetic resonance: principles of pulsed gradient spin echo NMR*, Oxford University Press, Oxford, 2011.

26. S. W. Provencher, *Comp. Phys. Comm.*, 1982, **27**, 213.

27. S. W. Provencher, *Comp. Phys. Comm.*, 1982, **27**, 229.

28. S. J. Law, PhD Thesis, University of Birmingham, 2015.

29. M. Instruments, *Zetasizer Nano Series User Manual*, 2004.

30. P. T. Callaghan, *Principles of Nuclear Magnetic Resonance Microscopy*, Oxford University Press, New York, 1991.

31. J. Nordstrom, L. Aguilera and A. Matic, *Langmuir*, 2012, **28**, 4080.

32. V. N. Manoharan, *Science*, 2015, **349**, 942.

33. F. Sciortino and P. Tartaglia, *Adv. Phys.*, 2005, **54**, 471.

34. C. J. Dibble, M. Kogan and M. J. Solomon, *Phys. Rev. E*, 2008, **77**, 050401-I.

35. E. Zaccarelli, *J. Phys.-Condens. Mat.*, 2007, **19**, 323101.

36. V. Trappe, V. Prasad, L. Cipelletti, P. N. Segre and D. A. Weitz, *Nature*, 2001, **411**, 772.

37. J. R. Stokes and W. J. Frith, *Soft Matter*, 2008, **4**, 1133.

38. A. Hess, M. Pretzl, L. Heymann, A. Fery and N. Aksel, *Phys. Rev. E*, 2011, **84**, 031407.

39. V. J. Anderson and H. N. W. Lekkerkerker, *Nature*, 2002, **416**, 811.

40. P. J. Lu and D. A. Weitz, in *Annu. Rev. Condens. Matter Phys.*, ed. J. S. Langer, 2013, vol. 4, p. 217.

41. P. J. Lu, J. C. Conrad, H. M. Wyss, A. B. Schofield and D. A. Weitz, *Phys. Rev. Lett.*, 2006, **96**, 028306.

42. N. Kovalchuk, V. Starov, P. Langston and N. Hilal, *Adv. Colloid Interfac.*, 2009, **147**, 144.

43. T. H. Zhang, J. Klok, R. H. Tromp, J. Groenewold and W. K. Kegel, *Soft Matter*, 2012, **8**, 667.

44. J. Novak and M. M. Britton, *Soft Matter*, 2013, **9**, 2730.

5. Studying Local Rheological Behaviour Using Velocity Imaging

5.1 Introduction

In chapter 3, the bulk rheology of four different ionic liquids with varying concentrations of silica was studied using a cone and plate geometry in a rheometer. All of the neat ionic liquids showed Newtonian behaviour. Suspensions in $[C_2mim][NTf_2]$ and $[C_4mim][NTf_2]$ showed shear thinning behaviour at all silica concentrations investigated. This was proposed to be due to the breaking of networks of silica nanoparticles.[1] Evidence for the formation of these aggregated networks was observed using dynamic light scattering measurements in the previous chapter. Suspensions in $[C_2mim][BF_4]$ and $[C_4mim][NTf_2]$ showed shear thinning at low silica concentrations and shear thickening at high silica concentrations. It has been proposed that at high shear rates the silica nanoparticles form clusters that cause the increase in viscosity.[2] However, rheology is a bulk technique that provides an average of the behaviour over the sample.

To investigate the differences in rheological behaviour further, magnetic resonance velocity imaging has been used. This technique allows the rheological behaviour to be studied at a local level.[3, 4] This enables shear banding and shear localization to be directly observed.[4, 5] Shear banding occurs when unstable flow occurs in a sample, so it forms into different bands, which have different shear rates and different microstructures. These bands allows the sample to avoid the unstable regions of flow.[4] Shear banding has been observed in both colloidal gels and glasses.[6, 7]

Velocity imaging has previously been used to study $[C_4mim][BF_4]$ with hydrophilic silica nanoparticles.[5] Shear thickening was observed in both the bulk rheology and using velocity imaging. The degree of shear thickening was observed to increase with increase in shear rate. An ionic liquid with an NTf_2 anion, with the same silica nanoparticles, was also

studied.[5] The bulk rheology for this suspension showed a plateau in the flow curve, indicating unstable flow. Velocity imaging was used to demonstrate that the shear banding was responsible for the observed rheological behaviour.

In this chapter, $[C_4mim][BF_4]$ and $[C_4mim][NTf_2]$ have been investigated at selected silica concentrations using both bulk rheology measurements and magnetic resonance velocity imaging. As the anions appear to influence the rheological behaviour, comparing these two ionic liquids has allow the effects of the anion, and not the cation, to be studied, unlike previous studies.[5] Velocity imaging has allowed the flows of these systems to be investigated over a range of shear rates in a Couette cell. It has also allowed a comparison between the observed behaviour in bulk rheology and velocity imaging of rheology.

5.2 Experimental

5.2.1 Materials and Sample Preparation

1-butyl-3-methylimidazolium tetrafluoroborate, $[C_4mim][BF_4]$ (98 %) and 1-butyl-3-methylimidazolium bis(trifluoromethylsulfonyl)imide, $[C_4mim][NTf_2]$ (98 %) were obtained from Sigma Aldrich, UK and used without further purification. Aerosil 200 silica nanoparticles (Evonik, Germany) have a diameter of 12 nm, a surface area of 200 ± 25 $m^2 g^{-1}$ and Si-OH surface functionalisation. Aerosil 200 was dried overnight at 70 °C in a vacuum oven prior to use. Aerosil 200 was dispersed in $[C_4mim][BF_4]$ at concentrations from 0 to 10% wt. (0.29 mole fraction) and in $[C_4mim][NTf_2]$ from 0 to 5% wt. (0.28 mole fraction). The suspensions were stirred until they appeared homogeneous and placed in a vacuum oven overnight at least 70 °C to minimise the water content. Water content was monitored by observed the water peak in the ^1H NMR spectrum.

5.2.2 Magnetic Resonance Imaging Velocity Measurements

NMR velocity measurements were performed on a Bruker DMX 300 spectrometer, which has a ^{1}H resonance frequency of 300.13 MHz. Measurements were performed at a temperature of 20 ± 0.3 °C. Experiments were performed using a 25 mm ^{1}H birdcage radio-frequency resonator with a maximum gradient strength was 96 G cm^{-1}. A 90° pulse duration of ca. 20 μs was used. Velocity measurements were performed on fluid inside the annulus of a Couette cell, which had an inner cylinder with a radius, r_i, of 2.6 mm and an outer cylinder,r_o, with radius of 5.7 mm. The inner cylinder of the Couette cell was rotated using a drive shaft, which was controlled by a stepper motor (Bruker Rheo-NMR System). A pulsed gradient spin echo (PGSE) imaging sequence, with a 180° Gaussian pulse of 1000 μs with an attenuation of ca. 16.2 dB, was used to acquire velocity images.[8] Horizontal images were acquired with a slice thickness of 3 mm, field of view of 13 mm × 13 mm and a matrix size of 64 × 64 pixels, which gave a pixel size of 0.20 × 0.20 mm^2. The resolution was limited by the large spectral width of the ^{1}H resonances in the cations (figure 4.2). Velocity images were acquired at rotation rates, ω, of 0.5 – 4 Hz with gradient values from 0 to a maximum gradient, $\boldsymbol{G}_{max}$, which varied from 9.5 to 80 G cm^{-1}. 8 $\boldsymbol{q}$ steps were acquired for each experiment. Values of δ = 1 ms and Δ = 15 ms, as well as 8 dummy scans and a repetition time of 1 s were used. Velocity profiles were taken along the centre of the Couette cell. These were fitted to the power law equation (equation 2.28) in Kaleidagraph (Synergy, USA) to obtain values for power law exponent.[5, 8]

5.2.3 Rheometry

Rheometry measurements were performed on an AR-G2 rheometer (TA Instruments) with a cone and plate geometry. The measurements were performed at 20 ± 0.1 °C, with shear stress recorded logarithmically with 10 points per decade, between shear rates of 0.1 and

1000 s^{-1}. For the neat ionic liquids, a 60 mm diameter cone with a 2° angle was used. For the ionic liquid suspensions, a cone with a 20 mm diameter and a 2° angle was used.

5.3 Results and Discussion

5.3.1 Suspensions of [C_4mim][BF_4]

Velocity imaging experiments were performed to allow the rheology of these systems to be studied at the local level. The radial velocity profiles for [C_4mim][BF_4] with 0, 0.10, 0.25 and 0.29 mole fractions of silica are shown in figure 5.1. It can be observed in the radial

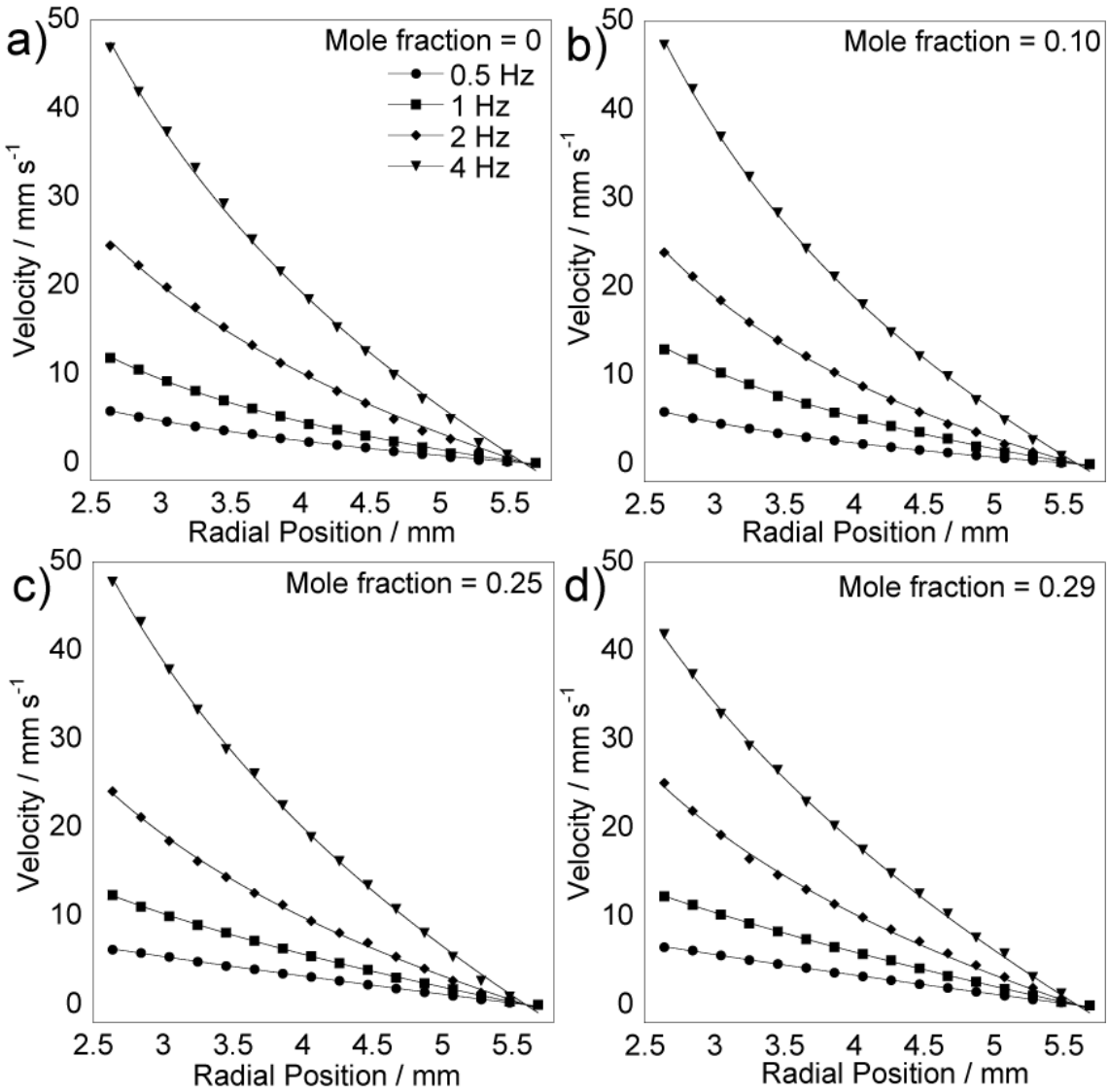

Figure 5.1: Radial velocity profiles across a Couette cell, showing a fit to the power law relationship (equation 4.1), for [C_4mim][BF_4] with 0 (a), 0.1 (b), 0.25 (c) and 0.29 (d) mole fractions of silica.

velocity profiles that there is no deviation from the power law model at any of the shear rates or in any of the concentrations of silica. The power law exponent values obtained from the radial velocity profiles are shown in figure 5.2, along with the bulk rheology measurements for these suspensions.

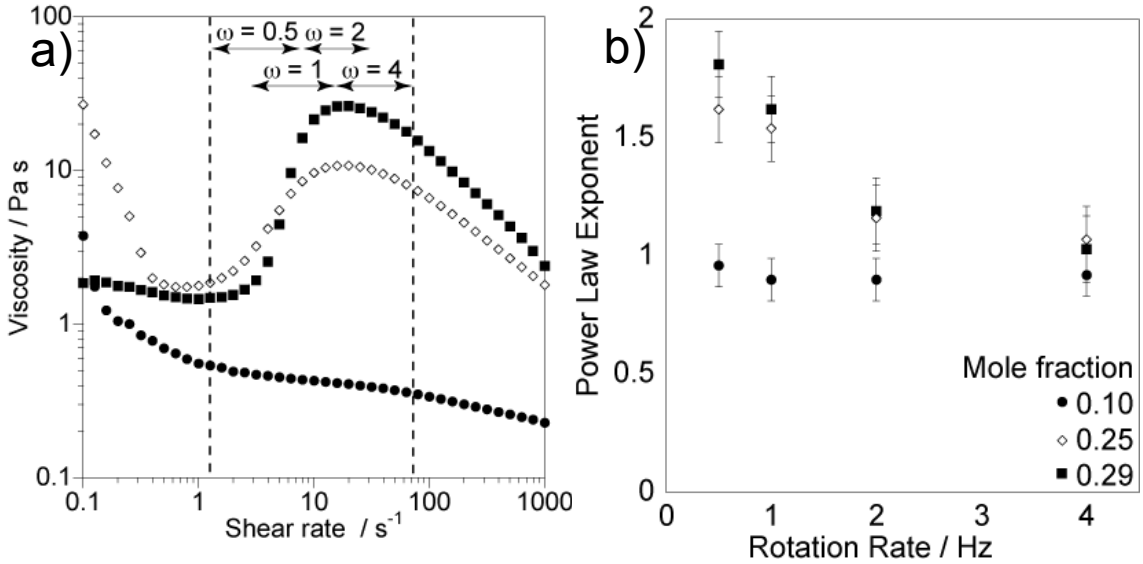

Figure 5.2: a) Plot of viscosity against shear rate and b) plot of power law exponent against rotational rate for $[C_4mim][BF_4]$ with 0.10, 0.25 and 0.29 mole fractions of silica. The range of shear rates accessed by the rotation rates in the Couette cell is shown. The calculation of these shear rates are described in appendix 6.

$[C_4mim][BF_4]$ with 0.10 mole fraction of silica shows a decrease in viscosity with an increase in shear rate, indicating that this suspension is shear thinning. The power law exponent values obtained from the velocity data are all below 1, also indicating shear thinning behaviour. These values for the power law exponent were all above 0.9, indicating that the suspension is only slightly shear thinning, and shows almost Newtonian behaviour. This is reflected in the bulk rheology measurements. Over the range of shear rates that are accessed in the Couette cell, shown on figure 5.2a, the curve observed for $[C_4mim][BF_4]$ with 0.10 mole fraction of silica is shallower than that observed at lower shear rates. This indicates that in this regime, the suspension is showing more Newtonian behaviour, reflected in the power law exponents. This shear thinning is most likely due to the ordering of the silica

nanoparticles into layers, which can easily move past each other causing a decrease in the viscosity or due to the breaking up of the small clusters that were observed in chapter 4.[9]

At the lowest shear rates accessed in the Couette cell, at rotational rates of ω = 0.5 and 1 Hz, suspensions of [C_4mim][BF_4] with 0.25 and 0.29 both show power law exponents that are greater than 1.5, indicating a high degree of shear thickening. This corresponds to the increase in viscosity with increase in shear rate observed between 1 s^{-1} and 10 s^{-1} for these suspensions in the bulk rheology. There is a larger increase in the viscosity for suspensions with a 0.29 mole fraction of silica, which is reflected in a higher power law exponent value for this suspension n = 1.8 and 1.6, compared with n = 1.6 and 1.5 for 0.25 mole fraction of silica (figure 5.2b). This shear thickening is due to aggregation of clusters into larger clusters, which cause the viscosity to increase. These clusters are transient and are constantly being formed and broken.[2, 10] At higher rotation rates in the Couette cell, there is a decrease in the power law exponent for both of these silica concentrations in [C_4mim][BF_4]. This reflects the bulk rheology as, at the shear rates accessed at rotation rates of ω = 2 and 4 Hz, there is little change in the viscosity. This decrease in the viscosity is due to the shear forces overwhelming the hydrodynamic forces that cause the formation of the clusters, causing the clusters to break and hence a decrease in the viscosity and the power law exponent values.[2, 10] The viscosity is still high as there is a balance between the forming and breaking of the clusters that cause the increase in viscosity. It is this balance which leads to power law exponent values of around 1 being observed at these shear rates, as the shear thinning and shear thickening effects cancel each other out, leading to overall Newtonian behaviour at the range of shear rates accessed at ω = 4 Hz. At the highest shear rates, the clusters are broken up completely, which leads to shear thinning behaviour at the highest silica concentration.[2]

These results show that there is a good match between the bulk rheology and velocity data, and demonstrate the sensitivity of the velocity imaging. As the data fits well to

the power law model, it indicates that the suspensions of $[C_4mim][BF_4]$ with silica are behaving as power law fluids. However, there is no variation in the data to indicate the differences between the shear thinning and shear thickening observed at different silica concentrations. The differences in structure that cause this different rheological behaviour, discussed in chapter 4 are not evident here.

5.3.2 Suspensions of $[C_4mim][NTf_2]$

Velocity imaging experiments were also performed for suspensions of $[C_4mim][NTf_2]$ with 0, 0.18 and 0.27 mole fractions of silica. The power law exponents from these experiments along with the bulk rheology are shown in figure 5.3. There was no change in the viscosity with increase in shear rate for the neat ionic liquid, indicating Newtonian behaviour (figure 5.3a). The power law exponent values for $[C_4mim][NTf_2]$ are all 1 ± 0.1 also demonstrate that the ionic liquid is Newtonian (figure 5.3b). The radial velocity profiles for this neat ionic liquid are shown in figure 5.4. The data show a good fit to the power law relationship.

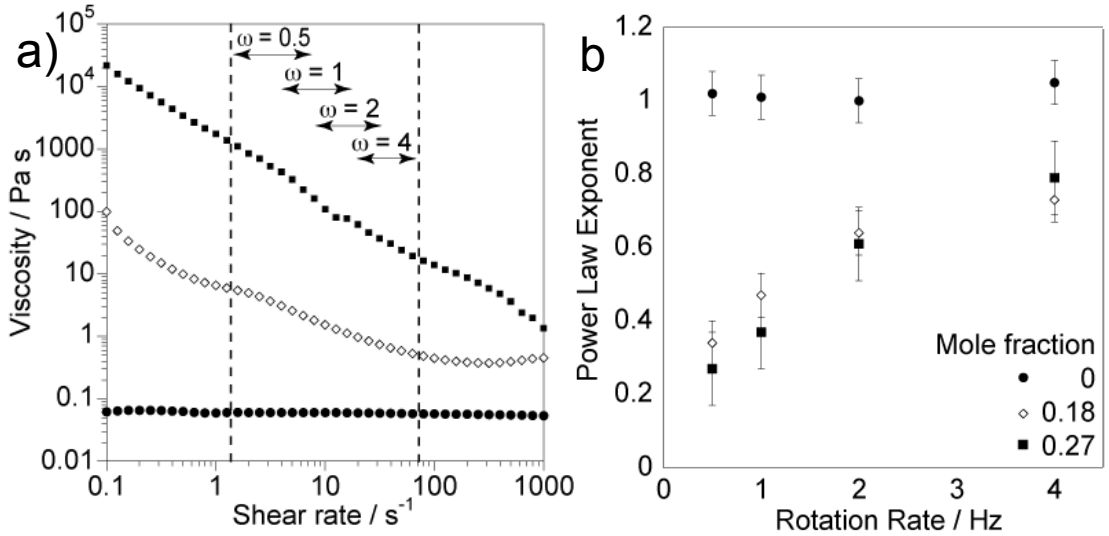

Figure 5.3: a) Plot of viscosity against shear rate and b) plot of power law exponent against rotational rate for $[C_4mim][NTf_2]$ with 0.18 and 0.28 mole fraction of silica. The range of shear rates accessed by the rotation rates in the Couette cell is shown.

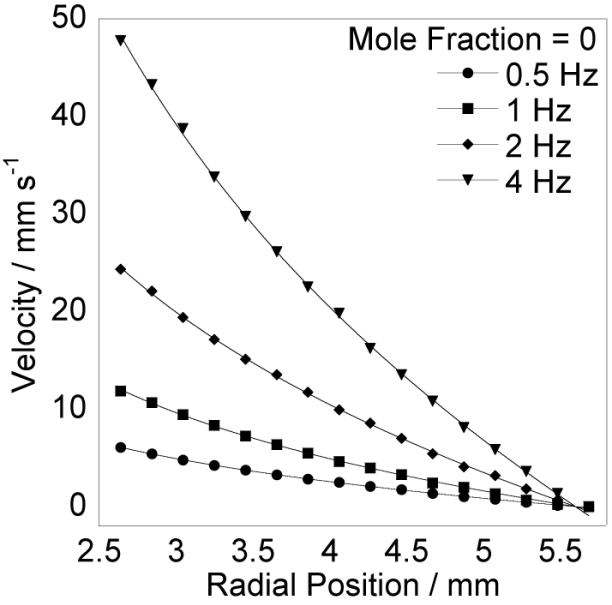

Figure 5.4: Radial velocity profiles across a Couette cell, showing a fit to the power law relationship (equation 2.28), for neat $[C_4mim][NTf_2]$.

Suspensions of $[C_4mim][NTf_2]$ with 0.18 and 0.27 mole fractions of silica both show a decrease in viscosity with increase in shear rate, showing these suspensions are shear thinning (figure 5.3a). The power law exponents obtained for these suspensions are all below 1, also indicating shear thinning behaviour. Therefore, these suspensions are showing the same behaviour in the rheology and the velocity imaging experiments. However, the power law exponent values for both of these suspensions increase with increasing rotation rates, indicating that the suspensions are showing more Newtonian behaviour at the higher shear rates accessed in the Couette cell. However, there is little change in the gradient of the curve for the viscosity observed in the bulk rheology over the range of shear rates that are accessed in the Couette cell. This implies that there is a subtlety to the rheology of these suspensions that is not being shown in the bulk rheology.

The radial velocity profiles for suspensions of $[C_4mim][NTf_2]$ with 0.18 and 0.27 mole fractions of silica are shown in figure 5.5. These appear to show a good fit to the power law equation. However, at a rotation rate of 3 Hz for $[C_4mim][NTf_2]$ with 0.27 silica mole fraction, it can be observed that there is not a good fit to the power law relationship. It can also be

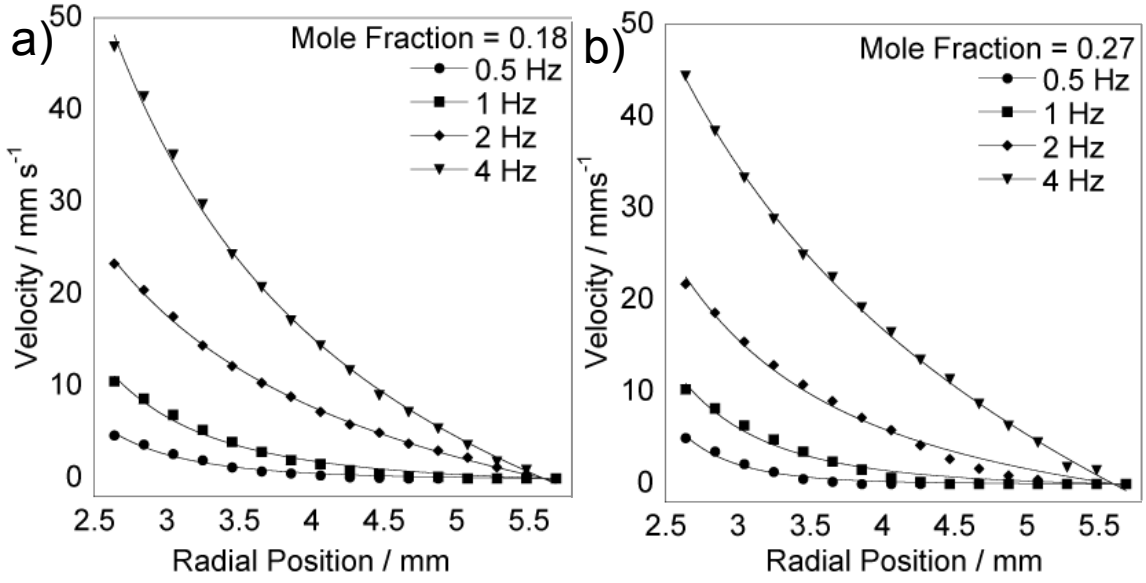

Figure 5.5: Radial velocity profiles across a Couette cell, showing a fit to the power law relationship (equation 2.28), for $[C_4mim][NTf_2]$ with 0.18 (a) and 0.28 (b) mole fractions of silica.

observed that the velocity of the suspensions at rotation rates of ω = 0.5 and 1 Hz, that the velocity of the fluids falls to 0 around a radial position of 4 to 4.5 mm. This indicates that the fluid is not flowing. A region of flow next to a region of no flow indicates there is shear localisation within these samples.[11]

Figure 5.6 shows these plots of velocity against radial position with an expanded scale. This allows the fits of the power law exponents to be more clearly shown. Above a rotational velocity of 2 Hz in 0.18 mole fraction of silica, and 4 Hz in 0.28 mole fraction of silica, a good fit to the power law relationship can be observed, indicating that the sample is flowing in a single regime across all the shear rates. However, there is not a good fit to the power law relationship for the other rotation rates. This is why there is not a good agreement be tween the bulk rheology and the power law exponent values. In these plots r_o has also used as a fitting parameter to see if the flowing part of the suspensions can be fitted to a power law relationship. There is still not a good fit, indicating the flowing part of this suspension is showing complex flow behaviour, as it cannot be described by a power law relationship.[12] This suggests that this system is undergoing shear banding. This shear

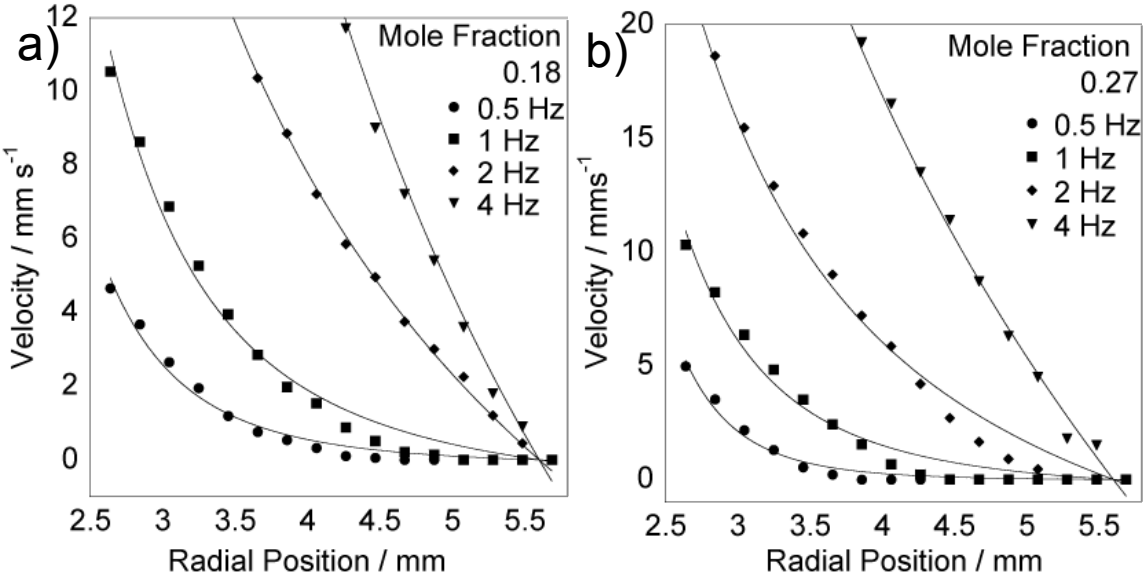

Figure 5.6: Radial velocity profiles across a Couette cell, showing a fit to the power law relationship (equation 2.28), for $[C_4mim][NTf_2]$ with 0.18 (a) and 0.28 (b) mole fractions of silica. The data shown is the same as figure 5.5 with an expanded scale.

banding occurs when the shear causes a region of instability. The material then splits into regions of different shear rates to avoid this unstable structure. This reorganisation then affects the flow behaviour.[13] Hence, it is this coupling that causes the non-linear flow behaviour to be observed. This has also been observed for a colloidal suspension of hydrophilic nanoparticles in an ionic liquid that has an NTf_2 anion, but a different cation.[5] More investigation is required to understand the cause of the complex shear behaviours in these systems. Also, different ionic liquids need to be investigated to explain why this is observed in these ionic liquids and whether it is only the NTf_2 anion where this is observed.

From these measurements, the cause of the differences in the rheological behaviour of these two systems is not clear. Why does one show shear thinning and shear banding and the other show shear thinning and shear thickening behaviour? Shear banding has previously been observed in colloidal systems, including both weakly and strongly flocculating system, as well as colloidal gels and glasses.[12] Macroscopic behaviour of suspensions is characterised by volume fraction, particle diameter and internal energy

between particles.[6] The only difference between these systems is the anion of the ionic liquid – the volume fraction and the particles used are the same. It has been previously calculated that the nanoparticles are unstable in the ionic liquids, regardless of their hydrophilicity.[14] More investigation is required into a wider range of ionic liquids so that the cause of the shear banding in these systems can be understood.

5.3.3 Effects of Sample Preparation

Two different samples of $[C_4mim][BF_4]$ containing 0.29 mole fraction of silica were prepared on the same day, using the same method and treated identically so that the variation in the rheological behaviour could be studied. The bulk rheology and the power law exponents from the velocity experiments for these samples are shown in figure 5.7. In the bulk rheology, figure 5.7a, it can be observed that these samples have different zero shear viscosities. The onset of shear thickening occurs at a different shear rate in these samples but the increase in viscosity observed during shear thickening is the same. The same viscosities are observed for these samples during the shear thinning regime at a shear rate of 100 s^{-1} and higher. This shows that the small differences in the samples have a discernable effect on the bulk rheology.

The difference in these samples can also be observed in the power law exponents extracted from the velocity data. Sample A shows a higher power law exponent at the lower rotational velocities, which corresponds well with the maximum shear thickening in the bulk rheology. Sample B has a lower viscosity maximum when shear thickening. The power law exponents for sample B are below 1 at the highest rotational velocities, ω = 4, indicating shear thinning, which correlates with the bulk rheology. The power law exponent for sample A is not less than 1 as the shear thinning regime is not reached in the range of shear rates accessed in the velocity experiment. These results indicate that the rheology of these samples is extremely sensitive to small variations in the samples. These variations can be

detected in bulk rheology and velocity imaging studies of these systems. In a previous study, it was shown that the shear thickening within suspensions of $[C_4mim][BF_4]$ and silica nanoparticles was reversible – the viscosity dropped as soon as the shear rate was below the critical value.[2] However, the repeatability of the critical shear rate within a sample has not been investigated. In general, the same critical shear stress is required for the same system, but more work needs to be done into the repeatability of these measurements of the same sample.

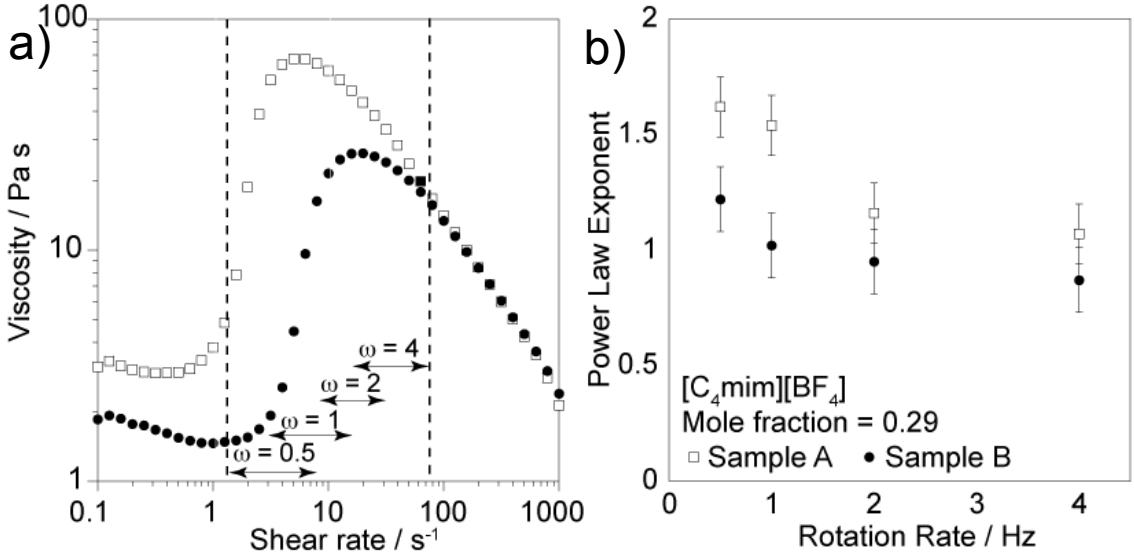

Figure 5.7: a) Plot of viscosity against shear rate for $[C_4mim][BF_4]$ with 0.29 mole fraction of silica and b) plot of power law exponent against rotational velocity data. The different shapes represent the different samples prepared. The range of shear rates accessed by the rotation rates in the Couette cell is shown.

The effect of different stirring methods on the rheological behaviour of the samples has been shown in previous chapters. Figure 5.8 shows the bulk rheology and the power law exponents from velocity experiments for two samples of $[C_4mim][BF_4]$ with 0.10 mole fraction of silica prepared by two different stirring methods. The sample prepared using a stirrer bar showed no change in viscosity with increase in shear rate, indicating Newtonian behaviour. The power law exponents obtained for this sample are all 1.0 ± 0.1, which also indicates

Newtonian behaviour. For the sample stirred using a spatula a higher zero shear viscosity was observed in the bulk rheology. A decrease in the viscosity in observed with an increase in shear rate, indicating shear thinning behaviour. The power law exponents are all less than 1, indicating shear thinning behaviour. This shows that both velocity imaging and bulk rheology are sensitive to the differences in the systems caused by the stirring method used.

In the previous chapter, dynamic light scattering measurements were used to show that larger silica nanoparticle cluster sizes are observed when the sample is prepared using a magnetic stirrer bar. This is possibly due to the stirring using a magnetic stirrer bar giving the clusters more time to form. However, it is unclear as to why this causes Newtonian behaviour and the smaller cluster sizes show shear thinning behaviour. This requires further investigation, such as dynamic light scattering measurements of the suspensions under shear, to understand what is causing the differences in rheological behaviour.

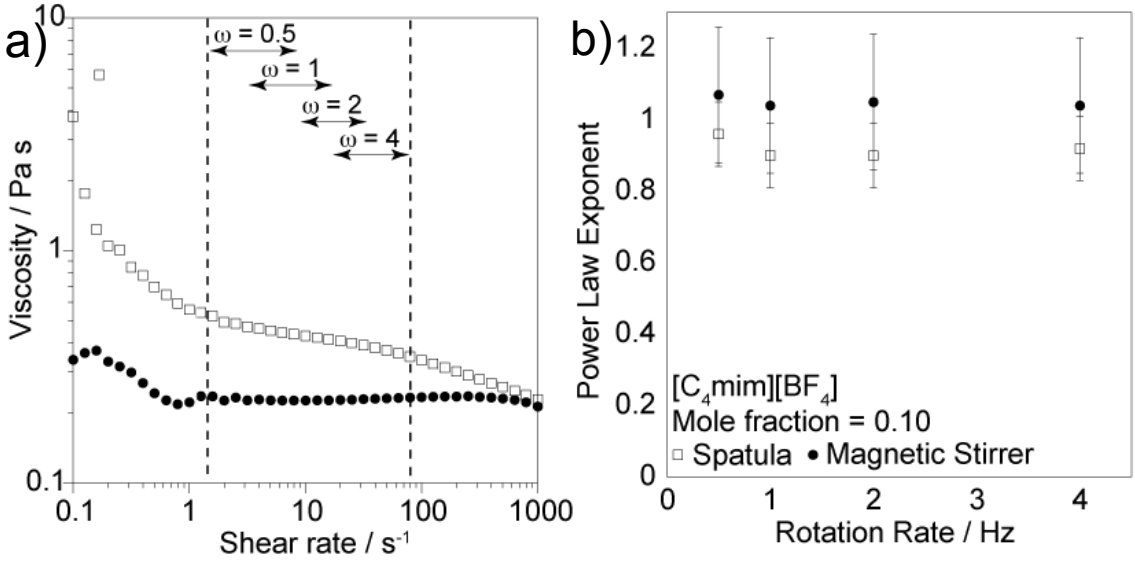

Figure 5.8: a) Plot of viscosity against shear rate for $[C_4mim][BF_4]$ with 0.10 mole fraction of silica and b) plot of power law exponent against rate for $[C_4mim]\{BF_4]$. Filled circles - sample stirred using magnetic stirrer bar. Open squares – sample stirred using spatula. The range of shear rates accessed by the rotation rates in the Couette cell is shown.

5.4 Conclusion

Colloidal suspensions of two ionic liquids with the same cation and different anions have been studied under shear, using magnetic resonance velocity imaging. $[C_4mim][NTf_2]$ silica suspensions demonstrated possible shear banding at lower shear rates in the Couette rates, indicating that these systems demonstrate complex rheology. In the future other ionic liquids with NTf_2 anions should be studied to see if this shear banding is a function of this anion. The data from $[C_4mim][BF_4]$ showed the shear thinning at low silica concentrations and shear thickening at high concentrations in both the bulk rheology and the magnetic resonance velocity experiments. It was shown that the rheological behaviour of these samples depends on the way they are prepared. Velocity imaging has allowed the localised rheology of these suspensions to be studied, but further investigation is required to understand the structures of these suspensions under shear.

5.5 References

1. K. Ueno and M. Watanabe, *Langmuir*, 2011, **27**, 9105.
2. J. Qin, G. Zhang, X. Shi and M. Tao, *J Nano. Res.*, 2015, **17**, 333.
3. M. M. Britton and P. T. Callaghan, *Magn. Reson. Chem.*, 1997, **35**, 37.
4. P. T. Callaghan, *Rheo. Acta*, 2008, **47**, 243.
5. J. Novak and M. M. Britton, *Soft Matter*, 2013, **9**, 2730.
6. A. Hess, M. Pretzl, L. Heymann, A. Fery and N. Aksel, *Phys. Rev. E*, 2011, **84**, 031407.
7. P. C. F. Møller, S. Rodts, M. A. J. Michels and D. Bonn, *Phys. Rev. E*, 2008, **77**, 041507-I.
8. P. T. Callaghan, *Translational dynamics and magnetic resonance: principles of pulsed gradient spin echo NMR*, Oxford University Press, Oxford, 2011.

9. H. Watanabe, M. L. Yao, K. Osaki, T. Shikata, H. Niwa, Y. Morishima, N. P. Balsara and H. Wang, *Rheo Acta*, 1998, **37**, 1.

10. X. Cheng, J. H. McCoy, J. N. Israelachvili and I. Cohen, *Science*, 2011, **333**, 1276.

11. P. Coussot, L. Tocquer, C. Lanos and G. Ovarlez, *J. Non-Newton. Fluid* 2009, **158**, 85.

12. P. Coussot, J. Raynaud, F. Bertrand, P. Moucheront, J. Guilbaud, H. Huynh, S. Jarny and D. Lesueur, *Phys. Rev. Lett.*, 2002, **88**, 218301-I.

13. S. M. Fielding, *Rep. Prog. Phys.*, 2014, **77**, 102601.

14. K. Ueno, A. Iaba, M. Kondoh and M. Watanabe, *Langmuir*, 2008, **24**, 5253.

6. Comparing Suspensions of Hydrophilic and Hydrophobic Nanoparticles

6.1 Introduction

In the previous chapters, the behaviour of hydrophilic silica nanoparticles has been studied in four ionic liquids, with focus on comparing suspensions in the hydrophilic ionic liquid [C_4mim][BF_4] with those in the hydrophobic ionic liquid [C_4mim][NTf_2]. It was shown, using NMR relaxation measurements, that in all of the ionic liquids it is the imidazolium ring of the cation that interacts with the hydrophilic silica. DLS and rheology measurements were used to demonstrate that at low silica concentrations, the nanoparticles were forming a fluid of clusters in both [C_4mim][BF_4] and [C_4mim][NTf_2]. At above 0.20 silica mole fractions, the suspensions underwent a jamming transition. [C_4mim][BF_4] suspensions showed one peak in the DLS size distribution, corresponding to a cluster of nanoparticles, indicating that these suspensions had formed a glass-like state consisting of nanoparticle clusters. [C_4mim][BF_4] suspensions also demonstrate shear thickening rheology at silica mole fractions above 0.20. Whereas, suspensions of [C_4mim][NTf_2] demonstrated shear thinning rheology at all silica concentrations. They showed a large increase in the zero shear viscosity as the silica concentration increased and large distributions of nanoparticles were present in the DLS particle size distributions, suggesting that suspensions in [C_4mim][NTf_2] formed a colloidal gel at high silica concentration.

In this chapter, hydrophobic nanoparticles of the same size, 12 nm, have been studied in [C_4mim][BF_4] and [C_4mim][NTf_2]. The comparison of hydrophilic and hydrophobic interactions with ionic liquids is important in applications such as energy storage, where silica and carbon electrodes are often used. The interaction between ionic liquids with the hydrophilic silica and the hydrophobic carbon need to be characterised so that the electrochemical reactions can be understsood.[1] Also, ionic liquids can be used to extract

hydrophobic nanoparticles from organic solvents, such as oil, by providing a preferential environment for hydrophobic nanoparticles, such as sand.[2] The interactions between the hydrophobic nanoparticles and the ionic liquids need to be understood so that the ionic liquid that is most attractive to the hydrophobic nanoparticles can be identified.[2] Also, if water sensitivity is a problem in solid-state electrolytes, hydrophilic nanoparticles can make the system more hydrophilic. By using hydrophobic ionic liquids in a hydrophobic ionic liquid, it can make the system less hygroscopic, which is a major problem for applications of ionic liquids.

In previous studies[3-5], rheology has been used to compare suspensions of ionic liquids with hydrophilic and hydrophobic nanoparticles. Suspensions of hydrophobic nanoparticles in hydrophilic ionic liquids ($[C_2mim][BF_4]$, $[C_4mim][BF_4]$ and $[C_6mim][BF_4]$) have been observed to show shear thinning behaviour.[3-5] This indicates that the hydrophobic nanoparticles are unstable in the hydrophilic ionic liquids.[3-5] This same behaviour is observed when hydrophilic nanoparticles are suspended in hydrophobic ionic liquids.[6, 7] This shear thinning implies that the silica nanoparticles have not been stabilised in the ionic liquids. The instability of these nanoparticles is most likely due to the difference in hydrophobicity between the ionic liquids and the nanoparticles. When low concentrations of hydrophobic nanoparticles are suspended in hydrophobic ionic liquids, Newtonian behaviour is observed. Also, these suspensions demonstrate a single distribution of nanoparticles in DLS particle size distribution measurements, indicating that the nanoparticles had been stabilised.[4, 5] However, above hydrophobic nanoparticle concentrations of 2 wt. %, shear thinning behaviour is observed, indicating that the nanoparticles are not stabilised in the ionic liquid and hence forming aggregates that are broken on the application of shear thinning.[7] This seems to show that hydrophobic ionic liquids can only stabilise hydrophobic nanoparticles at concentrations less than 5 wt. %. This is explored in this chapter.

Suspensions of hydrophobic silica nanoparticles were prepared in the ionic liquids $[C_4mim][BF_4]$ and $[C_4mim][NTf_2]$ at a range of silica concentrations. The bulk behaviour of

these suspensions has been studied using rheometry and magnetic resonance velocity imaging. IR spectroscopy and NMR relaxation measurements have been used to study the interaction between the nanoparticles and the ionic liquids. Size distributions of the suspensions from DLS measurements have been used to characterise the structures formed by the hydrophobic nanoparticles in the ionic liquids. These findings have been compared with the behaviour of suspensions of hydrophilic nanoparticles that have been studied in the previous chapters.

6.2 Experimental

6.2.1 Materials and Sample Preparation

1-butyl-3-methylimidazolium tetrafluoroborate, $[C_4mim][BF_4]$ (98 %) and 1-butyl-3-methylimidazolium bis(trifluoromethylsulfonyl)imide, $[C_4mim][NTf_2]$ (98 %) were obtained from Sigma Aldrich, UK and used without further purification. Aerosil R104 silica nanoparticles (Evonik, Germany) had a diameter of 12 nm, a surface area of 150 ± 25 g cm^{-1} and CH_3 surface functionalisation. Aerosil R104 was dispersed in $[C_4mim][BF_4]$ at concentrations from 0 to 10% wt. % (0.29 mole fraction) and in $[C_4mim][NTf_2]$ at concentrations from 0 to 10% wt. (0.45 mole fraction). The suspensions were stirred until they appeared homogeneous and placed in a vacuum oven overnight at least 70 °C to minimise the water content. Water content was monitored by observing the water peak in the ^1H NMR spectrum.

6.2.2 Rheometry

Rheometry measurements were performed on an AR-G2 rheometer (TA Instruments) with a cone and plate geometry. The measurements were performed at 20 ± 0.1 ^oC, with shear stress recorded logarithmically with 10 points per decade, between shear rates of 0.1 and

1000 s^{-1}. For the neat ionic liquids, a 60 mm diameter cone with a 2° angle was used. For the ionic liquid suspensions, a cone with a 20 mm diameter and a 2° angle was used.

6.2.3 Magnetic Resonance

All NMR measurements were performed on a Bruker DMX 300 spectrometer, which has a ^{1}H NMR resonance frequency of 300.13 MHz and a ^{19}F NMR resonance frequency of 282.37 MHz. All measurements were performed at 20 ± 0.3 °C. All data was analysed using Prospa (Magritek, New Zealand).

6.2.3.1 T_1 Relaxation Measurements

^{1}H and ^{19}F NMR relaxation measurements were performed by placing samples in a 5 mm tube inside a 10 mm ^{1}H or ^{19}F resonator of a Bruker Diff30 probe. A 90° pulse duration of ca. 45 µs was used during the ^{1}H NMR experiments. For the ^{19}F NMR experiments, a 90° pulse duration of ca. 30 µs were used. An inversion recovery sequence was used to measure T_1 relaxation times.[8] 16 k points for ^{1}H NMR measurements and 32 k points for ^{19}F NMR measurements were collected with 8 signal averages and a spectral width of 10 kHz. A variable delay list with 20 points logarithmically spaced between 5 ms to 6 s or 8 s (ensuring that the repetition time was ≥ 5 × T_1) was used. T_1 values were obtained by curve fitting (equation 2.19) in Kaleidagraph (Synergy, USA). Each measurement was repeated at least three times and the error determined from an analysis of the variation in the value obtained for a given system.

6.2.3.2 Velocity Imaging Measurements

Velocity imaging experiments were performed using a 25 mm ^{1}H birdcage radio-frequency resonator with a maximum gradient strength was 96 G cm^{-1}. A 90° pulse duration of ca.

20 μs was used. Velocity measurements were performed on fluid inside the annulus of a Couette cell, which had an inner cylinder with a radius, r_i, of 2.6 mm and an outer cylinder,r_o, with radius of 5.7 mm. The inner cylinder of the Couette cell was rotated using a drive shaft, which was controlled by a stepper motor (Bruker Rheo-NMR System). A pulsed gradient spin echo (PGSE) imaging sequence, with a 180° Gaussian pulse of 1000 μs and an attenuation of ca. 16.2 dB, was used to acquire velocity images.[9] Horizontal images were acquired with a slice thickness of 3 mm, field of view of 13 mm × 13 mm and a matrix size of 64 × 64 pixels, which gave a pixel size of 0.20 × 0.20 mm^2. The resolution was limited by the large spectral width of the ^1H resonances in the cations (figure 4.2). Velocity images were acquired at rotation rates, ω, of 0.5 – 4 Hz with gradient values from 0 to a maximum gradient, $\boldsymbol{G}_{max}$, which varied from 9.5 to 80 G cm^{-1}. 8 $\boldsymbol{q}$ steps were acquired for each experiment. Values of δ = 1 ms and Δ = 15 ms, as well as 8 dummy scans and a repetition time of 1 s were used. Velocity profiles were taken along the centre of the Couette cell. These were fitted to the power law equation (equation 2.28), using curve fitting in Kaleidagraph to obtain values for power law exponent.[9, 10]

6.2.4 IR Measurements

A Perkin-Elmer Spectrum 100 FT-IR spectrometer was used to record IR spectra between 4000 cm^{-1} and 650 cm^{-1}, with 4 signal averages. IR spectra were recorded for $[C_4mim][BF_4]$ with 0 and 5 % wt. silica (0.16 silica mole fraction) and $[C_4mim][NTf_2]$ with 5% wt. silica (0.26 silica mole fraction). Water was added drop wise to these systems, with each drop of water equivalent to ca. 2 % volume. An IR spectrum was recorded for each additional drop of water.

6.2.5 DLS Measurements

DLS measurements were performed on a Zetasizer Nano ZS (Malvern Instruments, UK). The samples were allowed to equilibrate at 20.0 °C for 60 seconds and the data was accumulated for 120 seconds with 6 repetitions. A refractive index of 1.42, viscosity of 99.6 mPa s and a dielectric constant of 11.7 were used for measurements of $[C_4mim][BF_4]$ suspensions.[11] A refractive index of 1.43, viscosity of 49.9 mPa s and a dielectric constant of 11.5 were used for measurements of $[C_4mim][NTf_2]$ suspensions.[11] The time domain correlation method was used with CONTIN analysis, which applies a constrained of the inverse Laplace transformation to generate the particle sizes.[12-14] The intensity distribution is reported.[15] The experiments were repeated three times for each silica mole fraction recorded. The error was determined by calculating the standard deviation of the values obtained.

6.3 Results

6.3.1 Rheology

The rheology for $[C_4mim][BF_4]$ with hydrophobic silica is shown in figure 6.1. All suspensions in $[C_4mim][BF_4]$ are shear thinning, which implies the hydrophilic ionic liquid is not able to stabilise the hydrophobic silica nanoparticles. This is most likely due to the repulsion between the hydrophilic ionic liquid and the hydrophobic nanoparticles. At the mole fractions of 0.25 and above, a yield stress can be observed in the materials, indicating that a gel may have been formed. Up to a silica mole fraction of 0.25 in $[C_4mim][BF_4]$, an increase of more than an order of magnitude is observed in the viscosity with each silica concentration. This large change in the viscosity indicates that the hydrophobic silica is unstable and forming aggregates.[16] Above a silica mole fraction of 0.25, an increase is still

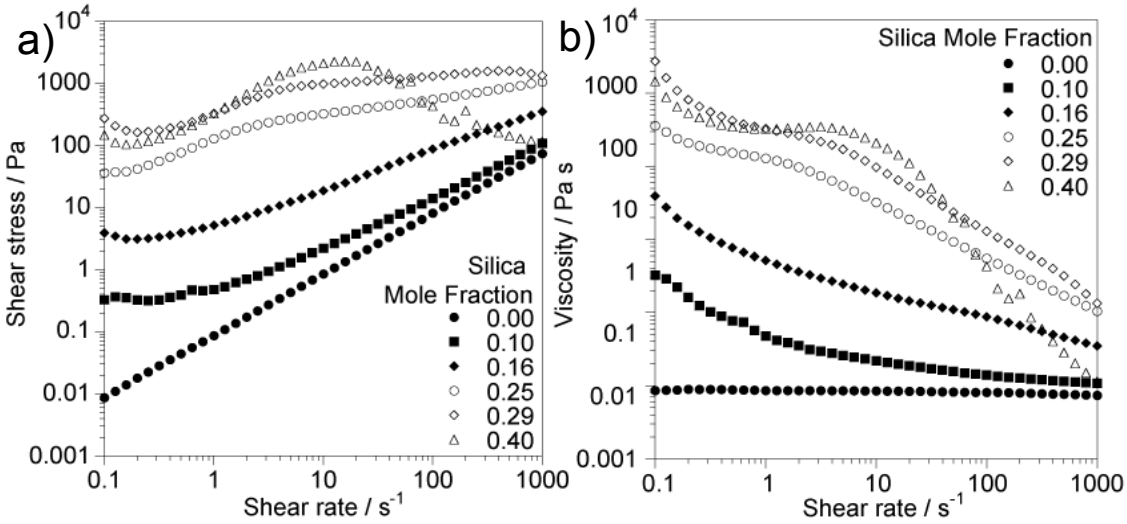

Figure 6.1: Plots of shear stress against shear rate (a) and viscosity against shear rate (b) for $[C_4mim][BF_4]$ with hydrophobic silica.

observed in the viscosity but this is much smaller. This indicates that the aggregated structures are still forming, but they are trapping about the same amount of ionic liquid; therefore at these concentrations of silica, similar structures are being formed.

The rheology for $[C_4mim][NTf_2]$ with hydrophobic silica is shown in figure 6.2. At low hydrophobic silica concentrations, 0.18 and 0.27 silica mole fractions, suspensions in $[C_4mim][NTf_2]$ behave like a Newtonian fluid. This indicates that these systems are stable. At shear rates above 10 s^{-1} for $[C_4mim][BF_4]$ with 0.27 mole fraction of hydrophobic silica, a decrease in the viscosity is observed with the increase in shear rate, indicating shear thinning behaviour. At a silica mole fraction of 0.39 and above, shear thinning behaviour is observed across all shear rates, indicating that the suspensions are not stable. This is most likely due to the formation of a flocculated structure, which is then broken on the application of shear to provide the shear thinning behaviour. These higher mole fractions of silica also show a yield stress, indicating the formation of a gel.

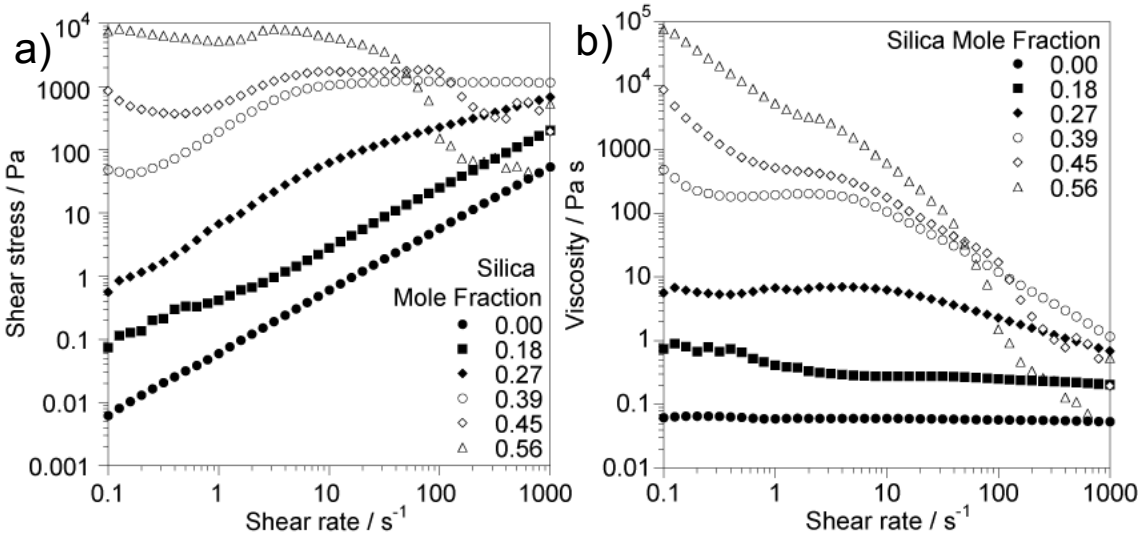

Figure 6.2: Plots of shear stress against shear rate (a) and viscosity against shear rate (b) for [C_4mm][NTf_2] with hydrophobic silica.

6.3.2 Velocity Imaging

Velocity imaging experiments were performed to allow the rheology of these systems to be studied at a local level. The radial velocity profiles for [C_4mim][BF_4] with 0.10 and 0.29 mole fractions of silica are shown in appendix 7. The power law exponent values obtained from these radial velocity profiles are shown in figure 6.4a. The values for the power law exponents are all below 1, indicating shear thinning behaviour. The rheology for these suspensions is also shown in figure 6.3. There is a decrease in viscosity with increase in shear rate, indicating that these suspensions are shear thinning. Therefore, the suspensions are showing the same behaviour in the rheology and the velocity imaging measurements.

[C_4mim][BF_4] with 0.10 mole fraction of hydrophobic silica has the same power law value, n = 0.88, for the lowest three rotational velocities, ω = 0.5, 1 and 2 Hz. At a rotational velocity of ω = 4 Hz, there is an increase in the power law exponent to n = 0.96. This indicates that the suspension is becoming less shear thinning and showing more Newtonian behaviour. By observing the region of the rheology plot highlight ω = 4 Hz, (figure 6.3b), it can be seen that the curve has a shallower slope than at lower shear rates, also

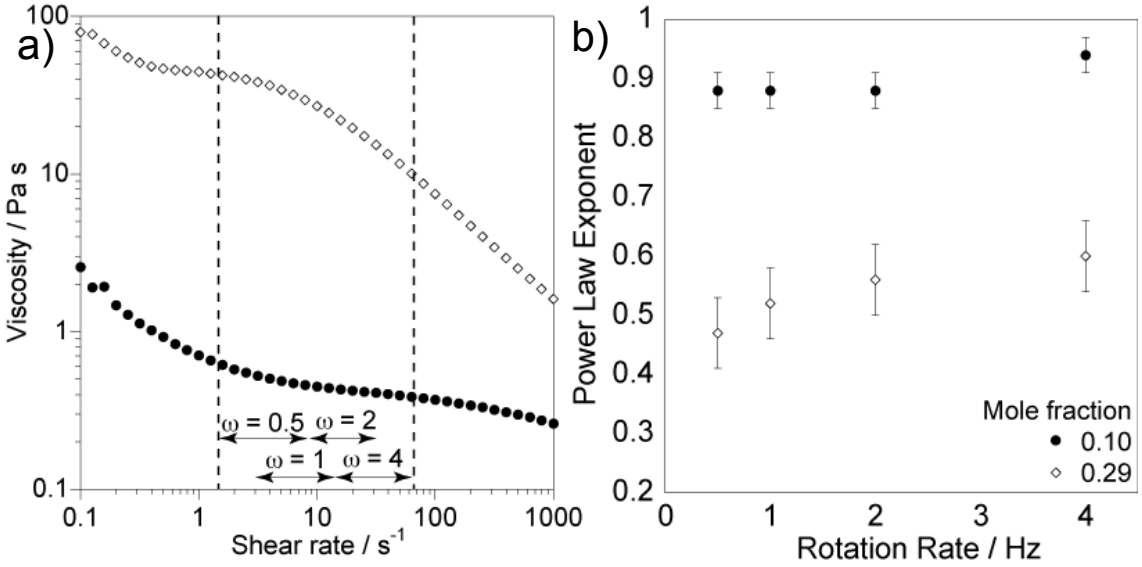

Figure 6.3: Plots of viscosity against shear rate (a) and power law exponent against rotation rate (b) for $[C_4mim][BF_4]$ with hydrophobic silica. The range of shear rates accessed by the rotational rates in the Couette cell is shown.

demonstrating that the suspension is becoming less shear thinning. This shows that the velocity data is as sensitive as the rheology to changes in the behaviour of this suspension.

The power law exponent values for $[C_4mim][BF_4]$ with 0.25 mole fraction of silica increases from n = 0.47 at ω = 0.5 Hz to n = 0.60 at ω = 4 Hz. (figure 6.3b). This indicates that the suspension is showing less shear thinning behaviour as the shear rate increases. This can also be observed in the bulk rheology (figure 6.3a). As the rotational velocity increases, the slope of the viscosity against shear rate for $[C_4mim][BF_4]$ with 0.25 mole fraction of silica becomes shallower (figure 6.3a). This again shows that there is a good agreement between the rheology and the velocity data for this system.

The power law exponents are shown in figure 6.4b and the bulk rheology for this data is in figure 6.4a. The radial velocity profiles for suspensions of $[C_4mim][NTf_2]$ with hydrophobic silica nanoparticles can be found in appendix 7. The bulk rheology data and the velocity data shown in figure 6.4 are from different samples. This means there is some variation in the behaviour when they are compared but the overall trends are the same. At

the lowest silica concentration, mole fraction of 0.18, the values for the power law exponent are 0.96 to 1.00, indicating Newtonian behaviour. As there is little change in the viscosity of the suspension with increasing shear rate (figure 6.4a), this also demonstrates that the suspension is showing Newtonian behaviour.

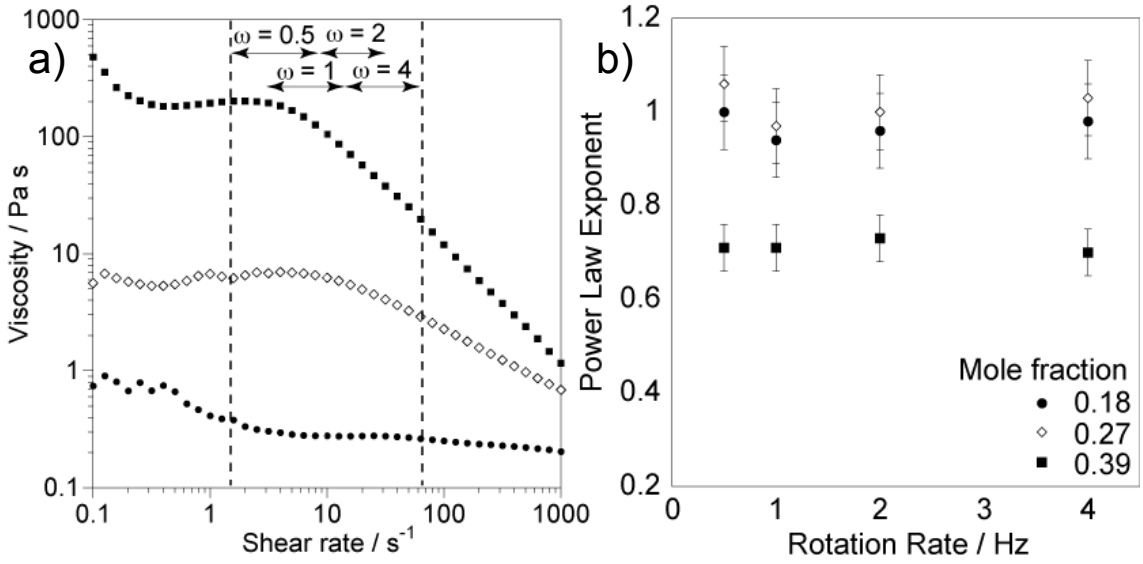

Figure 6.4: Plots of viscosity against shear rate (a) and power law exponent against rotation rate (b) for $[C_4mim][NTf_2]$ with hydrophobic silica. The range of shear rates accessed by the rotational rates in the Couette cell is shown.

$[C_4mim][NTf_2]$ with 0.27 mole fraction of hydrophobic silica has power law exponent values of 0.97 – 1.03. This indicates that this suspension is showing Newtonian behaviour at all the shear rates studied in the Couette cell. In figure 6.4a, the range of shear rates accessed in the Couette cell is shown on the rheology plots. At the highest shear rates accessed in the Couette cell, at a rotational rate of 4 Hz, shear thinning can be observed in the rheology. At this shear rate, a power law exponent value of 1.03 was obtained from the velocity data. The difference between these values is due to the data being from different samples and hence shows the variability in the rheological behaviour of these suspensions. Slight differences in the samples, such as different silica concentrations can have a large effect on the rheology, as was shown in chapter 5.

This variation can also be observed for [C_4mim][NTf_2] with 0.39 mole fraction of hydrophobic silica. The power law exponents extracted from the data are all less than 1, indicating shear thinning behaviour. The shear rates accessed in the Couette cell are shown on the rheology in figure 6.4. At the lowest rotational velocity in the Couette cell, 0.5 Hz, the rheology flow curve shows Newtonian behaviour, and the power law value obtained was 0.71. This demonstrates the variation between these different samples.

6.3.3 Infrared Spectroscopy

The IR spectrum for the hydrophobic nanoparticles is shown in figure 6.5. The IR spectra for [C_4mim][BF_4] with and without hydrophobic silica nanoparticles can be found in figure 6.6. It can be observed that there is little change in the IR spectra of [C_4mim][BF_4] on the addition of hydrophobic silica.

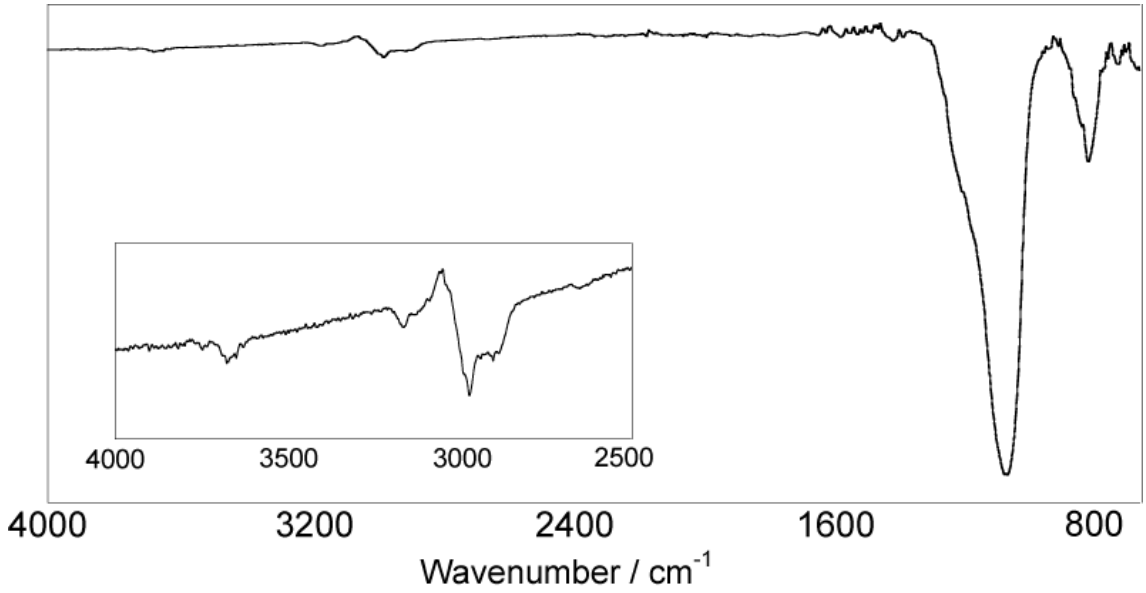

Figure 6.5: IR spectrum of hydrophobic silica nanoparticles. Inset shows the O-H stretching region.

The insets shown in figure 6.6 correspond to the O-H stretching region of the IR spectrum. By looking at the inset shown in figure 6.6a, it can be observed that there are two small peaks at ca. 3650 cm^{-1} and 3550 cm^{-1} in the spectrum of neat [C_4mim][BF_4]. These

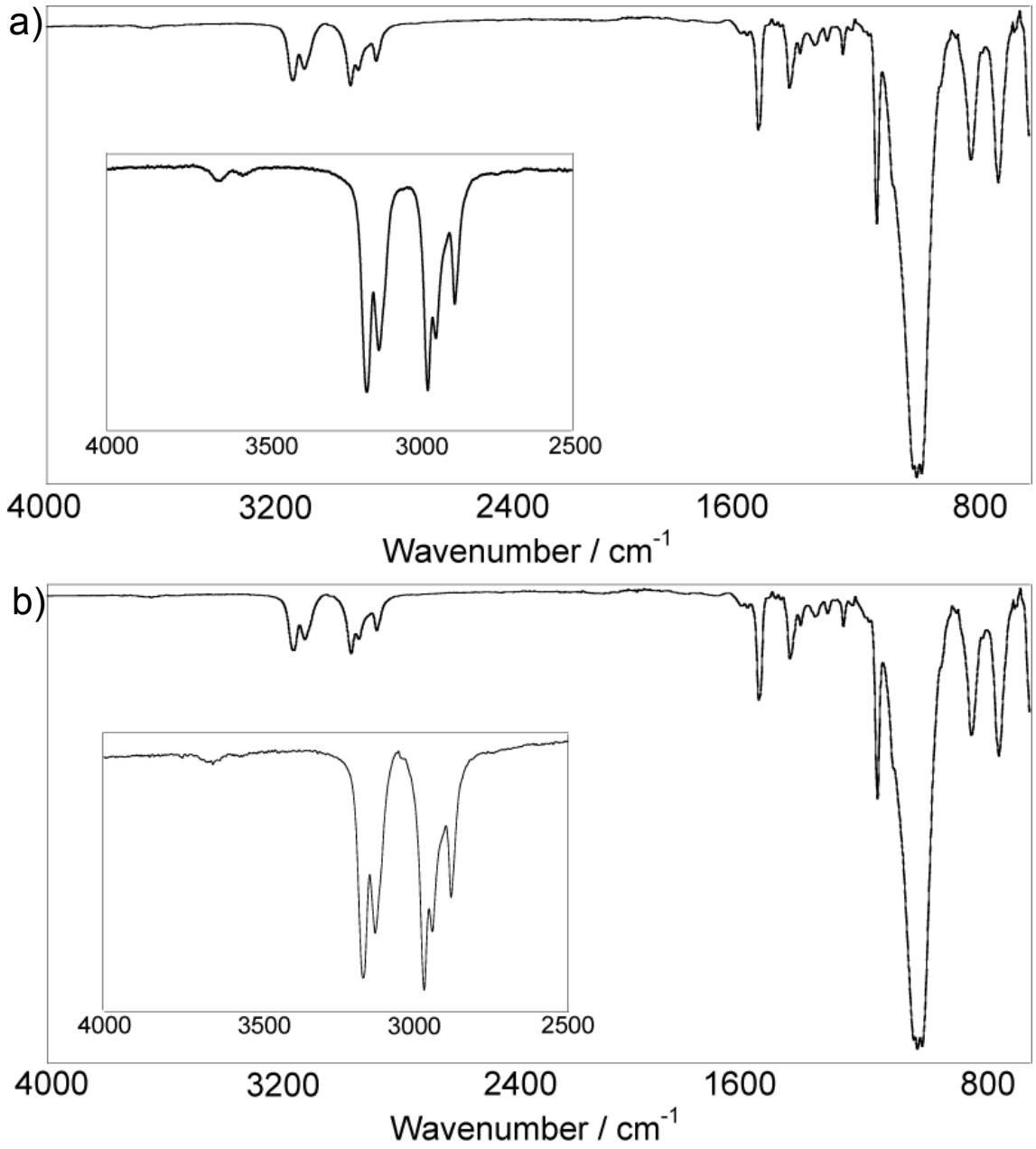

Figure 6.6: IR spectra for neat [C_4mim][BF_4] (a) and with 0.16 mole fraction of silica (b). Inset shows O-H stretching region of the IR spectrum.

peaks are due to small traces of water that cannot be removed from the ionic liquid. These peaks are also observed in the same position and at no greater intensity when the hydrophobic silica is added to the ionic liquid. This absence of change indicates that there is

little interaction between the silica and the ionic liquid. This lack of change was also observed when hydrophilic silica was added to the ionic liquid.

Figure 6.7 shows the 4000 – 2500 cm^{-1} region of the IR spectrum for $[C_4mim][BF_4]$ with and without hydrophobic silica, with the addition of water. It can be observed that the peaks at ca. 3650 cm^{-1} and 3550 cm^{-1}, increase in intensity on the addition of water and shift to slightly lower wavenumbers. This shift is present in both the neat ionic liquid and the suspension. Therefore, the shift does not indicate additional interactions occurring in the suspension. The growth of these peaks on the addition of water, in the absence of a vibrational shift, indicates that it is small traces of water that are the cause of these peaks in the neat ionic liquid. This small amount of water present in the neat ionic liquid is expected, as it is very hard to remove the last traces of water from the ionic liquid. This increase in intensity is observed for both the neat ionic liquid and the suspension with hydrophobic silica nanoparticles. The lack of shift in peaks is also observed for both. This is the trend as was observed for suspensions of hydrophilic silica nanoparticles in $[C_4mim][BF_4]$.

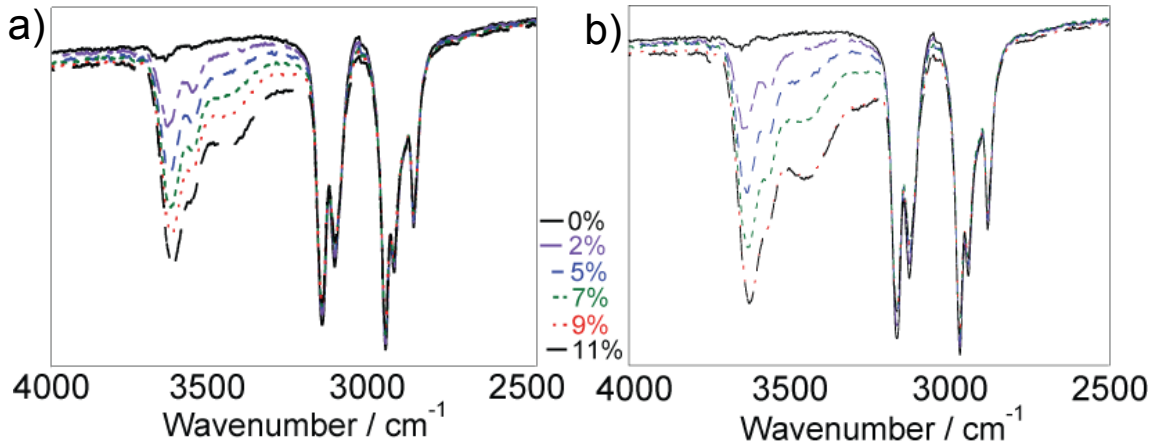

Figure 6.7: O-H stretching region of the IR spectra for neat $[C_4mim][BF_4]$ (a) and with 0.16 mole fraction of silica (b) with additions of water. Legend refers to the volume % of water added.

The IR spectra for $[C_4mim][NTf_2]$ with and without hydrophobic silica nanoparticles can be found in figure 6.8. There are only little differences between these spectra, indicating that there is little interaction between the ionic liquid and the hydrophobic silica nanoparticles. The inset shown for the spectra is the O-H stretching region of the IR spectrum. There are no peaks observed here in either neat $[C_4mim][NTf_2]$ or with hydrophobic silica nanoparticles, indicating that there are no noticeable O-H interactions

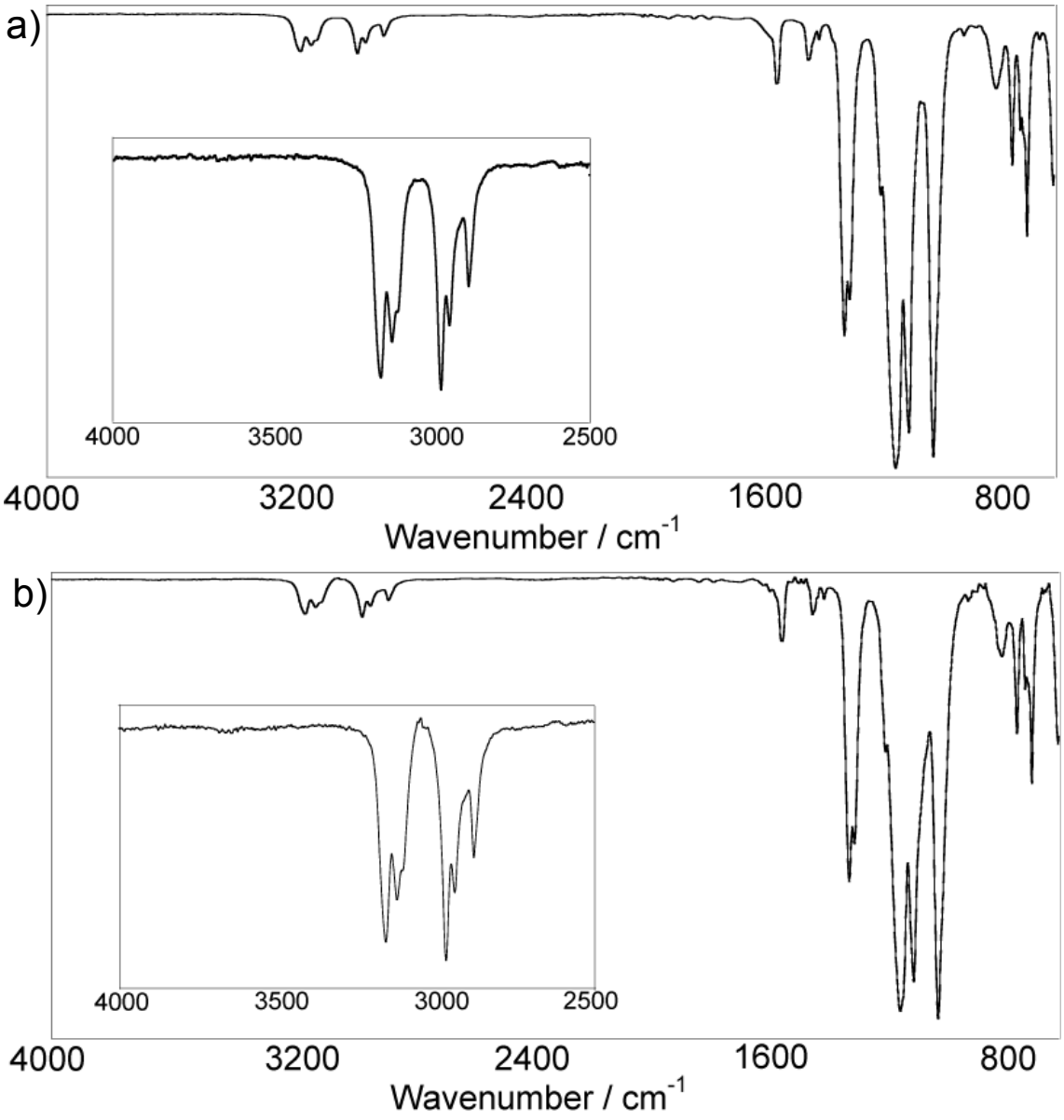

Figure 6.8: IR spectra for neat $[C_4mim][NTf_2]$ (a) and with 0.27 mole fraction of silica (b). Inset shows O-H stretching region of the IR spectrum.

present, even in the suspensions.

Figure 6.9 shows the spectra of $[C_4mim][NTf_2]$ with and without hydrophobic silica on the addition of water. The water was not miscible with the ionic liquid, even after vigorous stirring, as $[C_4mim][NTf_2]$ is a hydrophobic ionic liquid. The peaks observed in this region were present when regions of water within the formed emulsion could be observed. The presence and growth in intensity of these peaks, at ca. 3650 cm^{-1} and 3550 cm^{-1}, are therefore due to the presence of water within the system, as they only appear when water has been added.

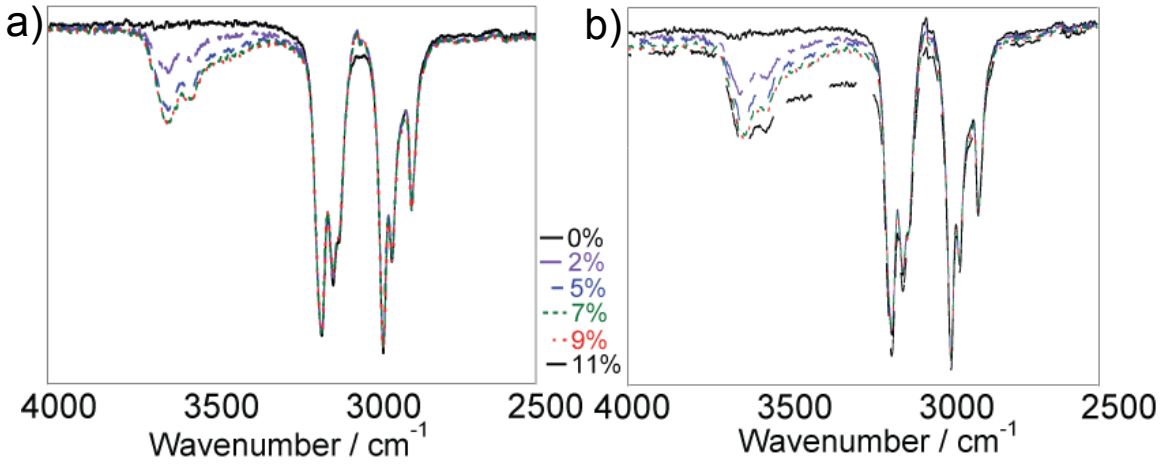

Figure 6.9: O-H stretching region of the IR spectra for neat $[C_4mim][NTf_2]$ (a) and with 0.27 mole fraction of silica (b) with additions of water. Legend refers to the volume % of water added.

As these peaks at ca. 3650cm^{-1} and 3550cm^{-1} appear at the same place in the spectrum in both ionic liquids, and their suspensions, regardless of which type of silica is present, it indicates that these peaks are due to the presence of water, and not due to an interaction between the ionic liquids and the silica. IR spectra of $[C_4mim][BF_4]$ with and without silica nanoparticles have previously been recorded.[17] The silica showed a broad peak in the O-H stretching region of the IR spectra, at ca. 3500 cm^{-1}. When the hydrophilic silica, from the same supplier, was added to $[C_4mim][BF_4]$, in the same concentration as shown in figure 6.6 peaks were observed at 3648 and 3572 cm^{-1}. The shift and growth of the peaks observed in the O-H stretching region of the IR spectrum was attributed to an

interaction between the ionic liquid and the hydrophilic silica nanoparticles. They proposed that the interaction observed in this system was therefore a hydrogen bonding interaction between the BF_4 and the silanol groups.[17] Other papers have also reported peaks in this area of the IR spectrum for ionic liquid and silica suspensions.[18, 19] However, other studies have not seen extra peaks in the IR spectrum on the addition of silica to ionic liquids.[3, 20] Here, it has been shown the extra peaks observed at ca. 3650 and 3550 cm^{-1} are more likely due to the presence of water within the suspension, than an indication of an interaction between the ionic liquid and the silica.

6.3.4 NMR Relaxation Measurements

The ^1H and ^{19}F NMR T_1 relaxation times for the cation and anion, respectively, have been recorded for $[C_4mim][BF_4]$ and $[C_4mim][NTf_2]$, over a range of concentrations of hydrophobic nanoparticles to see the effect the silica has on the rotational mobility of these components. The ^{19}F NMR T_1 relaxation times of the anion in suspensions of $[C_4mim][BF_4]$ and $[C_4mim][NTf_2]$ are shown in figure 6.10. No significant change is observed in the anion

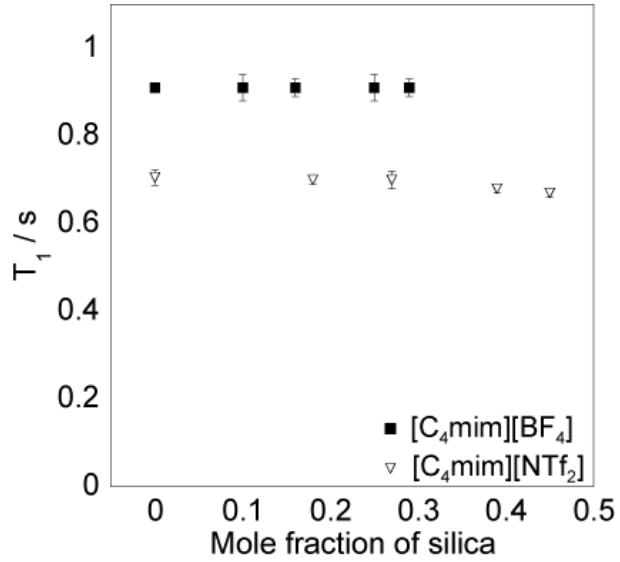

Figure 6.10: Plot of ^{19}F NMR T_1 relaxation times of the anion against mole fraction of hydrophobic silica.

relaxation time with increase in silica concentration. This suggests that the silica is not having an effect on the tumbling of the anion, implying that there is no interaction between the silica and the anion of either ionic liquid. This was also been observed for suspensions of hydrophilic nanoparticles in these ionic liquids. The BF_4 anion has a higher T_1 relaxation time than the NTf_2 anion, which would be expected, as it is a smaller molecule. However, this is not reflected in the viscosity, as $[C_4mim][NTf_2]$ is a less viscous ionic liquid. The increase in the viscosity suspension with increase in silica concentration is not reflected for either anion relaxation time.

The ^1H T_1 relaxation times for the H(4/5) protons, which are located on the imidazolium ring of the cations, are shown in figure 6.11. Suspensions of both ionic liquids, there is a decrease in the T_1 relaxation time with increase in silica concentration. This decrease indicates that there is a slowing in the tumbling of these protons. An interaction between these protons and the silica would cause this decrease, as the silica is larger and

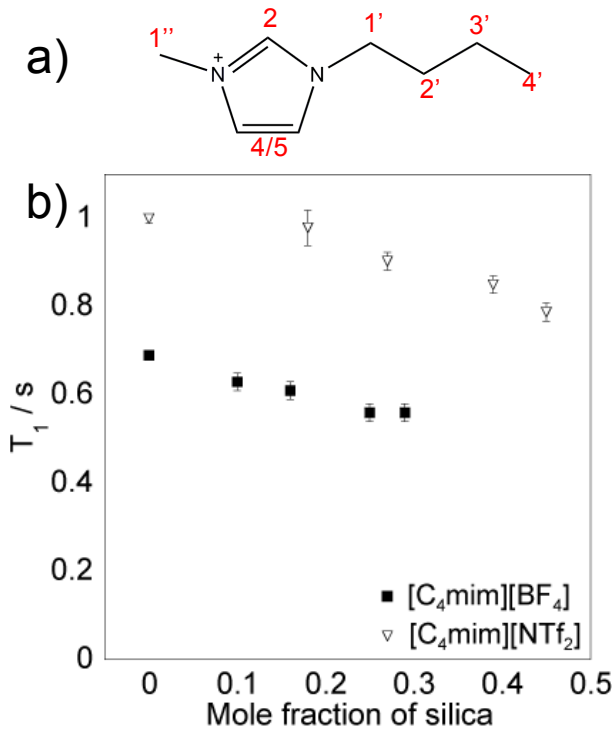

Figure 6.11: a) Structure of the C_4mim cation. b) Plot of ^1H T_1 relaxation times for H(4/5) against mole fraction of hydrophobic silica.

therefore will tumble slower. Since this decrease is not observed in the anion, this indicates that it is the imidazolium ring of both of the cations that is interacting with the hydrophobic silica nanoparticles, as was observed for the hydrophilic silica nanoparticles. The H(4/5) protons on the cation in $[C_4mim][NTf_2]$ have a higher mobility than those in $[C_4mim][BF_4]$. This higher mobility reflects the lower viscosity of this ionic liquid. In both ionic liquids, a decrease in the viscosity is observed with increasing silica concentrations, which corresponds with the decrease in the tumbling.

Suspensions in $[C_4mim][NTf_2]$ and $[C_4mim][BF_4]$ with hydrophobic silica show little change in the H(4') relaxation time with increase in silica concentration (figure 6.12). This possibly indicates a lack of the methyl group interaction with the silica surface, but is it most likely to be a reflection of the fast rotation of the methyl group bonds.

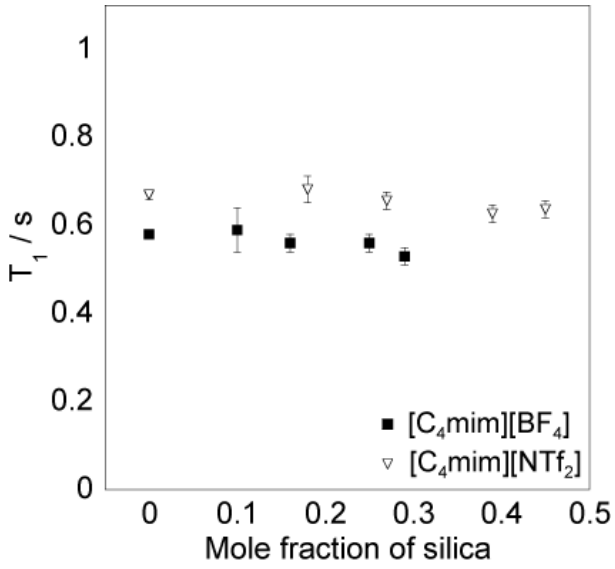

Figure 6.12: Plot of ^1H T_1 relaxation times H(4') against mole fraction of hydrophobic silica.

6.3.5 DLS Measurements

Finally, DLS measurements have been used to study the size distributions of the hydrophobic nanoparticles in $[C_4mim][BF_4]$ and $[C_4mim][NTf_2]$. Figure 6.13 shows the size of hydrophobic silica nanoparticles in $[C_4mim][NTf_2]$ obtained from DLS size distributions. The

sizes found are ca. 700 - 800 nm, indicating that clusters of nanoparticles have formed in the ionic liquid, as the nanoparticles have a diameter of 12 nm. The size of the clusters remains constant with the increase in silica concentration. A single peak was observed in the DLS size distributions up to a silica mole fraction of 0.28 (figure 6.15).

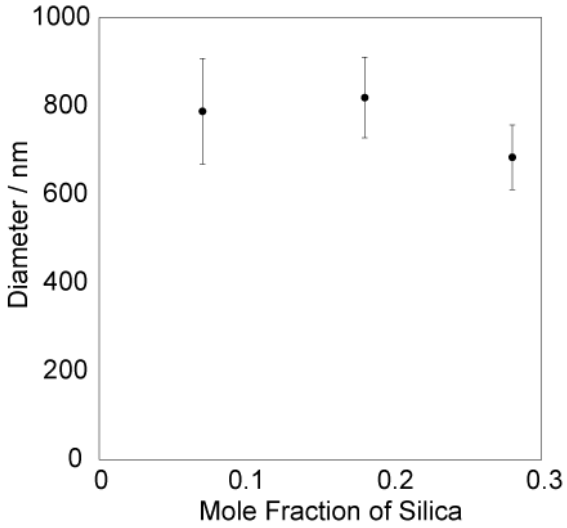

Figure 6.13: Plot of diameter against mole fraction of silica in $[C_4mim][NTf_2]$.

At 0.37 mole fraction of silica, two peaks are observed in the intensity spectrum (figure 6.14). The larger peak corresponds to clusters of nanoparticles that are ca. 800 nm, which is the same size observed at lower silica concentration. The smaller peak shows a diameter of 12 nm, the size of the nanoparticles, indicating that there are also individual silica nanoparticles present in this suspension. The presence of these single nanoparticles implies that a limit of the number of clusters present in the suspension has been reached and the nanoparticles are unstable. The volume distribution is also shown, as DLS intensity measurements are weighted towards larger cluster sizes. It can be observed from the volume distribution that there is a higher volume of clusters of silica nanoparticles in this ionic liquid.

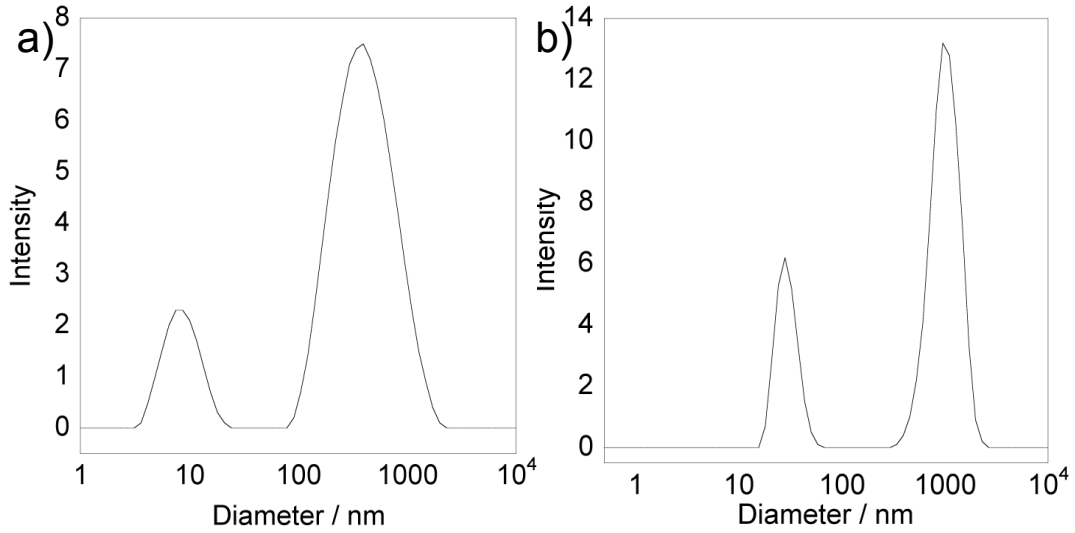

Figure 6.14: Plot of intensity against diameter for $[C_4mim][NTf_2]$ with 0.39 mole fraction of silica. (a) Intensity distribution (b) Volume distribution.

The suspensions of hydrophobic silica nanoparticles in $[C_4mim][BF_4]$ showed two peaks in the DLS intensity plot at silica mole fractions of 0.10 and above (figure 6.15 a, c & e), whereas the equivalent mole fractions of silica in $[C_4mim][NTf_2]$ showed one peak (figure 6.15 b, d & f). The peak that is smaller in intensity of the two peaks that appear for the $[C_4mim][BF_4]$ suspensions is at a diameter of 12 nm, corresponding to the presence of individual nanoparticles. The larger peak demonstrates that clusters of nanoparticles are also present.

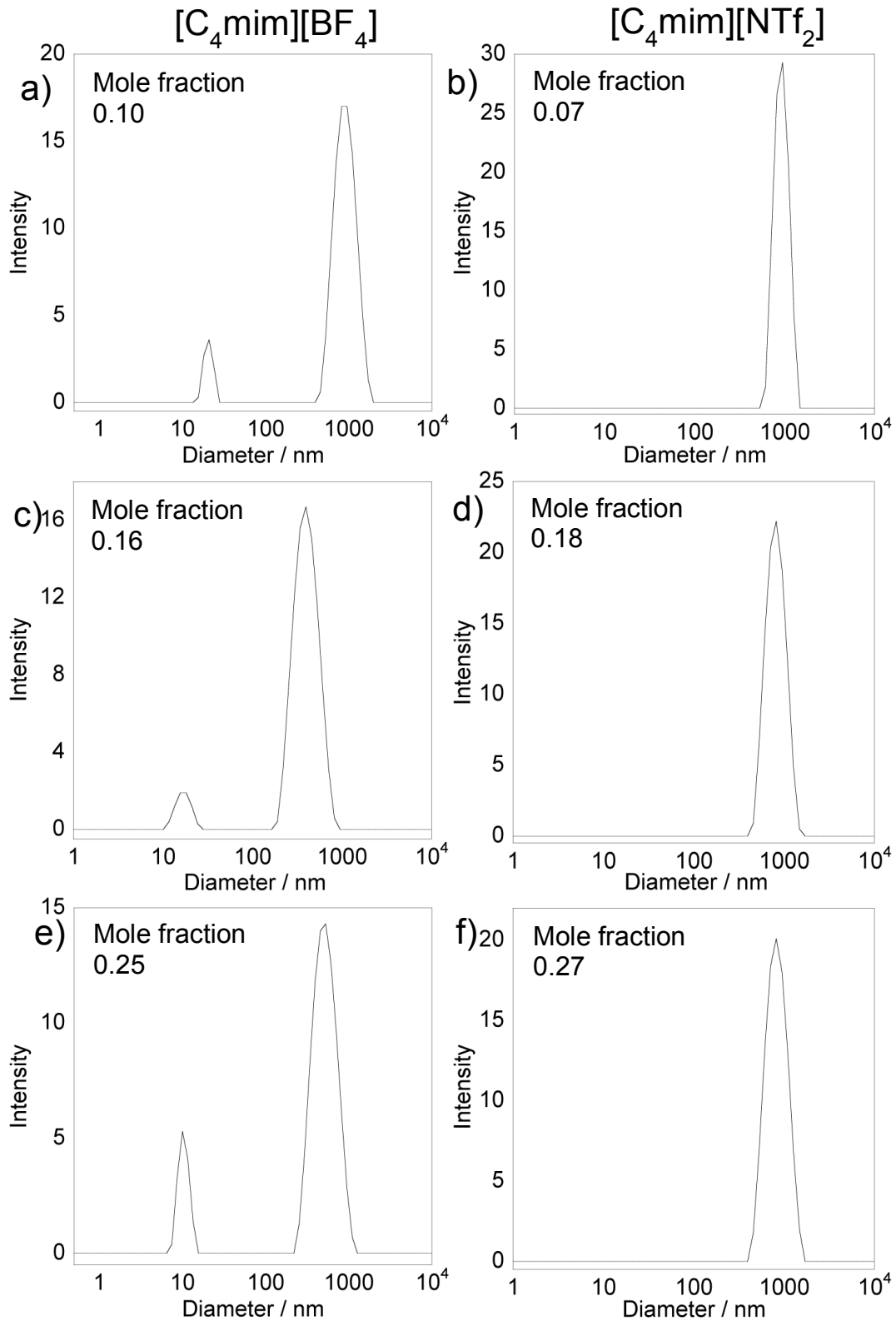

Figure 6.15: Plots of intensity against diameter for $[C_4mim][BF_4]$ with 0.10 (a), 0.16 (c) and 0.25 (e) mole fraction of silica and $[C_4mim][NTf_2]$ with 0.07 (b), 0.18 (d) and 0.27 (f) mole fraction of silica.

The intensity distributions and volume distributions for suspensions of $[C_4mim][BF_4]$ with hydrophobic nanoparticles are shown in figure 6.16. DLS measurements are weighted towards larger clusters of nanoparticles and this is reflected in the intensity distribution.[14, 15] By looking at the volume distributions, it can be observed that, by volume, there are more single nanoparticles present than clusters, potentially indicating the formation of a weakly flocculated gel.[21] This is different to what is observed in $[C_4mim][NTf_2]$ at the largest silica concentration (figure 6.14).

The presence of multiple peaks in the DLS distributions indicates that the silica nanoparticles are not being stabilised by the ionic liquids at these concentrations.[4, 5, 21] At the highest silica concentration, suspensions of hydrophobic nanoparticles in both ionic liquids show two peaks in the DLS size distribution plots. This indicates that the silica nanoparticles have aggregated in $[C_4mim][BF_4]$ and $[C_4mim][NTf_2]$, as uniform clusters are not present. The presence of the single nanoparticles is possibly a reflection of the lack of interaction between the hydrophobic silica nanoparticles. As their surface is methyl groups, there are only weak van der Waals forces to keep the nanoparticles together. At high concentrations, van der Waals attraction is most likely overcome by a steric repulsion between the particles.[22]

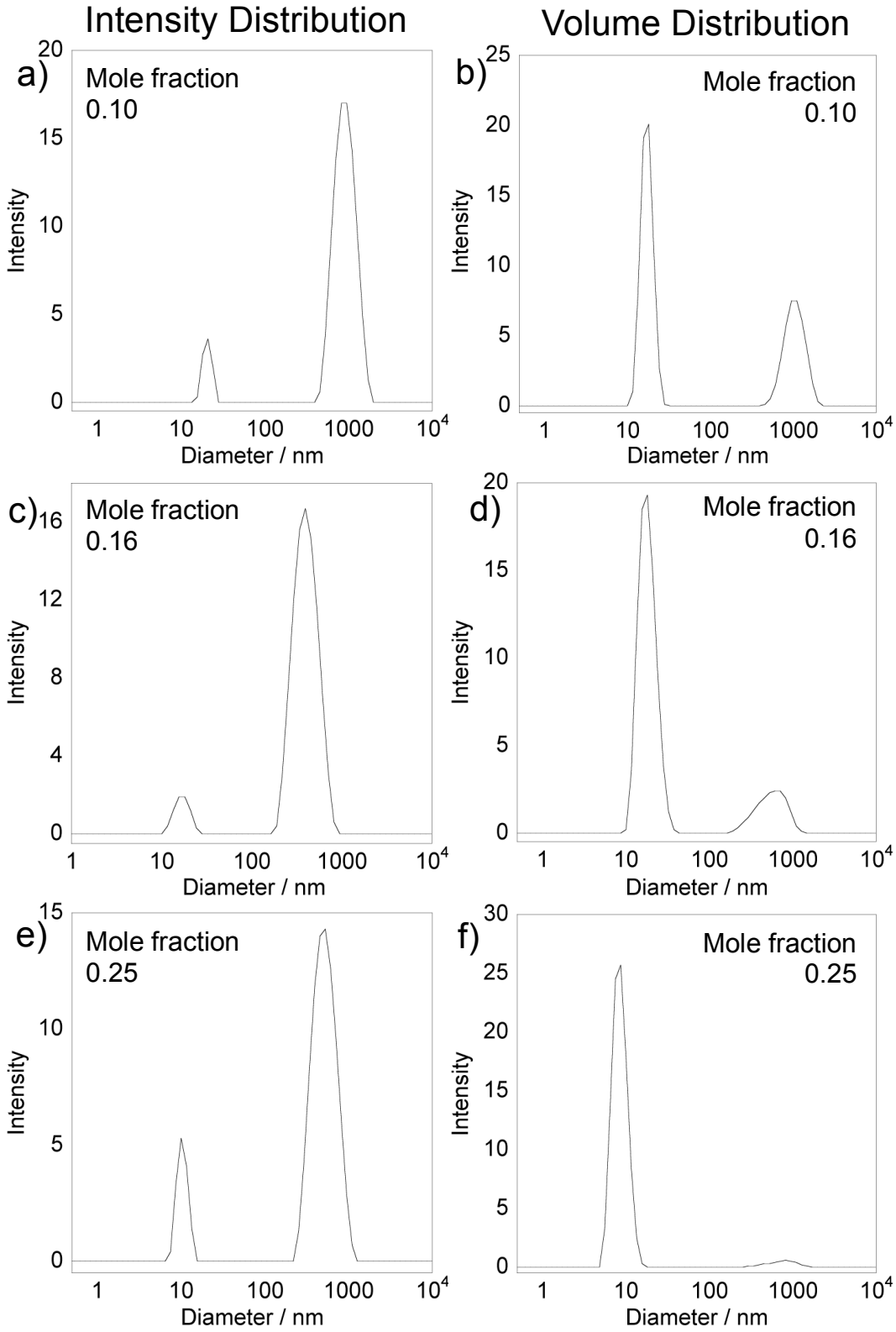

Figure 6.16: Plots of intensity against diameter for [C_4mim][BF_4] with 0.10 (a + b), 0.16 (c + d) and 0.25 (e + f) mole fraction of silica comparing the intensity (a, c, f) and volume (b, d, e) distributions.

6.4 Discussion

6.4.1 $[C_4mim][BF_4]$ with hydrophobic nanoparticles

The ^{19}F NMR T_1 relaxation times for the BF_4 anion in $[C_4mim][BF_4]$ do not change with increase in silica concentration, regardless of whether hydrophobic or hydrophilic silica is present. This agrees with the IR measurements that showed there is no significant interaction between the silica and the BF_4 anion. With increasing hydrophobic and hydrophilic silica concentration, the H(4/5) protons, which are located on the imidazolium ring of the cation, show a decrease in T_1 relaxation time in all of the suspensions studied. This indicates that there is a slowing in the tumbling of the imidazolium ring of the cation. This implies the imidazolium ring is interacting with the silica nanoparticles in all suspensions studied, as the silica nanoparticles are large and therefore will be tumbling slowly.

At low silica concentrations, up to a mole fraction of 0.10, both hydrophobic and hydrophilic nanoparticle suspensions in $[C_4mim][BF_4]$ show shear thinning rheology. This is observed both in the bulk rheology measurements and in the velocity imaging data. However, when hydrophilic silica nanoparticles are added to $[C_4mim][BF_4]$, there are small increases in the zero shear viscosity observed. In the hydrophobic silica suspensions, the zero shear viscosity increases by an order of magnitude at each silica mole fraction. Large increases in the viscosity of the suspensions with increases in silica concentration were also observed for $[C_4mim][NTf_2]$ with hydrophilic silica nanoparticles. Suspensions of hydrophilic silica nanoparticles in $[C_4mim][NTf_2]$ also showed shear thinning behaviour. $[C_4mim][NTf_2]$ with hydrophilic silica and $[C_4mim][BF_4]$ with hydrophobic silica both have a difference between the hydrophobicity of the ionic liquid and the silica. This similarity between the systems is reflected in the shear thinning behaviour and the changes in zero shear viscosity indicate that these systems are behaving similarly. However, there is a difference in the cluster sizes obtained for these suspensions.

The particle size distributions for $[C_4mim][NTf_2]$ and $[C_4mim][BF_4]$ with both types of silica, at low concentration are shown in figure 6.17. It can be observed that suspensions of $[C_4mim][BF_4]$ with hydrophobic and hydrophilic are the same size, within error, demonstrating that the different types of silica nanoparticles are forming the same structure type in this ionic liquid at low silica concentration. However, low hydrophilic silica concentrations in $[C_4mim][NTf_2]$ show much larger cluster sizes, showing that different structures are formed. This could be due to hydrophilic silica nanoparticles being able to interact with each other and therefore can form larger clusters than hydrophobic silica nanoparticles, which can only interact with each other through weak van der Waals forces.

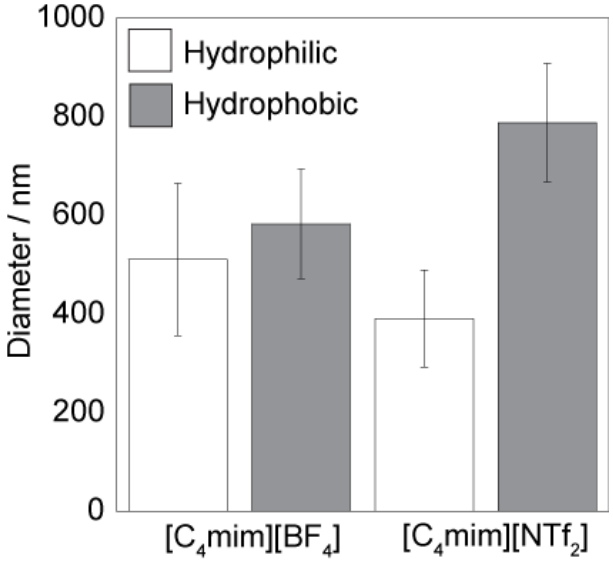

Figure 6.17: Plot of diameter against ionic liquid and nanoparticle type. The silica nanoparticles are at 0.04 mole fraction in $[C_4mim][BF_4]$ and 0.07 mole fraction in $[C_4mim][NTf_2]$.

These data indicate that at low silica concentrations, suspensions of $[C_4mim][BF_4]$ and hydrophobic silica nanoparticles are showing similar behaviour to suspensions in $[C_4mim][BF_4]$ and $[C_4mim][NTf_2]$ with hydrophilic silica. Therefore, they are forming a fluid of clusters, with cluster sizes of ca. 400 nm. The increase in zero shear viscosity is possibly caused by the trapping of ionic liquid in clusters of nanoparticles, as this is known to produce large increases in viscosity in similar systems.[16] The shear thinning observed is either due to

breaking of the clusters on the application of shear or ordering of the clusters into layers.[23] More investigation, such as performing small angle neutron scattering or DLS measurements of these systems under shear, is required to determine which of these mechanisms is occurring.

At a silica mole fraction of 0.16, there are differences observed between suspensions of the two types of silica in $[C_4mim][BF_4]$. Suspensions of hydrophobic nanoparticles show shear thinning behaviour at this silica concentration, whereas suspensions of hydrophilic nanoparticles show Newtonian behaviour. This Newtonian behaviour indicates that the hydrophilic silica is being stabilised, whereas the hydrophobic nanoparticles are unstable in the $[C_4mim][BF_4]$, as the suspensions show shear thinning behaviour. This is also reflected in the DLS measurements. At a hydrophilic silica mole fraction of 0.16 in $[C_4mim][BF_4]$, one peak is observed in the DLS size distributions, corresponding to one cluster size is present. However, there are two peaks observed in the DLS size distribution for $[C_4mim][BF_4]$ with 0.16 mole fraction of hydrophobic silica nanoparticles. One of these peaks corresponds to the presence of nanoparticle clusters. The second peak is at 12 nm, the size of the individual nanoparticles. The presence of these single nanoparticles indicates that there is a limit to the number of clusters or the size of the hydrophobic nanoparticle clusters in $[C_4mim][BF_4]$.

Multiple peaks are observed in the DLS size distributions of $[C_4mim][NTf_2]$ with 0.18 mole fraction of hydrophilic silica nanoparticles. The larger peak corresponded to clusters of nanoparticles and the smaller peak to individual silica nanoparticles, similar to that observed for $[C_4mim][BF_4]$ with 0.10 mole fraction of hydrophobic silica nanoparticles. This indicates that similar aggregated structures are being formed in these systems. This structure will trap ionic liquid, which causes the increase in viscosity observed in both of these systems.[16] When shear is applied, it causes the silica nanoparticles to break apart again, so the viscosity decreases and hence the shear thinning rheology. This shear thinning is observed for both $[C_4mim][BF_4]$ with hydrophobic silica nanoparticles and $[C_4mim][NTf_2]$ with

hydrophilic nanoparticles, indicating that these systems are behaving the same due to the different hydrophobicity of the ionic liquid and silica.

At silica concentrations of 0.25 mole fraction and above, there continues to be a difference in the behaviour of hydrophilic and hydrophobic silica suspensions in $[C_4mim][BF_4]$. At these concentrations, suspension of hydrophilic silica in $[C_4mim][BF_4]$ demonstrate shear thickening rheology, whereas suspensions of hydrophobic silica in this ionic liquid still show shear thinning behaviour. The hydrophobic silica suspensions in this ionic liquid also have a yield stress at 0.25 silica mole fraction and above. The hydrophilic suspensions still demonstrate one peak in the DLS size distributions, indicating one size of silica nanoparticle clusters is present. $[C_4mim][BF_4]$ with hydrophilic nanoparticles undergoes a jamming transition to form a colloidal glass-like structure at this concentration.[24]

At the highest two silica concentrations in suspensions of $[C_4mim][BF_4]$ with hydrophobic silica, there is smaller increase in the viscosity than is observed for other increases in silica concentration. This indicates that the structure of the suspensions is changing. The shear thinning rheology, as well as the presence of two peaks in the DLS for suspensions of $[C_4mim][BF_4]$ with hydrophobic silica demonstrate that this system is also undergoing a jamming transition, but not forming a colloidal glass. At silica mole fractions above 0.25 of hydrophilic silica in $[C_4mim][NTf_2]$, the variability in the peaks in the distributions indicates aggregation of the silica nanoparticles. The suspensions also show shear thinning behaviour, as well as a yield stress. This indicated that a colloidal gel had been formed, which has a continuous space-spanning network of silica nanoparticles (figure 6.18).[24-26] This network is broken on the application of shear and hence shear thinning rheology is observed.

The shear thinning rheology and multiple peaks in the DLS size distributions for $[C_4mim][BF_4]$ with hydrophobic silica indicate that these suspensions are also undergoing a jamming transition with increasing silica concentration to form a colloidal gel.[24-26] The gelation happens at a higher concentration that is observed for $[C_4mim][NTf_2]$ with hydrophilic silica. A

colloidal gel is possibly formed at lower silica concentrations in [C_4mim][NTf_2] with hydrophilic silica, as there is more attraction between the particles. The hydrophobic nanoparticles have methyl groups on the surface that can only interact via weak van der Waals forces. Hydrophilic nanoparticles are more attracted to each other and therefore form a network and hence a gel is formed at lower concentrations in the hydrophobic ionic liquid.

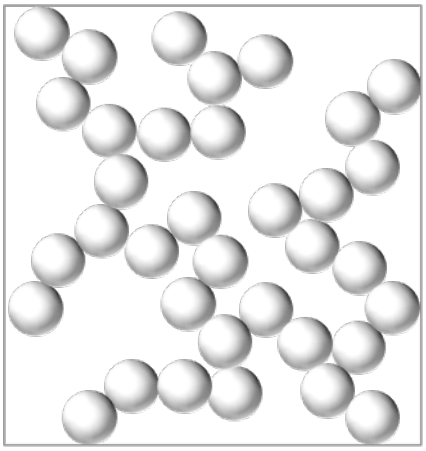

Figure 6.18: Schematic diagram of the network formed by silica nanoparticles in a colloidal gel. For the systems that are being described, each sphere represents a cluster of nanoparticles.

The similarity in behaviour between [C_4mim][BF_4] with hydrophobic silica and [C_4mim][NTf_2] with hydrophilic silica implies that the differences in hydrophobicity of the nanoparticles and the ionic liquid dominate the stability of these suspensions. A gel is formed at low concentrations in [C_4mim][NTf_2] with hydrophilic silica, which is most likely due to the attraction between the nanoparticles. The difference in the hydrophobicity means that the nanoparticles quickly aggregate to reduce contact with the ionic liquid. This leads to the possibility that ionic liquid gets trapped in nanoparticle clusters, and hence large increases in the viscosity of the suspensions are observed.[27, 28] These clusters break under shear to cause the shear thinning behaviour observed. As the silica concentration is increased, the nanoparticles start to form larger structures, which are observed by the presence of multiple peaks in the DLS size distribution. At the highest silica concentrations, the suspensions start

to phase separate, as they do at lower concentrations, but undergo spinodal decomposition and the nanoparticles form a space-spanning network – a colloidal gel.[28, 29] The formation of this network is characterised by very high zero shear viscosities and a yield stress in the plot of viscosity against shear rate.

6.4.2 [C_4mim][NTf_2] with hydrophobic nanoparticles

The ^{1}H NMR T_1 relaxation data for [C_4mim][NTf_2] with both types of silica show approximately the same decrease in the T_1 relaxation times of the protons on the imidazolium ring at the highest silica concentration. This indicates that the tumbling of the cations is being slowed by approximately the same rate, regardless of the type of silica, indicating that it is always the imidazolium ring of the cation that interacts with the silica. The decrease in the suspensions of [C_4mim][NTf_2] with hydrophobic silica is not linear. There is a smaller decrease observed at the highest silica concentrations, which is where the suspension is observed to show shear thinning behaviour. This indicates that there is a change in the structure of the silica, which leads to a reduced silica surface area for the cations to interact with so there is less change in the T_1 relaxation time.

[C_4mim][NTf_2] with hydrophobic silica at mole fractions of 0.27 or lower show Newtonian rheology at low shear rates, and slightly shear thinning at high shear rates. This is similar to [C_4mim][BF_4] with hydrophilic silica, where a Newtonian response was observed with 0.16 mole fraction of nanoparticles. The comparable response is due to the same hydrophobicity between the silica nanoparticles and the ionic liquids in both of these cases. This allows the silica to be stabilised and so Newtonian rheology is observed. However, when hydrophilic silica was suspended in [C_4mim][NTf_2], shear thinning behaviour was observed, indicating that the silica is unstable in this ionic liquid. Large increases in the zero shear viscosity with increasing silica concentrations were observed for [C_4mim][NTf_2] with

both hydrophilic and hydrophobic silica. This large increase is possibly due to the nanoparticles aggregating and trap ionic liquid in the nanoparticle clusters.[16]

At a mole fraction of 0.07, hydrophilic nanoparticles form clusters of ca. 400 nm in $[C_4mim][NTf_2]$, whereas the hydrophobic nanoparticles form cluster sizes of ca. 800 nm (figure 6.17). The larger cluster sizes in $[C_4mim][NTf_2]$ with hydrophobic silica could be due to more of the ionic liquid becoming trapped in the cluster. When the hydrophobic silica concentration in $[C_4mim][NTf_2]$ is increased, only one peak is observed in the DLS up to and including 0.27 mole fraction of silica, indicating that the nanoparticles have been stabilised. The sizes of the clusters remain constant, within error. However, multiple peaks are observed in the size distributions of $[C_4mim][NTf_2]$ with hydrophilic silica at these concentrations, indicating that the nanoparticles are no longer completely stabilised. Single peaks are still observed in $[C_4mim][BF_4]$ with hydrophilic silica at these concentrations, indicating that the silica nanoparticles are stabilised. The DLS size distributions show that suspensions of $[C_4mim][BF_4]$ with hydrophilic silica and $[C_4mim][NTf_2]$ with hydrophobic silica are still behaving similarly at silica concentrations at and below 0.27 mole fraction.

At hydrophobic silica concentrations of 0.39 mole fraction in $[C_4mim][NTf_2]$ shear thinning rheology and a yield stress are observed, whereas $[C_4mim][BF_4]$ with hydrophilic silica starts to show shear thickening behaviour at 0.25 silica mole fraction. This indicates these suspensions are forming different structures at these higher silica concentrations. The viscosity of $[C_4mim][NTf_2]$ with 0.27 mole fraction of hydrophobic silica is around 10 Pa s, which increases to almost 1000 Pa s at a mole fraction of 0.39. This large change in the viscosity indicates that there is a change in the structure of the suspension. At a silica mole fraction of 0.27, suspensions of $[C_4mim][NTf_2]$ and hydrophilic silica show shear thinning behaviour, and also large viscosity increases when silica is added, as well as yield stress. This implies that at these concentrations, suspensions of $[C_4mim][NTf_2]$ with hydrophobic or hydrophilic silica are behaving in the same way.

This similarity is also shown in the DLS size distributions. [C_4mim][NTf_2] with hydrophobic silica shows two peaks in the hydrophobic silica distribution at a silica mole fraction of 0.39, indicating the silica is not stabilised. At higher silica concentrations, [C_4mim][NTf_2] with hydrophilic silica nanoparticles also showed multiple peaks, where both clusters and single nanoparticles were present. This indicates the silica is not being stabilised by the ionic liquid and is starting to form aggregates. This, along with the shear thinning rheology, indicates that [C_4mim][NTf_2] is forming a colloidal gel with either type of silica at higher nanoparticle concentrations. At higher concentrations of hydrophilic silica nanoparticles in [C_4mim][BF_4] single peaks were still observed in the size distribution, indicating that the nanoparticles were still stabilised. This implies that hydrophilic silica nanoparticles are more stable in the hydrophilic ionic liquid than hydrophobic nanoparticles in a hydrophobic ionic liquid. This is possibility due the interaction between the nanoparticles themselves, as hydrophilic nanoparticles are attracted to each other, whereas the methyl groups on the surface of the hydrophobic nanoparticles can only interact through weak van der Waals forces.

A single peak in the DLS size distribution and Newtonian rheology indicate that at low silica concentrations, [C_4mim][NTf_2] with hydrophobic silica nanoparticles is forming a stable fluid of clusters, consistent with what is observed in the other suspensions studied in this work. The hydrophobic nature of the silica and the ionic liquid means that there is good compatibility and therefore the nanoparticles are stabilised, hence the single peak in the size distribution and the Newtonian rheology. When the hydrophobic silica concentration is increased to 0.39 mole fraction, the system undergoes a jamming transition as there is a larger increase in the zero shear viscosity, shear thinning rheology is observed and two broader peaks are observed in the DLS size distribution. This indicates that the system is forming a colloidal gel, similar to that observed in [C_4mim][BF_4] with hydrophobic silica nanoparticles. In both of these systems, the gelation happens at a lower concentration that in

[C_4mim][NTf_2] with hydrophilic silica. This is most likely due to the lack of attraction between the hydrophobic nanoparticles.

In both [C_4mim][BF_4] and [C_4mim][NTf_2], there is a comparable decrease in the T_1 relaxation times of the imidazolium ring protons with increase in silica concentration, regardless of whether hydrophobic or hydrophilic silica is added. This implies that it is the same interaction between the cation and the silica in all cases. At low silica concentrations, the systems have one peak in the DLS size distribution data and mostly show Newtonian behaviour. These indicate that a stabilised fluid of clusters has been formed. At higher silica concentrations, a jammed state is formed in all the systems. [C_4mim][BF_4] with hydrophilic silica nanoparticles continues to have one peak in the size distribution and shows shear thickening rheology. These indicate that the suspensions are forming a glass-like state, where clusters of nanoparticles are trapped in cages which are formed through short range bonds and repulsion.[25]

[C_4mim][BF_4] with hydrophobic nanoparticles and [C_4mim][NTf_2] with both types of nanoparticles form colloidal gels at higher silica nanoparticle concentrations. The concentration of silica nanoparticles required for gel formation depends on the system. Suspensions of [C_4mim][NTf_2] and hydrophilic silica form a colloidal gel at the lowest nanoparticle concentration – 0.18 mole fraction. This is due to the repulsion between the hydrophilic nanoparticles and hydrophobic ionic liquid meaning that the nanoparticles are not stabilised and the attraction between the hydrophilic silica nanoparticles means that they will aggregate at lower concentrations. There is less attraction between hydrophobic nanoparticles; hence hydrophobic nanoparticles in [C_4mim][BF_4] form a gel at a mole fraction of 0.25. There is repulsion between the hydrophilic ionic liquid and the hydrophobic nanoparticles, but there is less attraction between the nanoparticles to cause the aggregation, so the gelation happens at a slightly higher concentration. When hydrophobic nanoparticles are in the hydrophobic ionic liquid [C_4mim][NTf_2], they form a stable cluster of fluids up to a mole fraction of 0.39, as single peaks are observed in the DLS size distribution

and Newtonian rheology is observed. The large increase in zero viscosity and shear thinning at 0.39 mole fraction of silica indicate that it is at this silica concentration that a colloidal gel is formed.

6.5 Conclusion

Suspensions of hydrophobic surface-functionalised silica nanoparticles in $[C_4mim][BF_4]$ and $[C_4mim][NTf_2]$ have been studied using a variety of techniques. The hydrophilic ionic liquid, $[C_4mim][BF_4]$ stabilises the hydrophilic nanoparticles, evidenced by the shear thinning rheology and multiple peaks in the DLS size distribution. The hydrophobic ionic liquid, $[C_4mim][NTf_2]$, stabilised the nanoparticles at low concentrations, as shown by the Newtonian rheology and single peaks in the DLS size distribution. At higher silica concentrations, the suspensions of hydrophobic silica and both ionic liquids formed a colloidal gel. Large increases in the zero shear viscosity, shear thinning rheological behaviour, the presence of a yield stress and multiple peaks were observed in the size distribution demonstrating that these suspensions of hydrophobic nanoparticles had formed a colloidal gel. In future work, diffusion NMR measurements need to be performed on these systems to investigate the effect of the hydrophobic nanoparticles on the mobility of the ions. Also, transmission electron microscopy and oscillatory rheology should be used to fully characterise the jammed states that are formed.

6.6 References

1. S. Li, K. S. Han, G. Feng, E. W. Hagaman, L. Vlcek and P. T. Cummings, *Langmuir*, 2013, **29**, 9744.
2. D. S. Frost, M. Machas and L. L. Dai, *Langmuir*, 2012, **28**, 13924.
3. K. Ueno, S. Imaizumi, K. Hata and M. Watanabe, *Langmuir*, 2009, **25**, 825.

4. A. Wittmar, M. Gajda, D. Gautam, U. Dorfler, M. Winterer and M. Ulbricht, *J. Nano. Res.*, 2013, **15**, 12.

5. A. Wittmar, D. Gautam, C. Schilling, U. Dorfler, W. Mayer-Zaika, M. Winterer and M. Ulbricht, *J. Nano. Res.*, 2014, **16**, 14.

6. K. Ueno, K. Hata, T. Katakabe, M. Kondoh and M. Watanabe, *J. Phys. Chem. B*, 2008, **112**, 9013.

7. A. Wittmar, D. Ruiz-Abad and M. Ulbricht, *J. Nano. Res.*, 2012, **14**, 651.

8. R. L. Vold, J. R. Waugh, M. P. Klein and D. E. Phelps, *J. Chem. Phys.*, 1968, **48**, 3831.

9. P. T. Callaghan, *Translational dynamics and magnetic resonance: principles of pulsed gradient spin echo NMR*, Oxford University Press, Oxford, 2011.

10. J. Novak and M. M. Britton, *Soft Matter*, 2013, **9**, 2730.

11. K. Ueno, A. Iaba, M. Kondoh and M. Watanabe, *Langmuir*, 2008, **24**, 5253.

12. S. W. Provencher, *Comp. Phys. Comm.*, 1982, **27**, 213.

13. S. W. Provencher, *Comp. Phys. Comm.*, 1982, **27**, 229.

14. S. J. Law, PhD Thesis, University of Birmingham, 2015.

15. M. Instruments, *Zetasizer Nano Series User Manual*, 2004.

16. H. A. Barnes, J. F. Hutton and K. Walters, *An Introduction to Rheology*, Elsevier, Amsterdam, 1997.

17. H. Yang, C. Z. Yu, Q. L. Song, Y. Y. Xia, F. Y. Li, Z. G. Chen, X. G. Li, T. Yi and C. H. Huang, *Chem. Mater.*, 2006, **18**, 5173.

18. J. Y. Kim, T. H. Kim, D. Y. Kim, N.-G. Park and K.-D. Ahn, *J. Power Sources*, 2008, **175**, 692.

19. J. Nordstrom, L. Aguilera and A. Matic, *Langmuir*, 2012, **28**, 4080.

20. S. Shimano, H. Zhou and I. Honma, *Chem. Mater.*, 2007, **19**, 5216.

21. J. Smith, G. B. Webber, G. G. Warr and R. Atkin, *Langmuir*, 2014, **30**, 1506.

22. K. Ueno and M. Watanabe, *Langmuir*, 2011, **27**, 9105.

23. H. Watanabe, M. L. Yao, K. Osaki, T. Shikata, H. Niwa, Y. Morishima, N. P. Balsara and H. Wang, *Rheo Acta*, 1998, **37**, 1.

24. J. R. Stokes and W. J. Frith, *Soft Matter*, 2008, **4**, 1133.

25. E. Zaccarelli, *J. Phys.-Condens. Mat.*, 2007, **19**, 323101.

26. V. Trappe, V. Prasad, L. Cipelletti, P. N. Segre and D. A. Weitz, *Nature*, 2001, **411**, 772.

27. H. A. Barnes, *J. Rheol.*, 1989, **33**, 329.

28. V. J. Anderson and H. N. W. Lekkerkerker, *Nature*, 2002, **416**, 811.

29. C. J. Dibble, M. Kogan and M. J. Solomon, *Phys. Rev. E*, 2008, **77**, 050401-I.

7. Concluding Remarks and Future Work

In this work, suspensions of hydrophilic and hydrophobic nanoparticles in ionic liquids have been studied. The interactions between the ionic liquids and the silica nanoparticles have been characterised and the aggregation of the nanoparticles in the ionic liquids has been investigated.

The rheology of suspensions with hydrophilic nanoparticles was found to be influenced by the anion, rather than the cation, such that suspensions in $[C_2mim][NTf_2]$ and $[C_4mim][NTf_2]$ demonstrated shear thinning at all silica concentrations indicating the formation of a colloidal gel.[1-3] The suspensions of hydrophilic silica nanoparticles in $[C_2mim][BF_4]$ and $[C_4mim][BF_4]$ showed shear thinning at low silica concentrations and shear thickening at high silica concentrations. The shear thinning was proposed to be due to the ordering or breaking of these clusters and the shear thickening is due to the aggregation of these clusters at higher shear rates, causing an increase in the viscosity. For both $[C_4mim][BF_4]$ and $[C_4mim][NTf_2]$ with hydrophobic nanoparticles, shear thinning rheology was also observed, indicating the formation of a colloidal gel.

Magnetic resonance velocity imaging was used to study the rheology at a local level. The behaviour observed in the bulk rheology was consistent with the velocity imaging for suspensions of hydrophilic and hydrophobic nanoparticles in $[C_4mim][BF_4]$ as well as $[C_4mim][NTf_2]$ with hydrophobic nanoparticles. Suspensions of $[C_4mim][NTf_2]$ and hydrophobic nanoparticles demonstrated shear banding at low shear rates. More research is required to understand the cause of this shear banding in certain ionic liquid suspensions and not in others.

Previously, it had been proposed that the interaction between $[C_4mim][BF_4]$ and hydrophilic silica nanoparticles is hydrogen bonding between anions and hydroxide groups on the silica surface.[4] In the literature, this was shown using IR spectroscopy, but other studies have not been able to observe this interaction.[2, 5] In this work, it has been shown that

there is no detectable hydrogen bonding between the either type of silica nanoparticle and the ionic liquids. The hydrogen bonding observed in previous studies is most likely due to the presence of water within the suspensions.

Using NMR relaxation measurements, it has been shown that it is the imidazolium ring of the cation that interacts with the silica nanoparticles, regardless of the ionic liquid or the hydrophobicity of the silica nanoparticle. This is the first time that evidence for this interaction has been observed for suspensions of ionic liquids with hydrophobic silica nanoparticles. NMR diffusion measurements showed that there was an overall decrease in the cation and anion translational motion with increase in hydrophilic silica concentrations. A change in this translation motion of the cations and anions was observed for $[C_4mim][NTf_2]$ and $[C_4mim][BF_4]$ suspensions at silica mole fraction of ca. 0.20. To determine the precise concentration at which this change occurs, a range of silica concentrations around 0.20 mole fraction in both ionic liquids need to be studied. Also, diffusion measurements of the cations and anions in hydrophobic nanoparticle suspensions could be performed to see if this change is also observed.

To study the aggregation of silica nanoparticles within $[C_4mim][NTf_2]$ and $[C_4mim][BF_4]$, DLS measurements were carried out. At low silica concentrations in both ionic liquids with both hydrophilic and hydrophobic ionic liquids, clusters were observed in the size distributions, indicating a fluid of clusters state. The presence of multiple peaks in the DLS size distributions for suspensions of $[C_4mim][BF_4]$ with hydrophobic silica nanoparticles and $[C_4mim][NTf_2]$ with either type of silica indicated that a colloidal gel was formed in these systems. A colloidal glass of clusters has been proposed for suspensions of $[C_4mim][BF_4]$ with hydrophilic nanoparticles here. Microscopy techniques, such as scanning electron or transmission electron microscopy, should be conducted to see if these different structures of nanoparticles could be directly observed.

Further study into the effect of changing the length of the cation alkyl chain, different anions and different types of cations need to be carried out, so that more can be understood about what controls the aggregation and interactions of silica nanoparticles in ionic liquids.

7.1 References

1. K. Ueno, K. Hata, T. Katakabe, M. Kondoh and M. Watanabe, *J. Phys. Chem. B*, 2008, **112**, 9013.
2. K. Ueno, S. Imaizumi, K. Hata and M. Watanabe, *Langmuir*, 2009, **25**, 825.
3. K. Ueno and M. Watanabe, *Langmuir*, 2011, **27**, 9105.
4. H. Yang, C. Z. Yu, Q. L. Song, Y. Y. Xia, F. Y. Li, Z. G. Chen, X. G. Li, T. Yi and C. H. Huang, *Chem. Mater.*, 2006, **18**, 5173.
5. S. Shimano, H. Zhou and I. Honma, *Chem. Mater.*, 2007, **19**, 5216.

Appendix 1

The mole fraction of silica, x, was estimated from the molecular mass of the ionic liquid and SiO_2 and the ideal mass weighed, which allowed the moles of the ionic liquid, M_{IL}, and silica, M_S, for a given wt. % to be determined. The mole fraction was then calculated using:

$$x = \frac{M_S}{M_{IL} + M_S}$$

The volume fraction of silica, ϕ, was calculated using the density of the ionic liquids and the silica found in the table below.

Material	Density / g cm^{-3}
Aerosil R104	2.00
Aerosil 200	2.20
1-ethyl-3-methylimidazolium tetrafluoroborate	1.26
1-ethyl-3-methylimidazolium bis(trifluoromethylsufonyl)imide	1.49
1-butyl-3-methylimidazolium tetrafluoroborate	1.18
1-butyl-3-methylimidazolium bis(trifluoromethylsufonyl)imide	1.41

These densities allow the volume of the ionic liquid, V_{IL}, and the volume of the silica, V_S, to be calculated, which in turn allowed the volume fraction of the suspension to be calculated using:

$$\phi = \frac{V_S}{V_{IL} + V_S}$$

Appendix 2

The normalised diffusion coefficients for suspensions of $[C_2mim][BF_4]$ and $[C_2mim][NTf_2]$ with hydrophilic silica nanoparticles.

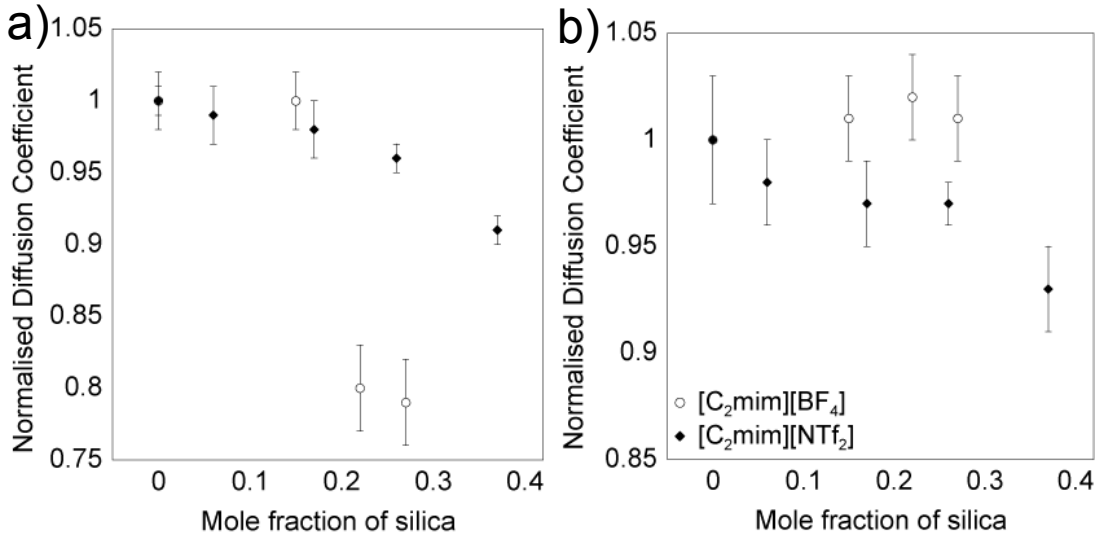

Plots of normalised diffusion coefficient against mole fraction of silica for a) cations and b) anions.

Appendix 3

The figure below shows the scatter in the data used to make figure 4.15.

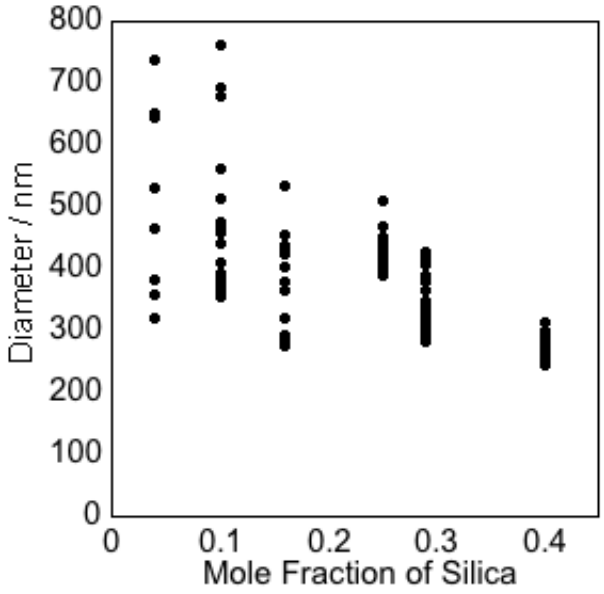

Plot of diameter against hydrophilic silica mole fraction of silica for $[C_4mim][BF_4]$ showing all repeats of the measurement.

Appendix 4

Representative size distribution obtained for $[C_4mim][BF_4]$ and $[C_4mim][NTf_2]$ with hydrophilic silica nanoparticles to show the variation in the size distribution intensities.

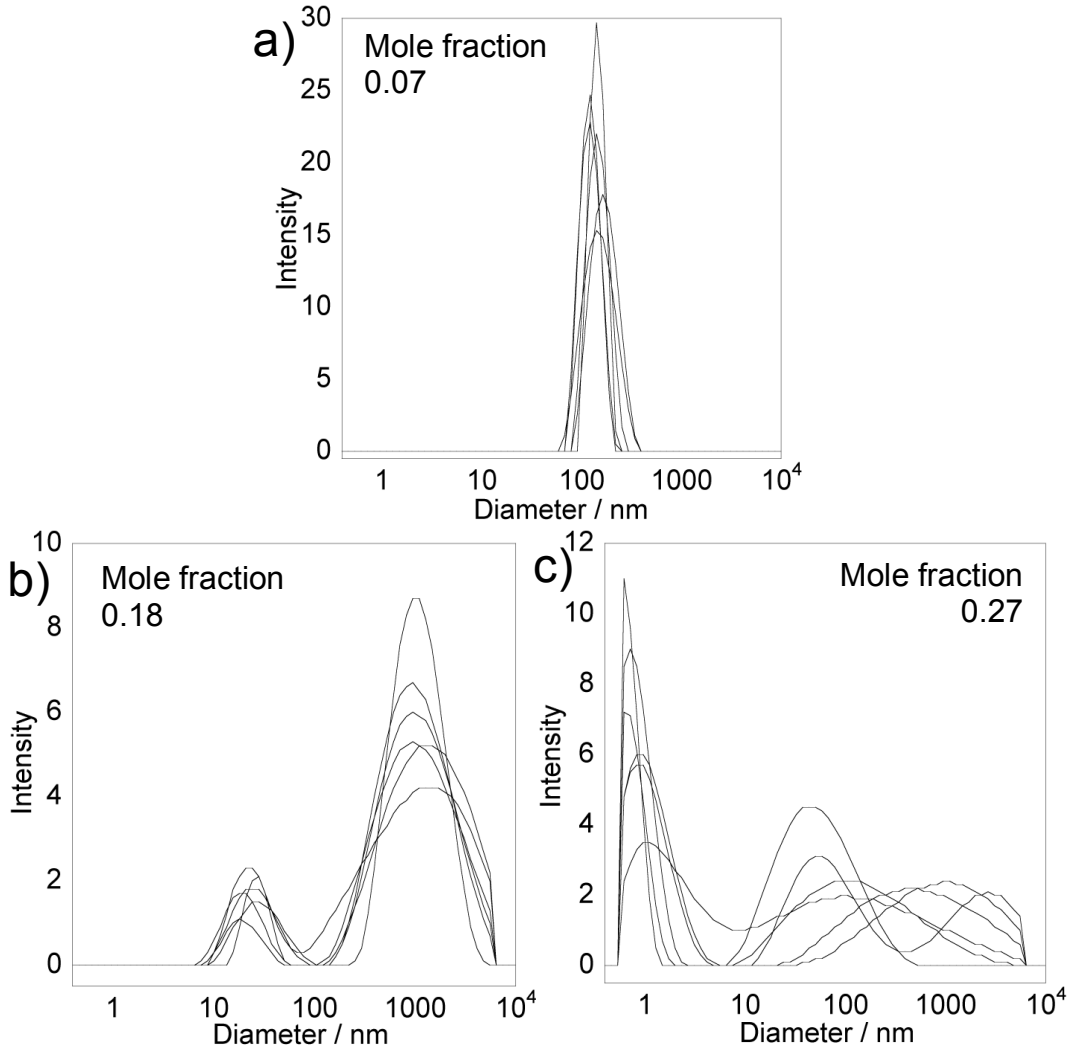

Plots of intensity against diameter for $[C_4mim][NTf_2]$ with hydrophilic silica nanoparticles.

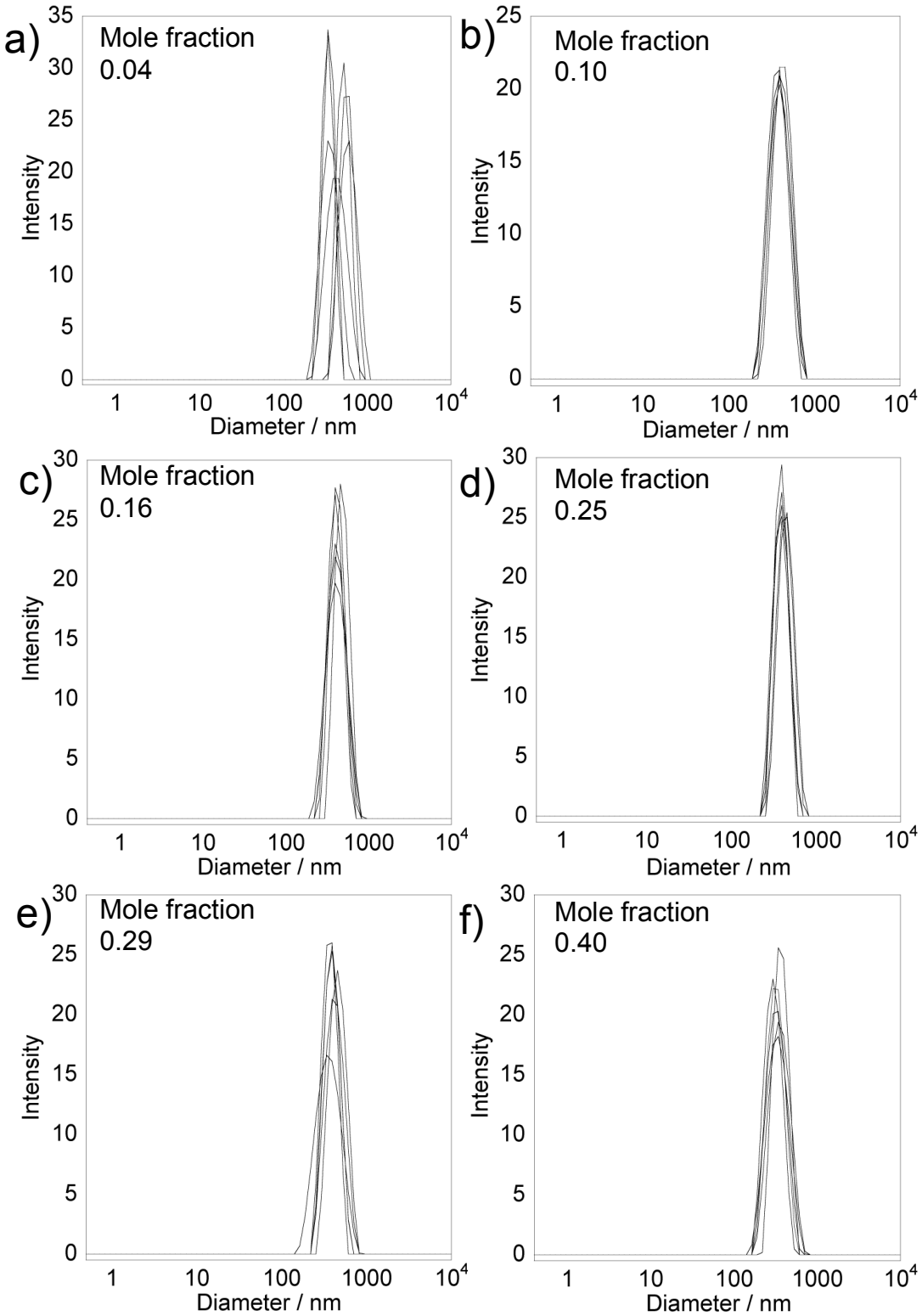

Plots of intensity against diameter for $[C_4mim][BF_4]$ with hydrophilic silica nanoparticles.

Appendix 5

The volume distribution from dynamic light scattering measurements for suspensions of $[C_4mim][NTf_2]$ with hydrophilic silica where polydispersity was observed

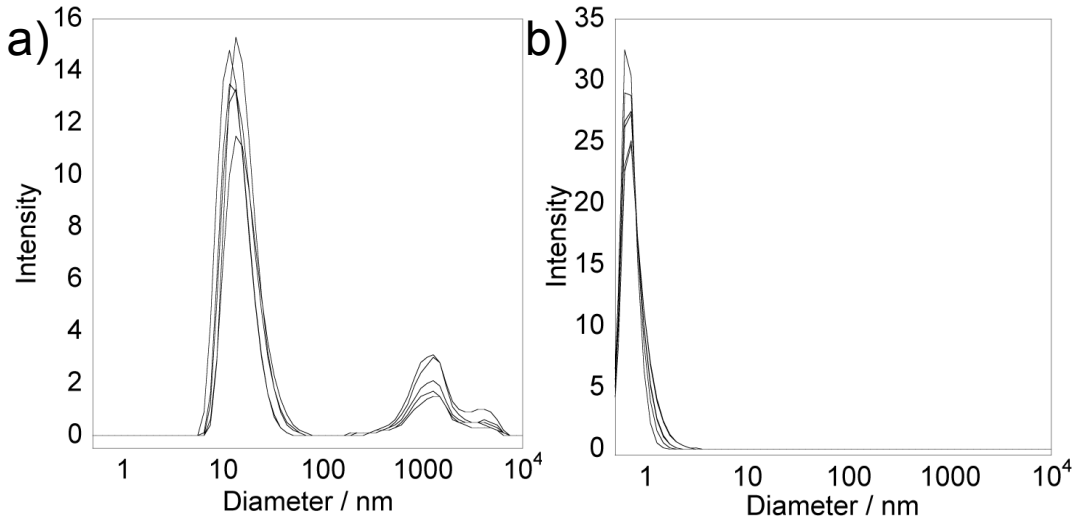

Plots of intensity against diameter $[C_4mim][NTf_2]$ with 0.18 (a) and 0.27 (b) mole fraction of hydrophilic silica nanoparticles. The volume distribution is shown.

Appendix 6

The shear rates, $\dot{\gamma}$, accessed in the Couette cell during the magnetic resonance velocity imaging measurements were calculated using,

$$\dot{\gamma} = \frac{2\omega}{n} \frac{R^{-2/n}}{1 - K^{-2/n}}$$

where ω is the rotation rate, $R = r/r_o$ and $K = r_i/r_o$. Values of the power law exponent, $n = 1$, inner cylinder radius, $r_i = 2.6$ and outer cylinder radius, $r_o = 5.6$ were used.

Appendix 7

Radial velocity profiles from magnetic resonance velocity imaging experiments used to obtain values for the power law exponent for suspensions of $[C_4mim][BF_4]$ and $[C_4mim][NTf_2]$ with hydrophobic silica nanoparticles.

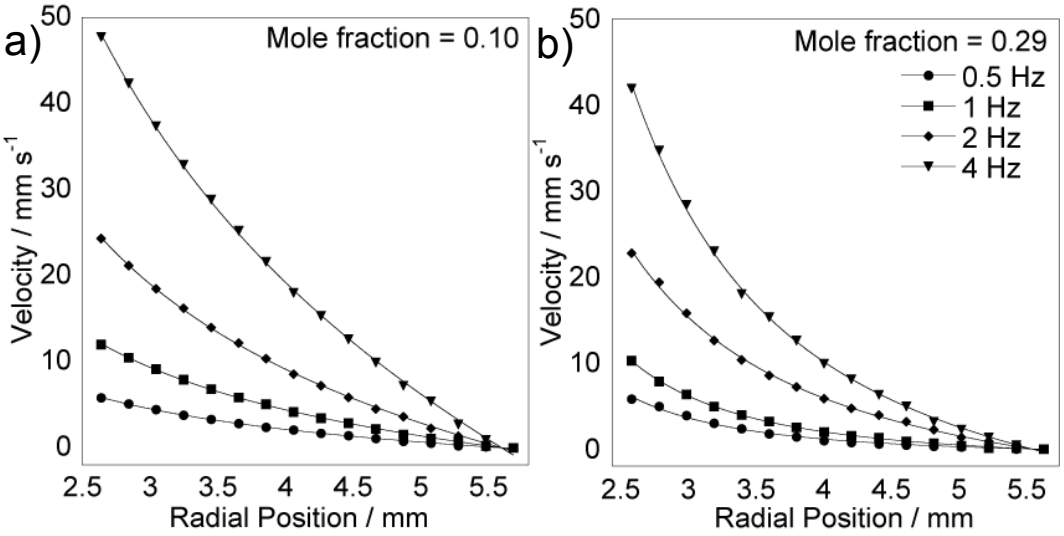

Radial velocity profiles for $[C_4mim][BF_4]$ with 0.10 (a) and 0.25 (b) mole fractions of hydrophobic silica.

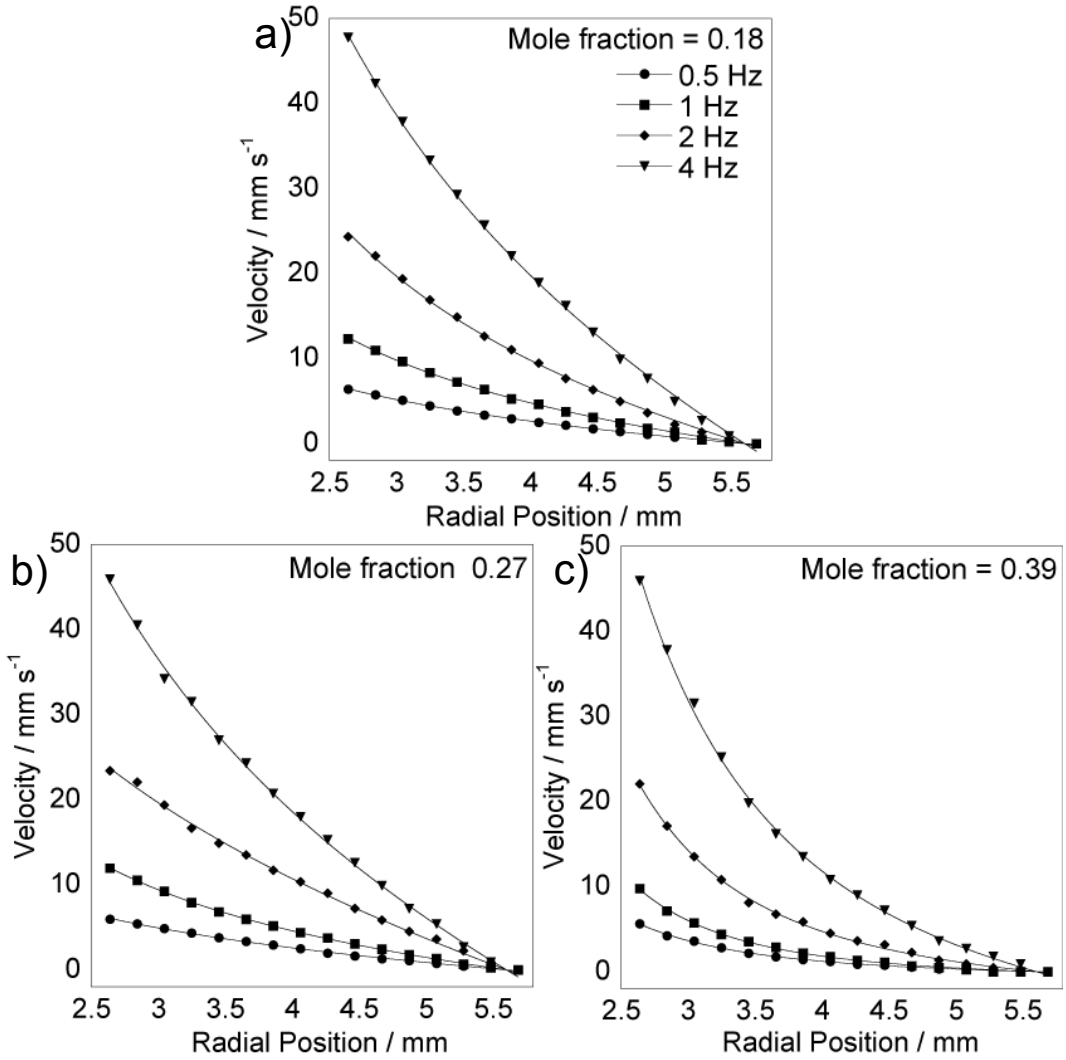

Radial velocity profiles for $[C_4mim][NTf_2]$ with 0.18 (a), 0.27 (b) and 0.39 (c) mole fractions of silica.

Appendix 8

Representative size distribution obtained for $[C_4mim][BF_4]$ and $[C_4mim][NTf_2]$ with hydrophobic silica nanoparticles to show the variation in the size distribution intensities.

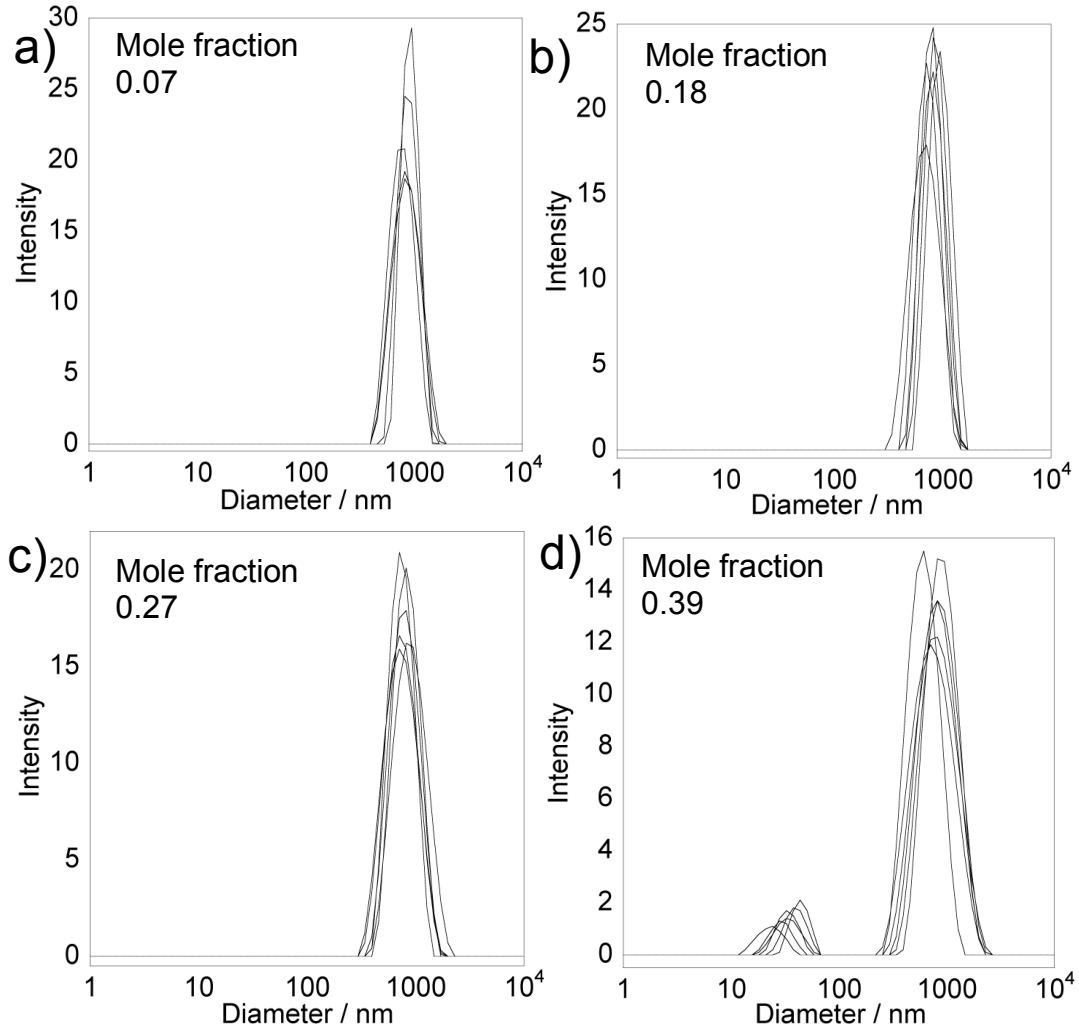

Plots of intensity against diameter for $[C_4mim][NTf_2]$ with hydrophobic silica nanoparticles.

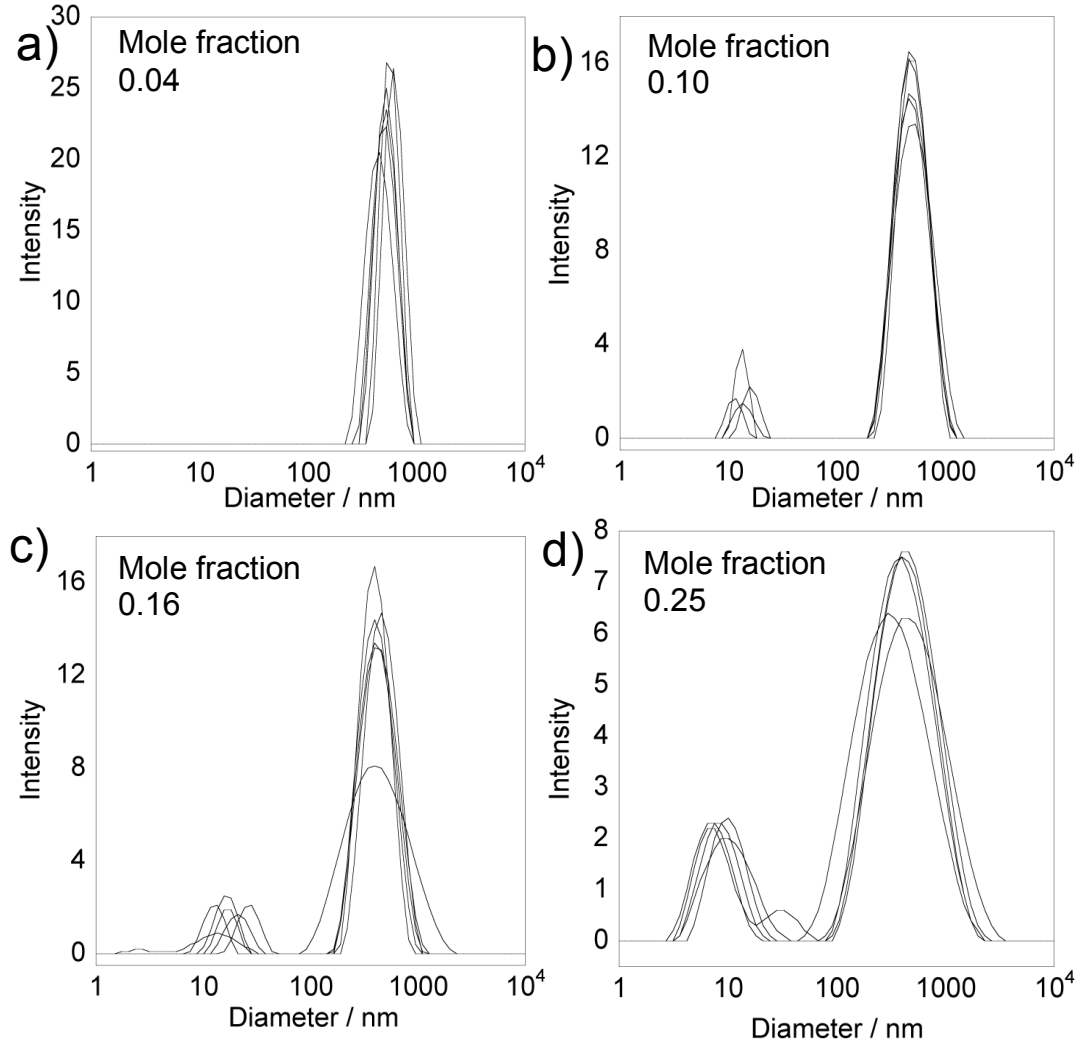

Plots of intensity against diameter for $[C_4mim][BF_4]$ with hydrophilic silica nanoparticles.

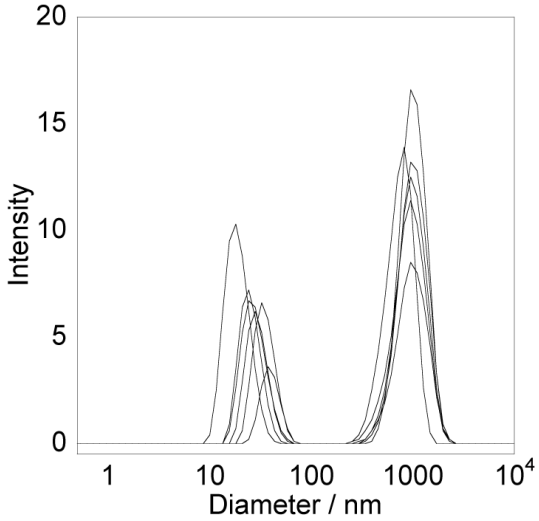

Plots of intensity against diameter for $[C_4mim][NTf_2]$ with 0.39 mole fraction of hydrophobic silica nanoparticles showing the variation in the volume distributions.

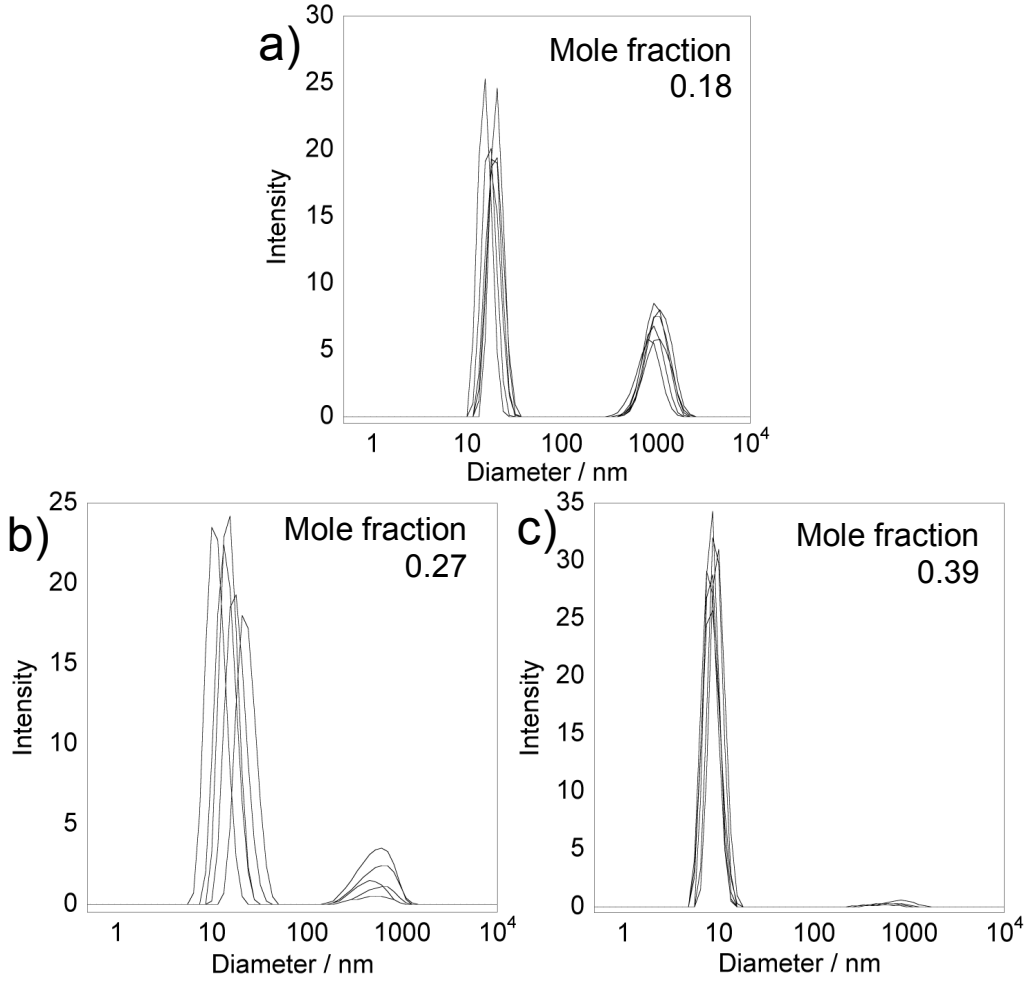

Plots of intensity against diameter for $[C_4mim][BF_4]$ with hydrophobic silica showing the variation in the volume distributions.